UNIVERSITY OF SHEFFIELD

Application of layout optimization to the design of bracing in buildings

by

Hongjia Lu

A thesis submitted in partial fulfillment for the

degree of Doctor of Philosophy

in the

Department of Civil and Structural Engineering

December 2017

Declaration of Authorship

I, Hongjia Lu, declare that this thesis entitled, 'Application of layout optimization to the design of bracing in buildings' and the work presented in it are my own. Where information has been derived from other sources or where the work is done in collaboration with my supervisors, I confirm that this has been indicated in the thesis.

Signed:

Date:

ABSTRACT

In civil engineering, techniques for the design and construction of tall buildings have expanded rapidly in recent decades. However, developments in layout / topology optimization techniques which can be applied to such structures have not kept pace. Consequently, currently the layout of structural members in buildings usually relies primarily on the engineer's experience. On the other hand, numerical layout optimization techniques appear potentially to be very suitable for building layout design, and yet have not been used in practical building design. Therefore, this thesis investigates the application of layout optimization in building layout / topology design, and especially focusses on the design of bracing layout.

The bracing structure (or lateral stability structure) is an essential component of any building that is used to provide stability against wind loads. Usually, the acting positions of the lateral loads are dependent on the building shape. However, this point has not been the subject of investigation in previous studies of bracing layout optimization. Therefore, two current numerical means of treating design dependent loads (i.e. transmissible loads) are investigated and compared in this thesis. The difference between these two means are identified and proved through the use of mathematical and numerical approaches. Additionally, during the investigation it has been found that taking advantage of pre-existing rigid bars in the optimization may lead to more efficient and simple structures. Therefore, in the following bracing design case studies, various assumptions about pre-existing bars are made.

The case studies involving bracing design comprise three main elements, covering a range of assumptions as follows: (1) Optimal bracing for pre-existing beam-column frames which are required to resist lateral loads are identified. (2): Optimal frames which are required to resist both vertical and lateral load cases are identified. (3): Optimal frames which are required to resist lateral load cases are identified with the assumption of pre-existing beams. This allows the bracing structure and external building envelope to be simultaneously identified.

It has been found in this study that cases with different assumptions lead to very different solutions, which may be selected for use based on the real situation. Additionally, some supplementary findings related to analytical optimal solutions and the use of the superposition approach in multiple load cases are outlined; details can be found in the main chapters.

Acknowledgements

Firstly, I would like to express my sincere gratitude to my advisors, Prof. Matthew Gilbert and Prof. Andrew Tyas, for their continuous support during my PhD studies and related research, and for their patience, motivation, and immense knowledge. Their guidance helped me in all aspects of my research and writing of this thesis. I cannot imagine having had better advisors and mentors for my PhD studies.

Also, I want to thank my colleagues and friends: without my interactions with you, my PhD life would not have been so enjoyable and colourful. I want to especially thank Dr Linwei He for his wise suggestions and generous guidance.

I want to thank my parents for their unconditional financial support; without them, I would never have had this chance to realize my dream.

Last but not least, I want to thank my dear wife, Yiling Zhang, who has been with me all these years and has made them the best years of my life so far.

Contents

Declaration . . . .

Abstract . . . .

Acknowledgements . . . .

Contents . . . .

List of Figures . . . .

List of Tables . . . .

1 Introduction **1**

1.1 Motivation 1

1.2 Objectives 2

1.3 Structure of the thesis 3

2 Literature review **5**

2.1 Mathematical programming 6

2.1.1 Convex and concave optimization 7

2.2 Linear programming 9

2.2.1 Approaches to solve linear programming problems 9

2.2.2 Duality theory 10

2.3 Non-linear programming 11

2.3.1 Optimality criteria for problems with equal constraints 12
2.3.2 Optimality criteria for problems with unequal constraints 13
2.4 Elastic and plastic design 14
2.4.1 Upper and lower boundary theory 15
2.4.2 Plastic vs. elastic beam design example 16
2.5 Mathematical theories of optimal structures 17
2.5.1 Michell's optimality criterion 17
2.5.2 Three regions in Michell structures 19
2.5.3 An example of interactive collaboration between analytical and numerical approach: optimal topology to withstand uniform load between pin supports 20
2.6 Discrete layout optimization 21
2.6.1 Ground structure approach 21
2.6.2 Hemp's theory 23
2.6.3 Member adding method 24
2.6.4 Geometry optimization 25
2.6.5 Structural optimization with multiple load cases and the superposition approach for solving multiple load case problems 26
2.7 Continuum topology optimization 27
2.8 Transmissible load 29
2.8.1 Prager structure 29
2.8.2 Rigid bar approach 30
2.8.3 Migrating load approach 30
2.9 Lateral stability system 30
2.9.1 Optimization of bracing system 34
2.10 Conclusions 36

3 On transmissible load formulations in topology optimization **37**

3.1 Introduction 38

3.2 Comparison between rigid bar and migrating load approaches 39

3.2.1 Conceptual formulation 39

3.2.2 Mohr's circle analysis. 40

3.3 Numerical examples 42

3.3.1 Example 1 - uniform load between pinned supports 42

3.3.2 Example 2 - Cantilever subject to uniform load 44

3.3.3 Commentary 45

3.4 Formal mathematical status of the rigid bar and migrating load appraches 47

3.4.1 Dual theory based proof of the difference between migrating load and rigid bar approach 47

3.4.2 Lagrangian function based proof of the difference between migrating load and rigid bar approach 49

3.5 Conclusion 51

3.6 Postscript 51

4 Optimal bracing systems in buildings:
bracing pre-existing frames **52**

4.1 Introduction 53

4.2 Assumptions 54

4.3 Problem specification 56

4.3.1 Cases considered 56

4.3.2 Single load case layout optimization formulation 57

4.3.3 Practical considerations 58

4.4 Optimized single bay bracing designs 59

4.4.1 Case 1: Tension only bracing 59
4.4.2 Case 2: Bracing connected only at corners 61
4.4.3 Case 3: Optimal reference bracing 63
4.5 Multi-storey / multi-bay buildings 66
4.6 Conclusions 68

5 Optimal bracing systems in buildings: holistic design 69

5.1 Introduction 69
5.2 Consideration of multiple load cases 71
5.2.1 Parameter governing the optimal layout, ΔV_{norm} 72
5.3 Examples: simple single and multi-storey braced frames 74
5.3.1 Problem definition 75
5.3.2 Optimal layout results 75
5.4 Bracing design of a small office building 78
5.5 Conclusions 81

6 Bracing topology optimization with transmissible loading condition 87

6.1 Introduction 87
6.2 Approaches and assumptions 87
6.3 2D Single load case optimization 89
6.3.1 Relation between topology simplicity and rigid floor number 91
6.3.2 Implication of single load case result 93
6.4 3D multiple load case optimization 93
6.5 Conclusion 98

7 Layout optimization formulation for combined structure of trusses and frames 100

7.1 Introduction 100
7.1.1 Optimization formulation 101
7.1.2 Numerical examples - Moment load 105
7.1.3 Numerical examples - bracing design under restricted design domain . . 107
7.2 Frame optimization formulation with multiple load cases 108
7.3 Use of an I section in frame optimization algorithm 110
7.4 Conclusion 113

8 Discussion **114**
8.1 Different optimized solutions under different assumptions 114
8.2 Optimal intersection angle with pre-existing bars 115
8.2.1 Pre-existing cases with non integer aspect ratio 120

9 Conclusions **122**

10 Recommendations for future work **124**

References **126**

List of Figures

1.1 Examples of tall buildings with exoskeleton structure: (a) Hearst Tower, New York (Alsandro 2006); (b) John Hancock Building, Chicago (Jovianeye 2011). 2

2.1 Local and Global optimal 7

2.2 Examples of convex and concave sets and functions: (a) Convex set S_1; (b) Concave set S_2; (c) Convex constraint $f(x) \geq 0$; (d) Concave function $g(x) \geq 0$ 8

2.3 Example of using the graphical approach to solve a linear program (2.2), where grey area is the search region, solid lines represent the constraints and dashed lines represent the contour lines of the objective function. 10

2.4 Optimality criteria of a non-linear mathematical program with equal constraints, where dashed lines are contour lines of objective function $f(x, y)$, and the solid line represents equal constraint $h(x, y) = c$. 13

2.5 Two situations of a non-linear mathematical program with inequality constraints: (a) Optimal point for $f_{max}(x, y)$ locates in the region of $g(x, y) \leq c$; (b) Optimal point for $f_{max}(x, y)$ locates outside of the region of $g(x, y) \leq c$; dashed lines are contour lines of objective function $f(x, y)$, and the grey area represents unequal constraint $g(x, y) \leq c$. 15

2.6 Steel stress/strain curve: (a) curve for a realistic scenario; (b) curve with assumptions made in plastic rigid design. 16

2.7 Elastic and plastic design example: (a) An I-section beam that takes uniform load across the span and has fixed supports at two ends; (b) Elastic design: moment distribution across the span and stress distribution at the middle and two ends; (c) Plastic design: moment distribution across the span and stress distribution at the middle and ends; where ω, l and f_y represent loading per unit length, total beam length and yield stress. 18

2.8 Michell cantilever with point load A and pin supports around circle B, where red and blue lines respectively represent bars in tension and compression. 19

2.9 Types of optimal regions in Michell trusses: (a) symbols of five types of region, where $+$ and $-$ represent tensile and compressive strain respectively; (b) a Michell structure with T-type structures in the middle region and R^{-}-type structures at the two sides; red and blue lines respectively represent bars in tension and compression. 20

2.10 Optimal topology for uniform gravity load between pin supports problem, where red and blue lines respectively represent bars in tension and compression 21

2.11 Ground structure approach: (a) initial design domain, support and loading conditions; (b) node discretization; (c) create all possible interconnections of discrete nodes (build ground structure); (d) use linear programming to select the optimal subset structure; red and blue lines respectively represent bars in tension and compression. 22

2.12 An optimized structure generated with the 99 line MATLAB script implementing the SIMP algorithm, where the command used is "top(50,50,0.3,3.0,1.5)" and the five parameters in the used command are design domain width, design domain height, volume fraction, penalty parameter p and filter diameter r_{min} respectively. (Sigmund 2001) 28

2.13 Four tubular buildings: (a) John Hancock Building, Chicago (Jovianeye 2011) (b) China World Trade Center Tower III, Beijing (Holton 2008) (c) Burj Khalifa, Dubai (Donaldytong 2012) (d) Willis Tower, Chicago (Soakologist 1998) 31

2.14 Three buildings using outrigger system: (a) Jin Mao Building, Shanghai (Airunp 2005); (b) International Commerce Centre, Hongkong (WiNG 2010); (c) U.S. Bank Center, Milwaukee (Sulfur 2006) 32

2.15 Three buildings using the diagrid bracing system: (a) 30 St Mary Axe, London (Guichard 2010); (b) Hearst Tower, New York (Alsandro 2006); (c) CCTV Headquarters, Beijing (Stojakovic 2013) 33

2.16 Three classical cantilever solutions, where red and blue lines respectively represent bars in tension and compression: (a) Michell-Hemp cantilever; (b) Michell-Hemp cantilever constrained within a half-strip; (c) Stromberg Bracing (Stromberg et al. 2012) 35

3.1 Rigid bar and migrating load approach for a problem involving six nodes: (a) the design problem and the trajectory of the transmissible load P; (b) solution obtained with rigid bar approach, where solid and dotted grey lines represent rigid bars have respectively non-zero and zero internal force; (c) possible solution obtained via migrating load approach, where P_1, P_2 and P_3 are the load variables and they must satisfy the sum and sign constraint in (c). 40

3.2 Migrating load approach: uniform load between pinned supports, where (a) is design domain description, (b) shows transmissible trajectory and result from discrete optimization and (c) shows final position of loads. Red bar takes tensile force and blue bar takes compressive force. 43

3.3 Rigid bar approach: uniform load between pinned supports, where (a) is discrete optimization result, (b) is early stage result of continuum optimization and (c) is final result of continuum optimization. Red, blue, grey solid, grey dotted lines represent, respectively, bars take tensile force, bars takes compressive force, rigid bars have non-zero internal force, rigid bars have zero internal force. 43

3.4 Migrating load approach: cantilever subject to uniform load, where (a) is design domain description, (b) shows transmissible trajectory and result from discrete optimization and (c) shows final position of loads. Red bar takes tensile force and blue bar takes compressive force. 45

3.5 Rigid bar approach: cantilever subject to uniform load, where (a) is discrete optimization result, (b) is early stage result of continuum optimization and (c) is final result of continuum optimization. Red, blue, grey solid, grey dotted lines represent, respectively, bars take tensile force, bars takes compressive force, rigid bars have non-zero internal forces, rigid bars have zero internal forces. 45

3.6 Rigid bar approach: uniform load between pinned supports, where (a) $\sigma^-/\sigma^+ = 3.33$, (b) $\sigma^-/\sigma^+ = 2.50$ and (c) $\sigma^-/\sigma^+ = 2.00$; where σ^- and σ^+ represents compressive and tensile stress capacity. Red, blue, grey solid, grey dotted lines represent, respectively, bars take tensile force, bars takes compressive force, rigid bars have non-zero internal forces, rigid bars have zero internal forces. 47

4.1 Bracing design case with pre-existing members around the edge of the bay, pinned supports at the bottom corners and a horizontal load at the top left corner. A 'ground structure' comprising interconnecting members (2×4 nodal division discretization shown, not including all connections for sake of clarity). 56

4.2 Optimized bracing layouts for various h:b aspect ratios (4:1, 3:1, 2:1, 1:1, 1:2, 1:3 & 1:4): (a) Case 1 - tension only bracing; (b) Case 2 - bracing connected only at corners; (c) Case 3 - optimal reference bracing. The corresponding analytical volume is indicated below each layout, where P is the magnitude of the horizontal load applied at the top left corner of the design domain, of breadth b and height h, and σ is the limiting tensile strength. Element color key: red = tensile, blue = compressive, grey = zero force, black = pre-existing (assuming left to right loading). 60

4.3 Volume comparison for the three bracing cases considered (where P is the magnitude of the horizontal load applied at the top left corner of the design domain, of breadth b and height h, and σ is the limiting tensile strength) 61

4.4 Ability of a pre-existing beam member with infinite reserves of strength to make an external load 'transmissible' (i.e. each of the above cases is equivalent) 62

4.5 Demonstrating the equivalence between Case 2 (bracing only connected at corners) and a Hemp-Michell cantilever: (a) starting problem, in this case with a frame with a 2:1 aspect ratio; (b) base supports replaced by reaction forces; (c) corner forces replaced by equivalent loads (since forces can be distributed arbitrarily along rigid members); (d) design domain divided along line of antisymmetry; (e) corner loads replaced by supports and appropriate forces added along line of division. 63

4.6 Optimized layout for Case 2 (connections only at corners) when the bracing elements are allowed to extend beyond the lines of the columns 64

4.7 Use of a Mohr's circle analysis to demonstrate that 45° is the optimal intersection angle between a pre-existing beam/column and an optimal tension/compression bracing member pairs. (An optimal bracing member follows the direction of principal strain (Hemp 1973), whilst the strain in a pre-existing member is zero due to its infinite strength. Thus the subtended angle between such members will be 90° on the circle, or 45° in reality.) 65

4.8 A standard knee bracing layout 65

4.9 Demonstrating the equivalence between Case 3 (optimal reference bracing) and Hemp-Michell cantilever solutions: (a) starting problem, in this case using frame with 1:3 aspect ratio; (b) rotate the problem by 90° clockwise; (c) design domain divided into Structure I & II along the line of antisymmetry; (d) point loads are replaced by distributed loads (since forces can be distributed arbitrarily along rigid members); (e) Structure I & II are combined into a Michell cantilever. 66

4.10 Comparison of optimal bracing layouts in multi-storey frames and sample braced tube structures constructed in practice: (a) the optimal layout for a 4:1 aspect ratio case with intermediate pre-existing beams and columns; (b) John Hancock Center in Chicago, a braced tube structure similar to (a); (c) an alternative optimal layout with the same volume as (a); (d) One Maritime Plaza in San Francisco, a braced tube structure qualitatively similar to (c). Element color key: red = tensile, blue = compressive, black = pre-existing (assuming Case 2 or 3 bracing and left to right loading). Note however that the angles in (b) and (d) differ from the 45° found to be optimal when bracing a pre-existing frame. 67

5.1 Use of superposition approach to derive the optimization result of multiple load cases: (a) three load cases based on British Standard load case combination, where $V = 1.0G_{\mathrm{k}} + 1.2Q_{\mathrm{k}}$, $\Delta V = 0.4G_{\mathrm{k}} + 0.4Q_{\mathrm{k}}$, $\Delta H = 1.2W_{\mathrm{k}}$, where G_{k}, Q_{k} and W_{k} are, respectively, characteristic permanent, imposed and wind loads; (b) as (a) but with additional dummy load case added to enable superposition principle to be applied; (c) using superposition, the solution to (b) can be obtained by superimposing the individual results from four single load case problems, $\overline{p}_1$ to $\overline{p}_4$. 73

5.2 Numerical verification of superposition approach using layout and geometry optimization: (a) example with $\Delta V_{\mathrm{norm}} = 3$; (b) example with $\Delta V_{\mathrm{norm}} = 6$, where ΔV_{norm} is the parameter governing layout for multiple load case problems. On the left hand side are optimized results from single component load cases $\overline{p}_2$ and $\overline{p}_3$, see Fig. 5.1c, and on the right hand side are multiple load case results. Red and blue bars represent, respectively, members taking tensile and compressive forces. For the multiple load case results the force distribution shown corresponds to the load case with horizontal loads acting from left to right. 74

5.3 Loads for single- and multi-storey bracing layout optimization study: (a) single-storey cases; (b) multiple-storey cases; values of V and H are given in Table 3. . 76

5.4 Volume comparison and optimized layout results for a single-storey frame based on British Standard loading with $c = 1.35$ and $\Delta V_{\text{norm}} = (0.4G_{\text{k}} + 0.4Q_{\text{k}})/(1.2W_{\text{k}})$, where c is the ratio of the vertical load between load cases (i.e. $(1.4G_{\text{k}} + 1.6Q_{\text{k}})/(1.0G_{\text{k}} + 1.2Q_{\text{k}})$); all the volumes are normalized against the volumes of standard cross bracing systems; red and blue bars represent, respectively, members taking tensile and compressive forces when horizontal loads are applied from left to right. 77

5.5 Volume comparison and optimized layout results of multi-storey cases based on British Standard loading with $c = 1.35$ and $\Delta V_{\text{norm}} = (0.4G_{\text{k}} + 0.4Q_{\text{k}})/(1.2W_{\text{k}})$, where c is the ratio in vertical load between load cases (e.g. $(1.4G_{\text{k}} + 1.6Q_{\text{k}})/(1.0G_{\text{k}} + 1.2Q_{\text{k}})$); all the volumes are normalized against the volumes of standard cross bracing systems;red, blue bars represent, respectively, members taking tensile and compressive forces in the load case which includes horizontal loads from left to right. 78

5.6 Plan of a typical small office building, after Brettle & Brown (2009) 79

5.7 Different braced bay designs for a typical small office building: (a) optimized bracing design; (b) optimized deisign with pre-existing beams; (c) conventional braced bay; (d) sections chosen for the structure shown in (b), with buckling effects considered; (e) sections chosen for the structure in (c), with buckling effects considered. Note that the selected bay could be found in Fig. 5.6 using reference points in this graph. 80

5.8 Visualization of small office building employing optimized bracing structure shown in Fig. 5.7b 82

6.1 Two examples show that acting positions of the wind loads are dependent on the structure shape. 88

6.2 Case description, where bold lines represent pre-existing beams. 89

6.3 Results of 2D bracing optimization: (a) Case 1: Bracing optimized with rigid floor members; (b) Case 2: Bracing optimized without rigid floor members; (c) Case 3: Fixed topology - Stromberg bracing; (d) Case 4: Fixed topology - Cross bracing; red, blue and grey lines represent bars in tension, compression and takes no forces respectively, when horizontal loads are applied from left to right 91

6.4 Results of 2D bracing optimization with different number of pre-existing beams: (a) 20 pre-existing beams across the height, (b) 8 pre-existing beams across the height, (c) 4 pre-existing beams across the height; red and blue lines represent bars in tension and compression respectively, when horizontal loads are applied from left to right. 92

6.5 Single load case result implementation example, where the building needs to take wind load from one major direction; red and blue lines respectively represent bars in tension and compression. 93

6.6 3D Case description, where red and blue arrows represent loads in load case 1 and 2. 94

6.7 Results from the 3D bracing optimization cases: (a) Case 5 - bracing member could exist anywhere within the cuboid design domain; (b) Case 6 - bracing members can only exist at the external surface of the design domain. 95

6.8 Relation between original load cases and component load cases in Case 5 where a bracing member could exist anywhere within the cuboid design domain: (a) top view graph of the original load cases on the building; (b) top view graph of the component load cases; (c) top view graph of the final acting positions of the transmissible loads in the component load cases; (d) numerical results of the component load cases; red and blue lines respectively represent bars in tension and compression. 96

6.9 Relation between original load cases and component load cases in Case 6 where bracing members could only exist at the external surface of the design domain: (a) top view graph of the original load cases on the building; (b) top view graph of the component load cases; (c) top view graph of the final acting positions of the transmissible loads in the component load cases; (d) numerical results of the component load cases. 97

7.1 Force components of a beam 101

7.2 Force distribution within a square section: (a) within a square section, the top and bottom area a_{M} is used to take moment and a_{N} is used to take axial force; (b) normal stress distribution within the section; (c) shear stress distribution within the section; (d) modified shear stress distribution within the section. 102

7.3 Cases with different in-plane moment load at the centre where the load magnitude for (a) 500kNm; (b) 2000kNm; (c) 4000kNm; red, blue and black lines represent members take tensile axial force, compressive axial force and bending moment. . 106

7.4 Cases with different design domain spaces: (a) only one layer of nodes located in the grey area; (b) one layer of nodes located on the two sides and 1.5m design space for the top and middle horizontal areas; (c) one layer of nodes located on the two sides and 3m design space for the top and middle horizontal areas. 108

7.5 Example of a single member's cross-sectional area in two load cases, where a_{M} is the area used to take moment and a_{N} is the area used to take axial and shear force. 109

7.6 Typical I section, (a) size parameters of an I section; (b) an area distribution with a_{N} only in the web; (c) an area distribution with a_{N} also in the flange; a_{N} is the area used to take axial and shear force, and a_{M} is the area used to take moment. . 111

8.1 Cost function, adjoint strain, and Mohr's circle analysis for three different members: (a) member with normal stress capacity σ; (b) member with increased stress capacity $n\sigma$; (c) member with infinite stress capacity. 117

8.2 Examples for pre-existing members with $n\sigma$ stress capacity and normal members with σ stress capacity:(a) n=1, pre-existing member not used; (b) n=1.1, the theoretical and numerical intersection angles are 77.690° and 78.173°; (c) n=2, the theoretical and numerical intersection angles are 60.000° and 61.650°; (d) n=5, the theoretical and numerical intersection angles are 50.768° and 51.590°; black members represent pre-existing members, and angles shown in the graph are numerical results. 118

8.3 Pre-existing member with area lower boundary, where a, f and σ represents area, material cost and adjoint strain : (a) curve of cost function; (b) relation between cost and adjoint strain. 120

8.4 Mohr circle analysis for R-region problem, where red, blue and black dash line represents, respectively, bracing member in tension, bracing member in compression and pre-existing member with infinite reserves of strength. 120

8.5 Pre-existing cases with none integer aspect ratios, where width : height equals to 1:1.5 in (a), 1:2.5 in (b) and 1:3.5 in (c). Element color key: red = tensile, blue = compressive, black = pre-existing (assuming left to right loading). 121

List of Tables

4.1 Comparison between optimal reference bracing (Case 3) and standard knee bracing volumes (where P is the magnitude of the horizontal load applied at the top left corner of the design domain, of breadth b and height h, and σ is the limiting tensile strength). 65

5.1 Calculation example of parameter ΔV_{norm}, where p_i represents the ith load case. . 73

5.2 Load values of V and H in different load cases, where p_i represents the ith load case; P is a unit load; c is a loading coefficient, assumed to be 1.35 based on British Standard 5950-1:2000 load case combinations, see Eqn. (1); ΔV_{norm} is the parameter governing layout for multiple load case problems (load positions are shown in Fig. 5.3). 77

5.3 Characteristic actions on the small office building 79

8.1 Optimization loads and targets of previous chapters 115

Chapter 1

Introduction

At present, the arrangement of key structural elements within a tall building is generally determined by hand, either to meet architectural objectives, or according to engineering intuition. Consequently, the resulting arrangements of components are often far from optimal in aspect of material consuming, leading to needless material consumption. In this thesis, computational layout optimization techniques will be applied to the design of tall buildings. The project involves computer programming, application of mathematical optimization techniques, and the development of improved guidance and software tools for engineers wishing to apply layout optimization in building design.

1.1 Motivation

The concept of optimal structure was established in the early 20th century, and nearly half a century later, a numerical optimization approach appeared in 1960. Currently, structural optimization has been widely used in the field of mechanical engineering. However, it is rarely used in the field of building design. One of the reasons for this may be that building structures often need to meet a large variety of different requirements. Hence, the optimization problem for building structures not only involves a high computational cost, but also, the final result is usually not satisfactory (e.g. many of the results from problems with multiple load cases are very complex and difficult to build). Consequently, the layout design of building structures is heavily reliant on the intuition and/or experience of engineers, or is just concerned with architectural objectives.

Moreover, because of the lack of knowledge about optimal structures, structures may cost even many times more with respect to material when compared with an optimized structure. Therefore, the study in layout optimization is very necessary and valuable.

Considering the working principles of buildings, braced frame or exoskeleton structures are very similar to a truss structure (e.g. Fig. 1.1). Therefore, among the numerous topology optimization approaches, truss layout optimization is the most suitable approach for this kind of problem (discussed in detail in Sections 2.6 and 2.7). In addition, because of the rapid development of layout optimization technology over the past two decades, the computational cost of large-scale problems has been significantly reduced, so now is a very good time for application of layout optimization techniques to be investigated.

(a) (b)

Figure 1.1: Examples of tall buildings with exoskeleton structure: (a) Hearst Tower, New York (Alsandro 2006); (b) John Hancock Building, Chicago (Jovianeye 2011).

1.2 Objectives

Previously layout truss optimization is not used by people to design buildings. This is mainly because transforming a real design problem into a layout optimization problem requires knowledge of building design, optimization theory and numerical algorithm. Consequently, this transformation process is difficult to be carried out for design engineers only or optimization

researchers only. Therefore, this thesis aims at bridging the gap between engineers and researchers through using layout optimization in building bracing design problems. Efforts will be made in four main aspects as following:

- Identify the important influencing factors of real design problems and find ways to involving them into a layout optimization problem.
- Adjust the layout optimization formulation to make it more suitable for the bracing design cases.
- Use the optimization tool in conceptual design stage of bracing design cases to identify simple and efficient design solutions.
- Carry out investigations on the optimized structures to obtain simple principles that lead to optimized structures.

1.3 Structure of the thesis

This thesis contains nine core chapters as follows.

- Chapter 2: Previous studies that are related to this thesis are reviewed in this chapter. This chapter contains five main parts: (1) mathematical programming, (2) the rigid plastic design approach, (3) analytical and numerical structural optimization approaches, (4) transmissible loads and their implementations in numerical optimization, and (5) optimization of tall building bracing structures. The former two cover fundamental knowledge of layout optimization, and the latter three contain information about previous studies that are related to this thesis.
- Chapter 3: For building bracing design, the numerical techniques that are used in this thesis are layout optimization, geometry optimization, and transmissible loads. The former two are well-developed techniques. However, currently there are two means of applying transmissible loads (i.e. the migrating load approach and the rigid bar approach), and it has been identified in a previous study that these two approaches may produce different solutions in the same cases. Therefore, before undertaking a case study on bracing optimization, the

difference in the formulations of these two approaches is investigated in this chapter through mathematical and numerical methods.

- Chapter 4: In this chapter, the column-beam frame is treated as a pre-existing column-beam frame in the design of bracing structures, and three different cases are studied: (1) Tension-only bracing, (2) Connection only at corner bracing, and (3) Optimal bracing with no additional constraints.

- Chapter 5: The assumptions for Chapter 4 are suitable for bracing structure design cases with a pre-defined column-beam frame. However, there are situations where column-beam frames are designed simultaneously with bracing elements. Therefore, the assumptions used in Chapter 4 are removed in this chapter, and a holistic design with multiple load cases is carried out. The efficiency of optimized results is compared with standard bracing structures.

- Chapter 6: Chapters 4 and 5 cover bracing optimization in different scenarios. However, although it was mentioned previously that wind load is naturally a kind of transmissible load, in these chapters, the external building shapes are potentially fixed and the transmissible loads are not significantly involved. Therefore, in this chapter, the rigid bar transmissible load approach is used with assumptions of pre-existing beams, and the aim is to simultaneously identify the bracing structure and the external building shape during the optimization. Under this setting, both 2D and 3D optimization cases are studied. Efficient and simple optimization results are identified for different scenarios.

- Chapter 8 discusses various issues relevant to the current research and a new approach for the optimization of members which can carry both axial forces and bending actions. Numerical examples are considered to illustrate the concepts involved.

- Chapter 9 presents the conclusions of the thesis.

- Chapter 10 presents several recommendations for future work.

Chapter 2

Literature review

The main problem of structural optimization is to find structures that satisfies certain conditions (e.g. boundary condition, equilibrium condition et al.) and are optimized in certain pre-defined proprieties (e.g. minimized in volume or maximized in stiffness et al.). To solve this problem, many different optimization methods have been developed in previous studies, such as discrete layout optimization approach (Dorn et al. 1964), continuum topology optimization approach (Bendsøe & Kikuchi 1988), evolutionary approach (Xie & Steven 1993) and genetic algorithm (Kane & Schoenauer 1996). The latter two are both none-gradient based approach and their disadvantage in solving large-scale problem have been pointed out in Sigmund (2011). Hence they are not used in this thesis. For the former two gradient based approach, despite the formulations themselves are entirely different, they are classified into a same kind of mathematical problem, which is mathematical programming. As stated in Chapter 1.2, in this thesis the problem formulations will be adjusted to be suitable for solving building optimization problem. Therefore, the relevant knowledge about mathematical programming is firstly reviewed in Sections 2.1 to 2.3.

Before all the numerical approaches, the underpinning theory of structural optimization area was identified in the early 19th century by Michell (1904). In this paper, Michell obtained an optimality criteria which can be used to judge the optimality of an existing structure. This criteria is important but the difficulty in solving a structural optimization problem with the proposed analytical approach is extremely high. Consequently, the numerical approaches mentioned in last paragraph were developed to identify the optimized structures. Since the aim of analytical and numerical approach is the same, optimality theory can be used to improve the efficiency

of numerical algorithm (Gilbert & Tyas 2003) or to prove the optimality of identified structure (Darwich et al. 2010). Therefore, this part of studies are reviewed secondly in Sections 2.4 to 2.8.

Although structure optimization research have been existed for over a century, current building conceptual design is still mainly based on the intuition of engineers or architects. For example, in the early design stage of the 122 Leadenhall Street building, the proposed layouts had simply started from aesthetic considerations, and included no structural evaluation (Baldock 2007). Consequently, this approach may lead to design difficulty in subsequent stages, or eventually an inefficient design. Therefore, optimization techniques can be used to search for a design that considers both beauty and economy. Some principles, identified from structural optimization research, can provide guidance for efficient design, and are very useful for the early design stage. Hence, many studies have focussed on these topics. These studies are reviewed in the final part of this chapter, which is Section 2.9.

2.1 Mathematical programming

Mathematical programming is a process of finding the optimal solution for a given set of variables and constraints. Usually, a mathematical programming problem is formulated as:

$$\begin{aligned}
&\text{maximize} && f(\mathbf{x}) && && \text{(2.1a)}\\
&\text{subject to} && h_i(\mathbf{x}) = 0, && i = 1, 2, \ldots, l && \text{(2.1b)}\\
& && g_j(\mathbf{x}) \leq 0, && j = 1, 2, \ldots, m, && \text{(2.1c)}\\
& && \mathbf{x} \in \mathbf{X} && && \text{(2.1d)}
\end{aligned}$$

where $\mathbf{x}$ is a vector of unknown *variables*; $f(\mathbf{x})$ is the *objective function*, and in this problem, the objective is to find values for $\mathbf{x}$ so that $f(\mathbf{x})$ can be maximum; (2.1b), (2.1c) and (2.1d) are the so-called *constraints* of this problem which means that for the values of $\mathbf{x}$, these conditions must not be violated. Additionally, (2.1b), (2.1c) and (2.1d) are usually called, respectively, equality constraints, inequality constraints, and bounds on the variables.

For different types of mathematical programming problems, there exists different kinds of optimal

solutions. As shown in Fig. 2.1, if the identified solution is an optimal within its neighbouring region, then it is a *local optimal*. Furthermore, if the solution is the optimal result in the whole search region, then the solution is a *global optimal*. From the definition, it is clear that a global optimal solution must also be a local optimal solution, but a local optimal solution is not necessarily a global optimal solution.

The global and the local optimal are very important concepts in mathematical optimization. If the final solution is not a global optimum, but only a local optimal solution, this solution may be misleading because some better solutions must exist somewhere in the search region, but are not identified.

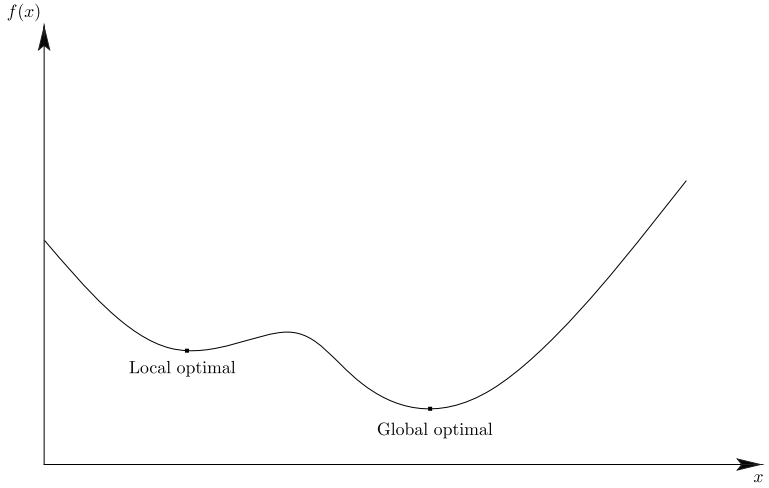

Figure 2.1: Local and Global optimal

2.1.1 Convex and concave optimization

Regarding the global and local optimal property, the convexity of a mathematical program is crucial, since in a convex optimization problem, identified optimal solutions are guaranteed to be global optimal (Bertsekas et al. 2003). To demonstrate the convexity of an optimization problem, the definition of a convex set must first be introduced:

For any two arbitrary points A and B within a set S, if all the points on line segment AB are also within S, then set S is a convex set (e.g. Fig. 2.2a). Otherwise, S is a concave set (e.g. Fig. 2.2b).

Based on this definition, convex and concave constraints can be further defined as the constraints that represent, respectively, convex and concave sets. Figures 2.2c and 2.2d show examples of convex and concave constraints. Finally, with the definition of convex and concave constraint,

a convex programming problem is defined as a mathematical program where every constraints within it are convex and the set represented by the objective function is also convex (i.e. $f(\mathbf{x}) \geq 0$ is convex for minimization problem or $f(\mathbf{x}) \leq 0$ is convex for maximization problem). It is worth noting that the a equal constraint is convex only if it is a linear constraint. This is because $h_i(\mathbf{x}) = 0$ can be transformed to $h_i(\mathbf{x}) \leq 0$ and $-h_i(\mathbf{x}) \leq 0$. If $h_i(\mathbf{x})$ is a non-linear convex constraint, then $-h_i(\mathbf{x})$ must be a non-linear concave constraint. Hence, convex equal constraints $h_i(\mathbf{x})$ must be linear.

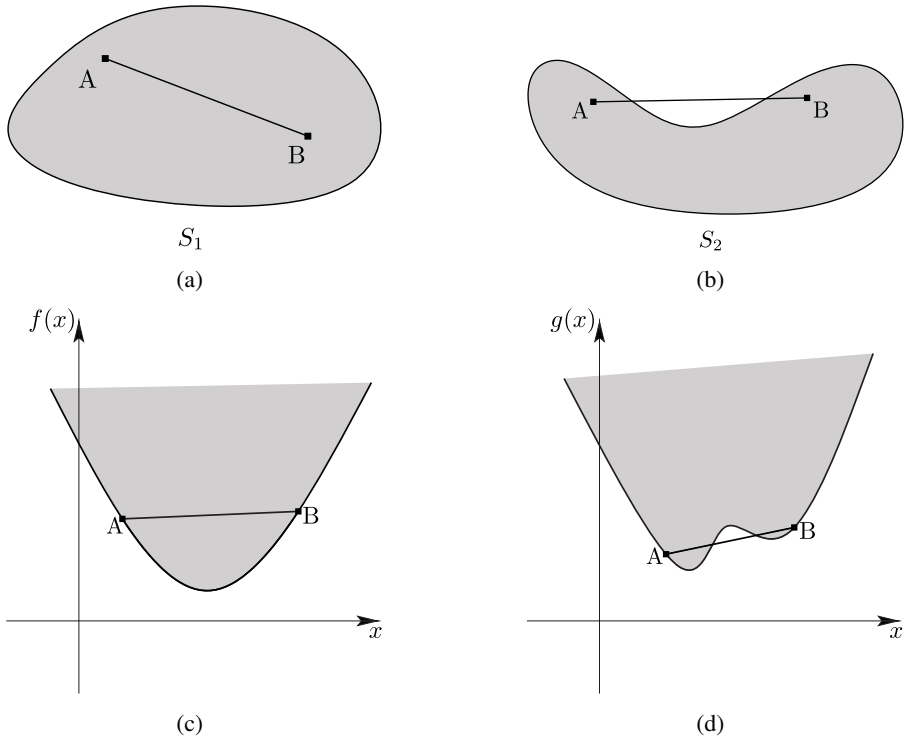

Figure 2.2: Examples of convex and concave sets and functions: (a) Convex set S_1; (b) Concave set S_2; (c) Convex constraint $f(x) \geq 0$; (d) Concave function $g(x) \geq 0$

Convexity is significantly important since it determines the reliability of a solution of a mathematical program. For this reason, convex formulations are usually preferred, when possible. Moreover, if an optimization problem can be formulated as a linear programming problem, then not only can a global optimal solution be guaranteed, but also the computational cost required to solve this problem is relatively small. Details about linear programming are presented in the next section.

2.2 Linear programming

The optimization problem shown in (2.1) is a linear programming problem when all the functions applied to the variable vector $\mathbf{x}$ are linear. Compared with a non-linear programming problem, a linear programming problem can be solved much more quickly. In addition, since linear programming problems are a special subset of convex programming problems, the solutions from linear programming problems are also guaranteed to be global optimal solutions.

2.2.1 Approaches to solve linear programming problems

Currently, three widely used approaches are available that can be used to solve a linear programming problem. The first one is the graphical approach, which could be applied to a linear programming problem with two variables. This approach is typically used in introductions to linear programming principles rather than real research investigations. Fig. 2.3 shows an example of applying the graphical approach to a linear programming problem (2.2). The second approach is the *simplex* method (Dantzig 1949), which is a mathematical extension of the graphical approach; it is suitable for problems with any number of variables. The simplex method solves a linear program through a number of steps of linear matrix transformation, which gradually moves the solution along the boundary of the search region towards the final optimal value. The last method is the *interior point method* (Karmarkar 1984, Gill et al. 1986, Wright 2004). In contrast to the simplex method, this method moves the objective function value across an interior line of the search region. In current state-of-the-art linear programming solvers, interior point solvers are more efficient than simplex solvers, especially for large-scale problems (Wright 2004). Therefore, in this study, interior point solvers are used to solve the optimization problems which arise.

$$\begin{aligned} \text{maximize} \quad & x_1 + 2x_2 && \text{(2.2a)} \\ \text{subject to} \quad & x_1 + x_2 \leq 5 && \text{(2.2b)} \\ & x_1 - 3x_2 \leq 0 && \text{(2.2c)} \\ & x_1 \geq 0, x_2 \geq 0 && \text{(2.2d)} \end{aligned}$$

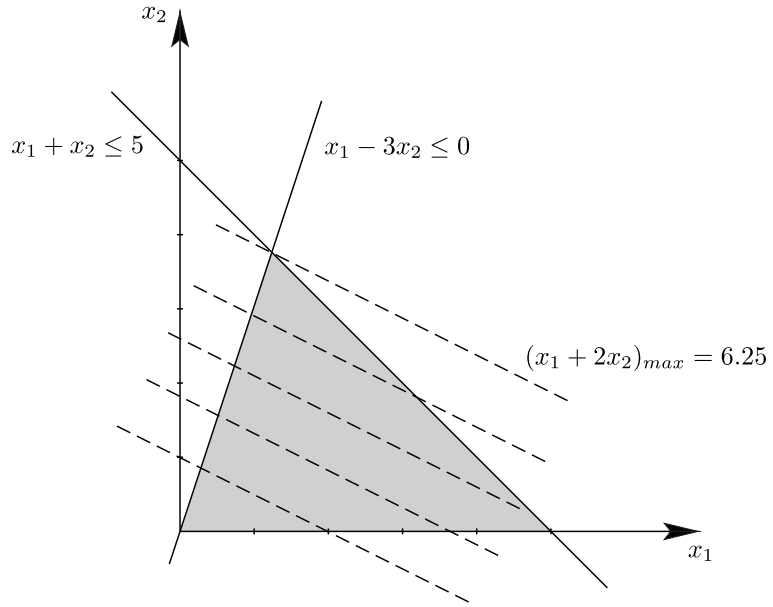

Figure 2.3: Example of using the graphical approach to solve a linear program (2.2), where grey area is the search region, solid lines represent the constraints and dashed lines represent the contour lines of the objective function.

2.2.2 Duality theory

Duality theory (Vanderbei 2001, Nocedal et al. 2006) is an important part of convex programming theory, especially for linear programming. Every linear programming problem has its dual-form formulation. For this pair of formulations, one feasible solution (e.g. those solutions that satisfy the constraints but are not necessarily optimal) of one of the problems could lead to a bound on the other problem. Therefore, more information about the original problem (the so-called primal problem) can be obtained from the investigation of its dual problem.

$$\text{maximize} \quad \sum_{j=1}^{n} c_j x_j \tag{2.3a}$$

$$\text{subject to} \quad \sum_{j=1}^{n} a_{ij} x_j \leq b_i \quad i = 1, 2, ..., m \tag{2.3b}$$

$$x_j \geq 0 \quad j = 1, 2, ..., n \tag{2.3c}$$

The dual problem of a general linear program as shown in Formulation (2.3) could be obtained through the following steps. First, take Constraint (2.3b) and multiply each side of the inequality

expression with a variable $y_i \geq 0$:

$$\sum_{j=1}^{n} a_{ij} x_j y_i \leq b_i y_i \tag{2.4}$$

Secondly, assume that any y_i satisfies Condition (2.5); thus the relation shown in (2.6) could be obtained based on Condition (2.5).

$$\sum_{i=1}^{m} a_{ij} y_i \geq c_j \tag{2.5}$$

$$\sum_{i=1}^{m} b_i y_i \geq \sum_{i=1}^{m} \sum_{j=1}^{n} a_{ij} x_j y_i \geq \sum_{j=1}^{n} c_j x_j \tag{2.6}$$

From the above derivation, it can be observed that, for any $\mathbf{y} = \{y_1, y_2, ..., y_m\}$ that satisfies Condition (2.5) and $y_i \geq 0$ could lead to a upper boundary $b_j y_j$ for the primal problem. Therefore, the dual problem of (2.3) is:

$$\text{minimize} \quad \sum_{i=1}^{m} b_i y_i \tag{2.7a}$$

$$\text{subject to} \quad \sum_{i=1}^{m} a_{ij} y_i \geq c_j \quad j = 1, 2, ..., n \tag{2.7b}$$

$$y_i \geq 0 \quad i = 1, 2, ..., m \tag{2.7c}$$

From (2.6), it is clear that there is always a gap between the value of the objective functions of the primal and the dual problem if the solution is only feasible but not optimal. This gap will be shortened as the solution approaches towards the optimal solution, and in the end when the optimal solution is identified, this gap will be eliminated and the objective function values of the primal and dual problems will be identical.

2.3 Non-linear programming

Compared with an equally sized linear programming problem, a non-linear programming problem usually involves higher computational cost to obtain a solution, and whether a global optimal solution can be found still depends on the convexity of this problem. Nevertheless, research on non-linear programming has always been an area of active interest since non-linearity

is an inevitable factor in complex and realistic cases. For such non-linear programming studies, derivative-based optimality criteria theory is a basic concept for algorithm development. Accordingly, details of derivative-based optimality criteria theory are described in the following sections.

2.3.1 Optimality criteria for problems with equal constraints

A non-linear problem with only equality constraints can usually be formulated as:

(for sake of simplicity, demonstration in Sections 2.3.1 and 2.3.2 is based on formulation with only two variables)

$$\text{maximize} \qquad f(x,y) \tag{2.8a}$$

$$\text{subject to} \qquad h(x,y) = c, \quad i = 1,2,\ldots,l \tag{2.8b}$$

Assume that $f(x,y)$ and $h(x,y)$ both have continuous first partial derivatives, then (2.8) could be transformed to this *Lagrange function*:

$$\mathcal{L}(x,y,\lambda) = f(x,y) - \lambda \cdot (h(x,y) - c) \tag{2.9}$$

where λ is a new variable introduced in a Lagrange function called *Lagrange multiplier*.

Based on (2.9), the optimality condition of point $(x^\star, y^\star, \lambda^\star)$ is given by:

$$\nabla(\mathcal{L}(x,y,\lambda)) = 0 \tag{2.10}$$

Fig. 2.4 presents a graphical demonstration of (2.10). It can be seen that if a point (x_1, y_1) is an intersection point between the contour line of $f(x,y)$ and the trajectory of $h(x,y) = c$, then there can be found a point (x_2, y_2) which neighbours (x_1, y_1) that could provide a more favourable solution $f(x_2, y_2)$. Hence, at the optimal point $(x^\star, y^\star)$, $f(x,y)$ and $h(x,y) = c$ must be tangential, which leads to the equation (2.10).

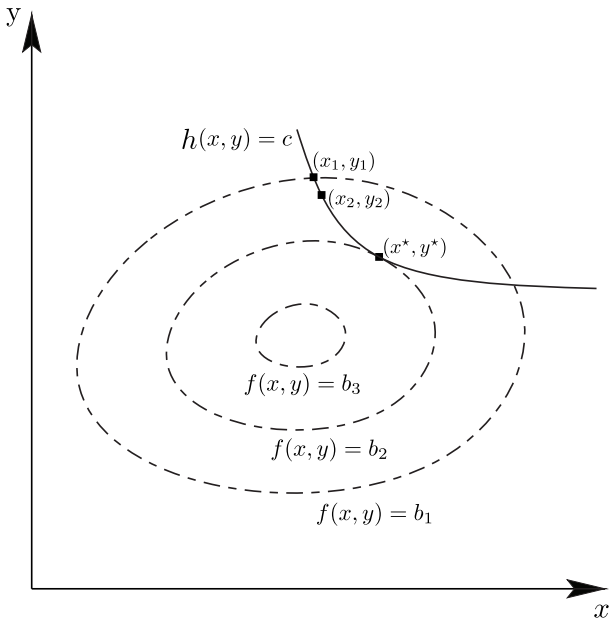

Figure 2.4: Optimality criteria of a non-linear mathematical program with equal constraints, where dashed lines are contour lines of objective function $f(x,y)$, and the solid line represents equal constraint $h(x,y) = c$.

2.3.2 Optimality criteria for problems with unequal constraints

The above optimality criteria only applies to non-linear problems with equality constraints (i.e. (2.8b)). For problems with inequaliity constraints, the optimality criteria are slightly different. For the sake of completeness, this will also be demonstrated through an example.

For a non-linear programming problem with inequaliity constraints, the formulation is:

$$\text{maximize} \qquad f(x,y) \tag{2.11a}$$

$$\text{subject to} \qquad g(x,y) \leq c, \quad i = 1,2,\ldots,l \tag{2.11b}$$

The corresponding Lagrange function is:

$$\mathcal{L}(x,y,\mu) = f(x,y) - \mu \cdot (g(x,y) - c) \tag{2.12}$$

And the optimality criteria of (2.12) are:

$$\mu \geq 0 \tag{2.13a}$$

$$\nabla(\mathcal{L}(x, y, \mu)) = 0 \tag{2.13b}$$

$$\mu \cdot (g(x, y) - c) = 0 \tag{2.13c}$$

Condition (2.13) is a widely used optimality criterion called the Karush-Kuhn-Tuker condition (Nocedal et al. 2006). In this condition, (2.13a) is the dual transformation result of (2.11b). (2.13b) is the same as (2.10), which represents the gradient relation between $f(x, y)$ and $g(x, y)$ at the optimal point. To understand (2.13c), we can usefully consider the optimization problem in two situations. In the first situation, as shown in Fig. 2.5a, it is assumed that the maximum point for $f_{max}(x, y)$ is located in the region of $g(x, y) \leq c$. In this situation, it is clear that the optimal result of (2.11) is effectively $f_{max}(x, y)$, which means that the constraint $g(x, y) \leq c$ is inactive in problem (2.11) (i.e. the removal of $g(x, y) \leq c$ will not affect the optimal solution of (2.11)) and the optimal solution only requires $\nabla(f(x, y)) = 0$. Therefore, in this situation $\mu = 0$. In the second situation shown in Fig. 2.5b where $f_{max}(x, y)$ is located out of the constrained region of $g(x, y) \leq c$, the optimal point must be located at the tangent point between the contour line of $f(x, y)$ and the boundary of $g(x, y) \leq c$. Therefore, in this situation, $g(x, y) = c$. From these findings it can be shown that $\mu \cdot (g(x, y) - c) = 0$, which is the condition shown in (2.13c).

2.4 Elastic and plastic design

In addition to knowledge of mathematical programming, the basic assumptions used in engineering design are also a crucial component of structural optimization. One of the most important assumptions is related to the strain-stress relation of the material. A demonstration of this starts with the typical steel stress/strain curve shown in Fig. 2.6a (Rees 2006). From this graph, it can be seen that the steel goes through an elastic deformation phase (i.e. where stress and strain have a linear relationship) and a plastic deformation phase (i.e. where stress and strain have a non-linear relationship) before it reaches the rupture point. Furthermore, the plastic deformation phase can be divided into three stages, which are the perfect plastic stage (i.e. stress is maintained at the same value as strain increases), the strain-hardening stage (i.e. stress increases as strain increases),

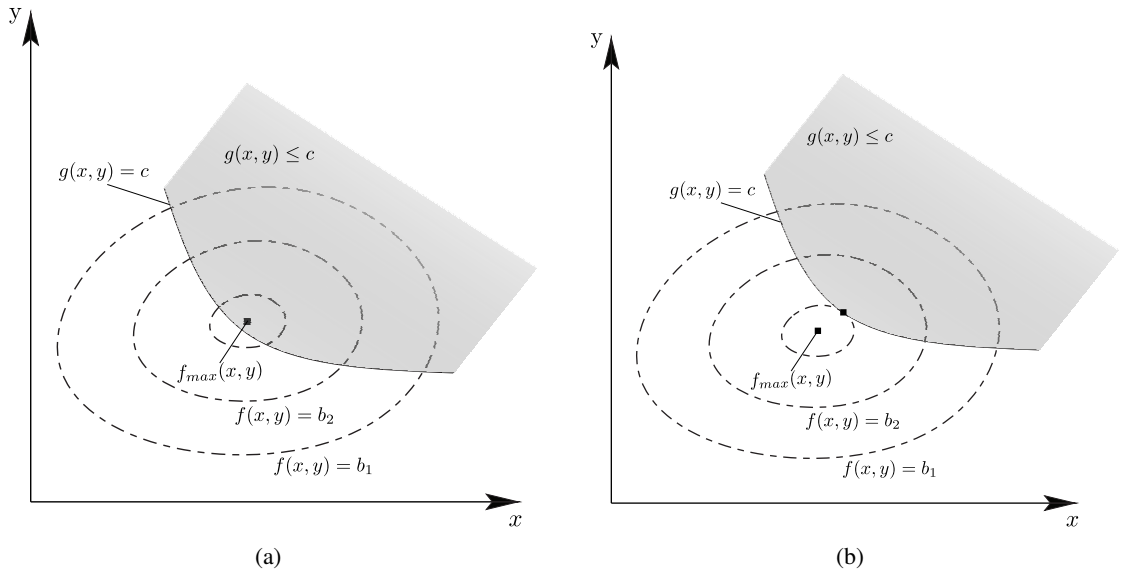

Figure 2.5: Two situations of a non-linear mathematical program with inequality constraints: (a) Optimal point for $f_{max}(x, y)$ locates in the region of $g(x, y) \leq c$; (b) Optimal point for $f_{max}(x, y)$ locates outside of the region of $g(x, y) \leq c$; dashed lines are contour lines of objective function $f(x, y)$, and the grey area represents unequal constraint $g(x, y) \leq c$.

and necking stage (i.e. stress decreases as strain increases). Therefore, it is clear that this typical stress/strain curve is a non-linear and non-convex function, which causes computational difficulty for design or research work. Consequently, one usually assumes that the material can only deform in the elastic phase, which leads to the currently widely used *elastic* design approach. In elastic design, as long as one position of the entire structure reaches the yielding stress, then the loading capacity of this structure is considered to be achieved. Nevertheless, from Fig. 2.6a it is clear that elastic deformation only takes up a small part of steel's strain capacity. Hence, the assumption of elastic design will lead to a waste of material. Therefore, a rigid-plastic model has been developed to make use of material's plastic capacity and also simplify the calculation process. In the rigid-plastic model, it is assumed that the relation between stress and strain is always plastic-perfect as shown in Fig. 2.6b. Although in reality this kind of material does not exist, for ductile material with plastic deformation much larger than elastic deformation, this model is still applicable (Nielsen & Hoang 2011).

2.4.1 Upper and lower boundary theory

In design with the rigid-plastic model, a structure is considered to collapse when a mechanism is formed, identified using upper or lower bound theory. To demonstrate this, three basic conditions

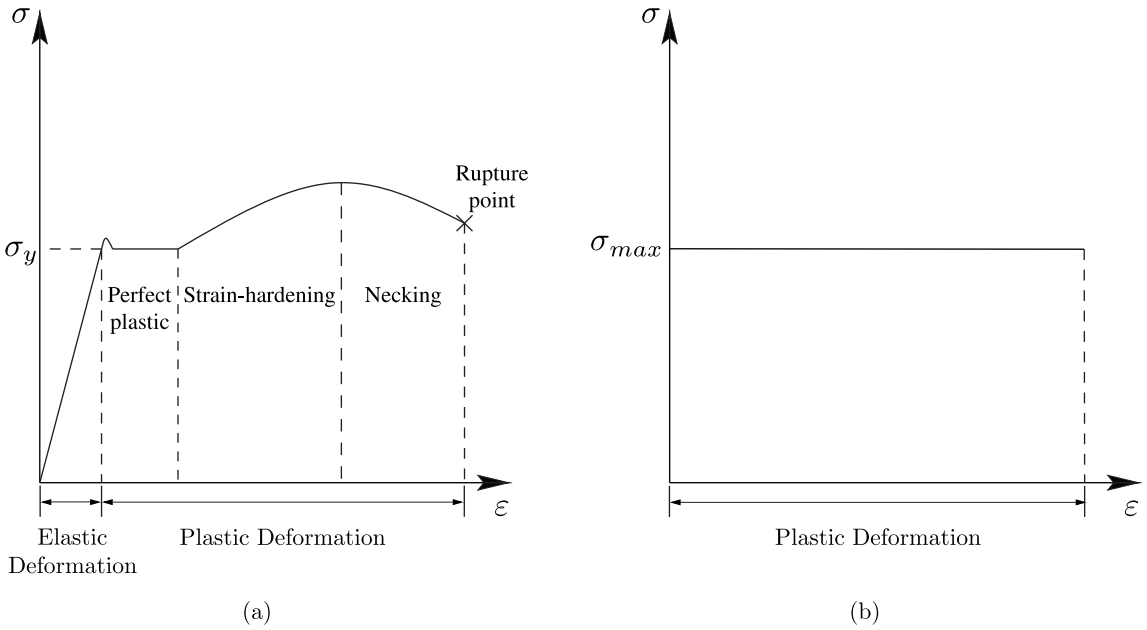

Figure 2.6: Steel stress/strain curve: (a) curve for a realistic scenario; (b) curve with assumptions made in plastic rigid design.

must first be introduced:

1) *Mechanism condition*: At the point of collapse, sufficient plastic hinges (at positions where the maximum material capacities are reached) form to create a mechanism.

2) *Equilibrium condition*: At the point of collapse, the internal bending moments are just in equilibrium with the applied loads.

3) *Yield condition*: At the point of collapse, stresses at all positions within the structure are smaller than or equal to the specified maximum stress (e.g. usually yield stress).

With these conditions, it is defined that for a specified structure, a loading that leads to satisfaction of *yield* and *equilibrium* conditions will be a lower bound on the plastic collapse load; a loading that leads to satisfaction of *mechanism* and *equilibrium* conditions will be an upper bound on the plastic collapse load; and a loading that leads the satisfaction of *mechanism*, *equilibrium*, and *yield* conditions will equal the exact plastic collapse load.

2.4.2 Plastic vs. elastic beam design example

The efficiency of the plastic design method can be demonstrated through a simple beam example (e.g. Fig. 2.7), which involves a beam having fixed supports at the two ends and takes a downwards

uniform load across the span. Fig. 2.7b shows the moment graph for elastic design where the moments at the support position are twice the moment at the middle position. Consequently, the maximum stress within the cross section located at the middle span position is only half of the yield stress. On the other hand, in plastic design (i.e. Fig. 2.7c), this beam collapses when three hinges form at the right end, midspan, and left end position. This collapse condition redistributes the moment such that the moments at the two ends equal the moment at midspan. Hence, the maximum stresses located at midspan and the two end positions are identical, which leads to a more efficient design to take the uniform load.

From the above demonstration, it can be seen that plastic design could lead to more efficient solutions than the elastic design approach. Considering that the purpose of this study is structural optimization, plastic design is accordingly used as the main design approach in this study.

2.5 Mathematical theories of optimal structures

2.5.1 Michell's optimality criterion

With the knowledge of mathematical programming and plastic design, we can now look at the fundamental mathematical theory of structural layout optimization. Michell (1904) first studied the least material truss problem and derived the criteria of the optimal truss topology based on the mathematical theory of Maxwell (1864). The specific problem studied by Michell (1904) is to find the optimal layout of the least material truss with stress constraints and a single load condition, and the optimality criterion is:

"A frame therefore attains the limit of economy of material possible in any frame-structure under the same applied forces, if the space occupied by it can be subjected to an appropriate small deformation, such that the strains in all the bars of the frame are increased by equal fractions of their length, not less than the fractional change of length of any element of the space."

This optimality criterion underpins the topology optimization area, and Michell has demonstrated its implications through several classical cases. Fig. 2.8 shows one of the examples presented by Michell, the cantilever problem with a single load and fixed supports around a circular boundary. In Fig. 2.8, it can be observed that tension and compression members intersect each other at 90°. This is a general member arrangement that appears in many other Michell structures (e.g.

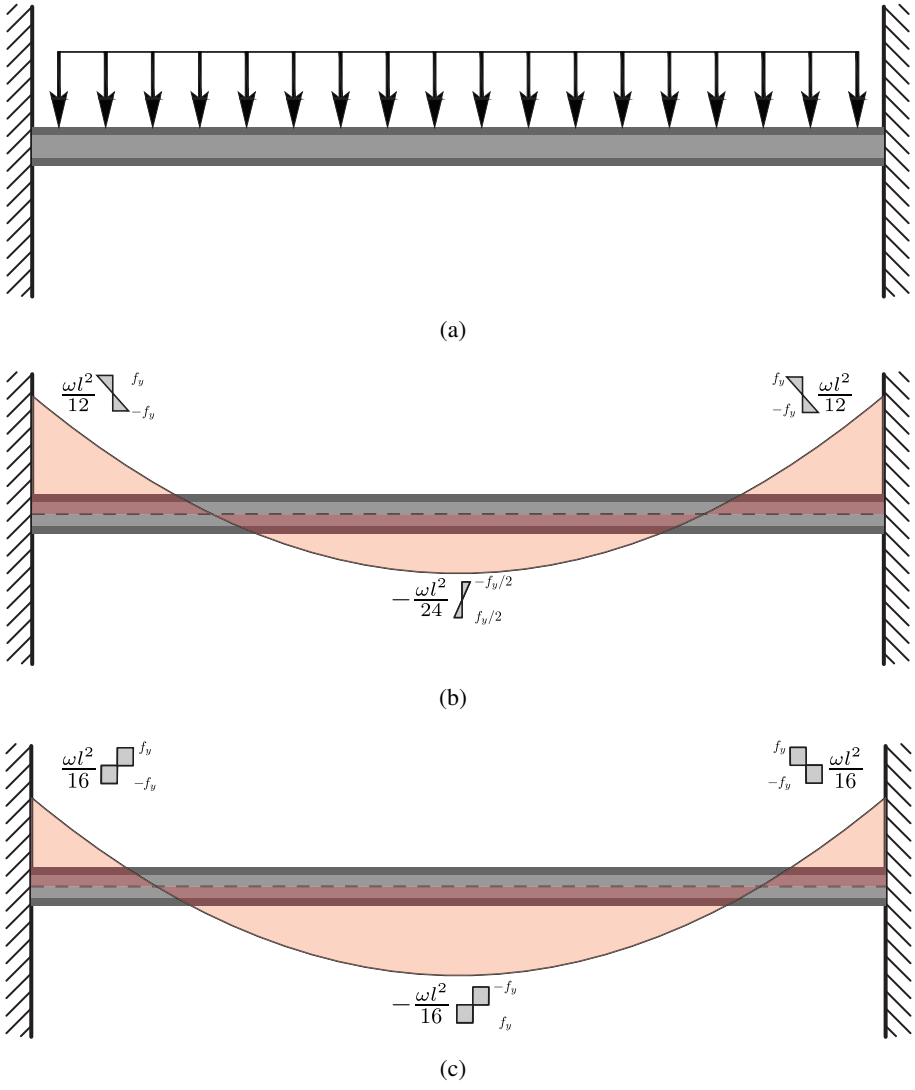

Figure 2.7: Elastic and plastic design example: (a) An I-section beam that takes uniform load across the span and has fixed supports at two ends; (b) Elastic design: moment distribution across the span and stress distribution at the middle and two ends; (c) Plastic design: moment distribution across the span and stress distribution at the middle and ends; where ω, l and f_y represent loading per unit length, total beam length and yield stress.

those structures that satisfy the optimality criterion). Similar to this member arrangement, Michell listed several other arrangements based on optimality criterion. By knowing these arrangements, one can derive the optimal topology of some cases as Michell did. However, this approach is rather difficult to apply to a case with arbitrary loading and support positions. Therefore, whilst Michell's analytical approach provides a strong foundation for this field, it is rarely helpful in specific structural design applications.

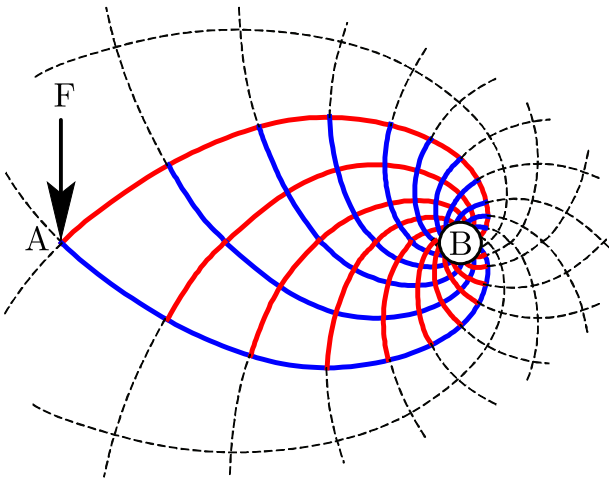

Figure 2.8: Michell cantilever with point load A and pin supports around circle B, where red and blue lines respectively represent bars in tension and compression.

2.5.2 Three regions in Michell structures

The general member arrangement that appear in Michell structures were extensively studied in Prager & Rozvany (1977), who derived that any point within a Michell structure must be located in one of the following three types of regions: (1) structurally rich forms in which (generally orthogonal) truss bars are strained to their respective limits in tension and compression; (ii) similarly rich forms but where all bars experience stresses in only one direction; and (iii) simpler flexureless line or surface structures. These have been defined respectively as: (i) T-type, (ii) S-type, and (iii) R-type structures. T-type region contains adjoint strains in two orthogonal directions. Thus optimized structure in this region usually have tension and compression members intersecting with each other at 90° (e.g. Fig. 2.8 and the fan structure in Fig. 2.9b). S-type region contains adjoint strains of only one sign in arbitrary directions. One example of S-type is the surface of a balloon, where every position is in tension. R-type region contains adjoint strain of one sign in one direction, thus optimized structures in this region usually are single or parallel bars

all in tension or all in compression (e.g. Fig. 2.9b). Additionally, based on the strain direction, S- and R-type structures can further be classified into R^+, R^-, S^+, S^- type structures (e.g. Fig. 2.9a).

Following on this theory, many studies have been performed using the analytical approach to identify the exact volume and member arrangement of Michell structures for different specific problems (Chan 1960, Rozvany 1998, Dewhurst 2001, Lewiński & Rozvany 2007, 2008, Graczykowski & Lewiński 2010). These are very useful to verify the correctness of a newly developed numerical approach.

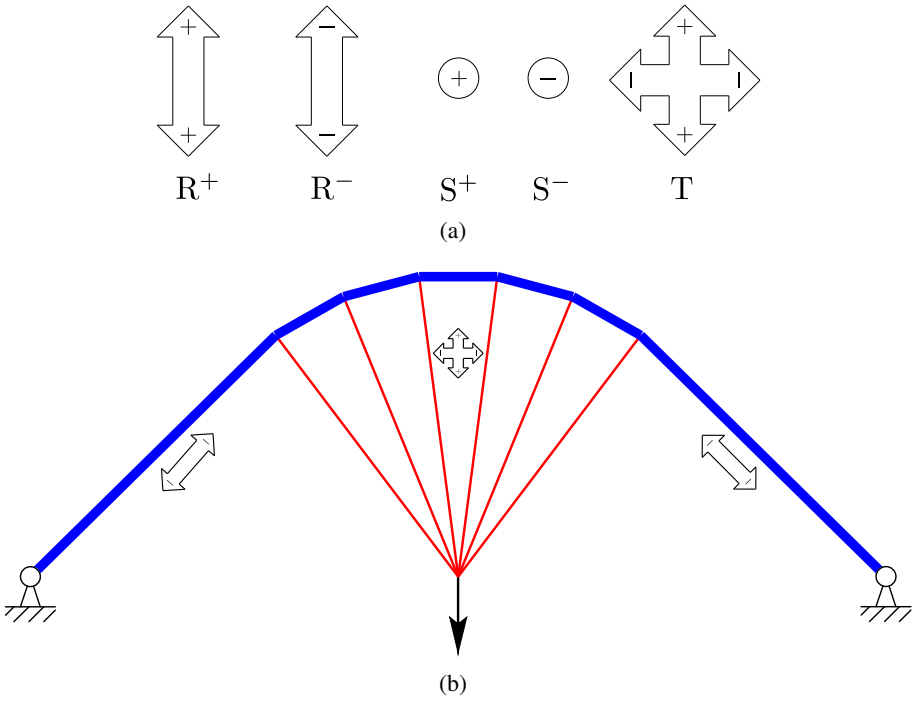

Figure 2.9: Types of optimal regions in Michell trusses: (a) symbols of five types of region, where + and − represent tensile and compressive strain respectively; (b) a Michell structure with T-type structures in the middle region and R^--type structures at the two sides; red and blue lines respectively represent bars in tension and compression.

2.5.3 An example of interactive collaboration between analytical and numerical approach: optimal topology to withstand uniform load between pin supports

Among all the classical topology optimization cases, the optimal topology to carry uniform gravity loads between pin supports is a problem that has been studied by engineers for hundreds of years. The widely accepted solution is a funicular parabola structure that uses only compressive internal force to resist the external applied loads (only for cases with supports located at he bottom

corners of the design domain). The theory behind this solution is the fundamental concept of arch bridges and other arch-shaped structural components. However, recently Darwich et al. (2010) investigated this problem using a numerical optimization approach and identified that the optimal solution is Fig. 2.10, which contains a rich structure that emerges from a given support position and ends at the one-third span position that connects a funicular structure in the middle part. Since surprisingly this solution conflicts with the long-held and widely accepted solution, the analytical approach is used in Tyas et al. (2010) to prove the optimality of the structure. It has been found that, in situations with $\sigma_c/\sigma_t \geq 3$, the parabola funicular structure is the optimal solution, where σ_c and σ_t represent, respectively, maximum compression and tension stresses. Nevertheless, in more the general situation with $\sigma_c/\sigma_t = 1$, Fig. 2.10 is the optimal solution. Although the volume difference between these two solutions is not significant, this example shows that the topology optimization technique could lead to solutions that could never be obtained using only engineering intuition.

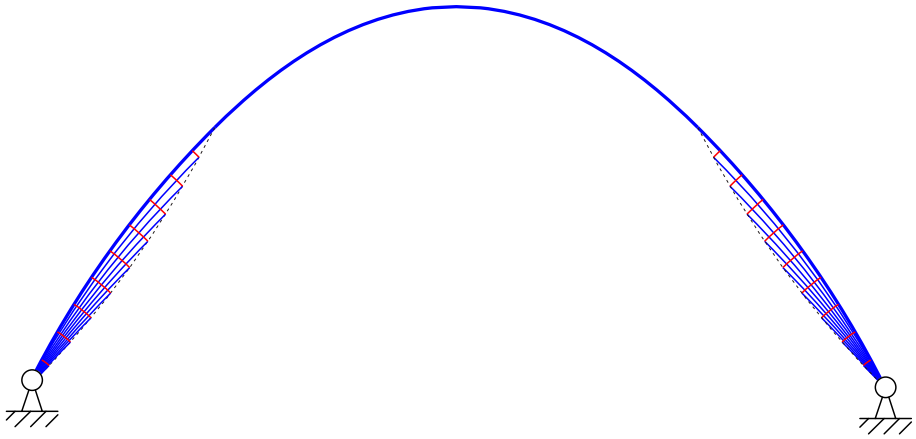

Figure 2.10: Optimal topology for uniform gravity load between pin supports problem, where red and blue lines respectively represent bars in tension and compression

2.6 Discrete layout optimization

2.6.1 Ground structure approach

Although analytical approaches could lead to exact optimal solutions, the significant effort required makes these methods unsuitable for solving general problems. Therefore, engineers have been using numerical methods to search for optimized structures. An automatic layout optimization scheme was first developed by Dorn et al. (1964). Prior to their work, the main

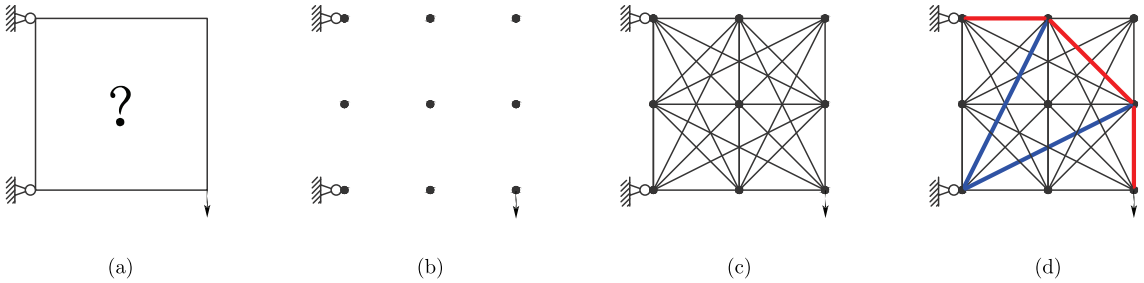

Figure 2.11: Ground structure approach: (a) initial design domain, support and loading conditions; (b) node discretization; (c) create all possible interconnections of discrete nodes (build ground structure); (d) use linear programming to select the optimal subset structure; red and blue lines respectively represent bars in tension and compression.

focus of structural optimization research was on size optimization (determining the size of already present members). Pearson (1958) found that some members would disappear when undertaking size optimization. Based on this finding, Dorn et al. (1964) proposed a ground structure-based approach in which each node was connected to every other node and the optimal subset of members was identified via optimization, with most members having zero area. Through this approach, layout optimization was transformed into a member sizing problem, which can be solved by LP.

As Fig. 2.11 shows, this approach can be divided into three steps. Firstly, the design domain is discretized into a grid of nodes. Secondly, all possible interconnections of discrete nodes are created (build ground structure). Thirdly, the optimal subset structure is selected from the ground structure using linear programming tool. The linear programming formulation for m bars and n nodes is stated as follows:

$$\begin{aligned} &\min && V = \mathbf{q}^T\mathbf{c} \\ &\textit{subject to} && \mathbf{Bq} = \mathbf{f} \\ &&& q_i^+, q_i^- \geq 0,\ i = 1, ..., m \end{aligned} \tag{2.14}$$

where V represents the total structure volume, $\mathbf{q}^T = \{q_1^+, q_1^-, ..., q_m^+, q_m^-\}$, $\mathbf{c}^T = \{l_1/\sigma_1^+, l_1/\sigma_1^-, ..., l_1/\sigma_m^+, l_1/\sigma_m^-\}$, $\mathbf{B}$ is a $2n \times 2m$ equilibrium matrix, and $\mathbf{f} = \{f_1^x, f_1^y, f_2^x, f_2^y, ..., f_n^x, f_n^y\}$; and $l_i, q_i^+, q_i^-, \sigma_i^+, \sigma_i^-$ represent, respectively, the length, tensile member force, compressive member force, tensile stress capacity and compressive stress capacity of member i. f_j^x and f_j^y represent the component of load in the x and y directions respectively for the load applied to node j.

Variables in this formulation are the axial forces of each member. By allowing the cross sectional areas to be able to become zero (or very close to zero), the optimal subset structure is selected from the ground structure via removing unnecessary members.

Despite the fact that Dorn's approach is capable of producing a similar solution to Michell's, it does not use Michell's optimality criteria theory. The central idea of the ground structure approach is to select the best solution from every possible one. Despite the efficiency of linear programming technology, the very large number of calculations required is the main limitation of the ground structure approach. The fact that the number of members increases as a function of the square of the number of nodes means that practically large 3D problems are unlikely to be solvable in the foreseeable future using the classical ground structure method.

2.6.2 Hemp's theory

Michell and Dorn pioneered, respectively, analytical and numerical approaches to structural optimization. Although these two approaches have the same goal, they were isolated from each other for many years until Hemp (1973) combined them together. Hemp applied LP duality theory to the ground structure approach formulation and obtained the following formulation:

$$\max W = \sum_{j=1}^{n} F_j u_j / \sigma\varepsilon \tag{2.15a}$$

subject to:

$$\sigma^{+}|\varepsilon_i|/\sigma + \sigma^{-}|\varepsilon_i|/\sigma \leq \varepsilon \tag{2.15b}$$

where W is the total virtual work; F_j, u_j are external force and displacement respectively of node j; ϵ_i is strain of member i; and σ and ϵ are constants of a Lagrangian multiplier.

From duality theory, it can be obtained that when the objective volume in formulation (2.14) reaches a minimum, the virtual work in formulation (2.15a) would be at its maximum. Additionally, the strain within each member must satisfy constraint (2.15b). Consider constraint (2.15b) together with Michell's optimality criterion: Hemp suggests that for those members that exist in the optimal structure, Constraint (2.16) must be satisfied, and for those members that do not exist, Constraint (2.17) must be satisfied.

$$\sigma^+|\varepsilon_i|/\sigma + \sigma^-|\varepsilon_i|/\sigma = \varepsilon \tag{2.16}$$

$$\sigma^+|\varepsilon_i|/\sigma + \sigma^-|\varepsilon_i|/\sigma < \varepsilon \tag{2.17}$$

Therefore, the optimality criteria proposed by Hemp are:

i. The structure should be capable of effectively carrying its alternative system of forces.

ii. Each member should be stressed to the limit σ^+ or σ^-.

iii. The framework allows a virtual displacement of its nodes, which produces non-negative strains in members loaded to stress σ^+, non-positive strains in members loaded to a stress σ^-, and zero strains in members not stressed to these limits.

iv. The strains of members that exist in the optimal topology satisfy Constraint (2.16).

v. The strains in all members (including those not present in the optimum structures), corresponding to the displacement of iii, satisfy Constraint (2.15b).

Hemp's work is significant because conditions iv and v above can be used to govern whether or not it is advantageous to include a given member in the optimal truss, which connects Michell's optimality criterion and Dorn's ground structure approach.

2.6.3 Member adding method

As computer technology has developed, the ground structure method has naturally lent itself to numerical implementation. However, despite the efficiency of LP approaches, even these methods become computationally intractable for large-scale problems, due to the numbers of potential members in the ground structure. With regard to this problem, Gilbert & Tyas (2003) proposed an iterative scheme called the 'member adding method', which could effectively decrease the computational cost of the classical ground structure approach. In the member adding method, a sparsely populated ground structure (e.g. a subset of the fully connected ground structure that usually contains only members connecting neighbouring nodes) is initially used, and necessary members are added in each iteration based on Hemp's optimality criteria (e.g. constraint (2.15b)). Since virtual displacements of each node could be automatically obtained when the primal problem

is solved, the strain of each potential member within the fully connected ground structure could be calculated with little computational cost. Hence, after each iteration, members that violate constraint (2.15b) could be easily picked out and added to the ground structure. Consequently, the size of the ground structure is gradually increased, and the objective function value is decreased. In the end, the iteration scheme stops when no member in the fully connected ground structure violates constraint (2.15b). Hence, the global optimality of the approach can be guaranteed.

The efficiency of the member adding method has been proved with numerical examples in Gilbert & Tyas (2003), and it has been used in many other truss optimization studies such as those by Pritchard et al. (2005), Darwich et al. (2010), Tyas et al. (2010), He & Gilbert (2016), and Smith & Gilbert (2007). From the previous studies, it could be concluded that this approach can effectively reduce the computational cost of layout optimization. Therefore, it will be used as a core method in this study.

2.6.4 Geometry optimization

With the member adding method, layout optimization can quickly produce solutions for various problems. However, it has been observed that the results are usually very complex. Due to this reason, He & Gilbert (2015) make an attempt to reduce the complexity of the solutions obtained via layout optimization by using geometry optimization as a post-processing method. In this approach, a non-linear, non-convex problem is solved to find the optimal positions of the nodes within a certain limit. Additionally, between iterations, nodes can also merge into one when two or more nodes are very close to each other. Although a non-linear optimization problem is required to be solved, this problem is started from an optimized structure that has most nodes and members in the ground structure eliminated. The computational cost is therefore relatively small. Additionally, with the optimized structure as the initial of the optimization, the results are usually more optimal than layout optimization results. From the examples in He & Gilbert (2015, 2016), He et al. (2017), it is clear that more rational structures can be identified by geometry optimization with only a slightly higher computational cost than when using only layout optimization. Therefore, this approach will also be used in this study to improve the quality of the optimized results.

2.6.5 Structural optimization with multiple load cases and the superposition approach for solving multiple load case problems

Previous sections have introduced optimization formulations for single load case problems. However, in reality, buildings usually need to take different load cases in different scenarios. Problems with multiple alternative load cases are therefore an important part of layout optimization. Hemp (1973) studied this problem and proposed the optimality criterion for a truss structure under multiple alternative load cases to be:

"that each member should be stressed to the limit σ_T or $-\sigma_C$ by at least one system of force"

which leads to the following multiple load case optimization formulation for M load cases, m members and n nodes:

$$\begin{aligned} \text{min} \quad & V = \mathbf{l^T a} \\ \text{subject to} \quad & \mathbf{B q}^\alpha = \mathbf{f}^\alpha \\ & \mathbf{a} \geq 0 \\ & a_i \geq \{q_i^+/\sigma_i^+ + q_i^-/\sigma_i^-\}^\alpha \\ & \{q_i^+\}^\alpha, \{q_i^-\}^\alpha \geq 0 \end{aligned} \tag{2.18}$$

where $\alpha = 1, 2, ..., M$ and $i = 1, 2, ..., m$; V represents total structure volume, $\mathbf{a} = \{a_1, a_2, ..., a_m\}$, $\mathbf{l} = \{l_1, l_2, ..., l_m\}$, $\mathbf{B}$ is a suitable $(2n \times 2m)$ equilibrium matrix, $\mathbf{q^T} = \{q_1^+, -q_1^-, ..., q_m^+, -q_m^-\}$, $\mathbf{f}^\alpha$ is the load case vector, where $\mathbf{f}^\alpha = \{f_1^x, f_1^y, ..., f_n^x, f_n^y\}^\alpha$; and $a_i, l_i, q_i^+, q_i^-, \sigma_i^+, \sigma_i^-$ represent, respectively, the cross section area, length, tensile force, compressive force, tensile stress capacity, and compressive stress capacity of member i and also $\{f_j^x\}^\alpha$ and $\{f_j^y\}^\alpha$ represent, respectively, the x and y direction component load applied on node j in load case α.

This formulation can be used to solve problems with arbitrary load cases. Nevertheless, in a situation with only two load cases, Hemp (1973) derived the dual formulation as:

$$\text{max} \qquad W = \sum_{a=1}^{2} W_a \tag{2.19}$$

where

$$W_a = \sum_{j=1}^{n} f_{aj} U_{aj} / \sigma\varepsilon \tag{2.20}$$

and

$$f_{1j} = (F_{1j} + F_{2j})/2, f_{2j} = (F_{1j} - F_{2j})/2 \tag{2.21}$$

This formulation indicates that the total virtual work of the optimal truss for two-load case F_1 and F_2 is equal to the sum of the virtual works of two optimal trusses for, respectively, load cases f_1 and f_2. With LP duality theory, the optimal truss for two alternative load cases F_1 and F_2 can be obtained by superimposing two optimal trusses for, respectively, single-component load cases f_1 and f_2.

Following Hemp's work, the superposition approach has been extensively studied by Rozvany & Hill (1978), and it is found that, when some special conditions are satisfied, the superposition approach can be applied to problems with more than 2 load cases, which can be used to reduce the computational cost of some special cases.

2.7 Continuum topology optimization

Compared with discrete layout optimization, more studies have focussed on finite element-based continuum topology optimization. This kind of optimization approach started with the homogenisation method (Bendsøe & Kikuchi 1988). In this approach, the material distribution in the design domain is represented by a finite number of elements, and each of them contains infinitely many microscopic voids. The optimization target is to seek the porosity of the elements under some user-defined optimality criteria. Unlike the philosophy underlying the ground structure approach, this approach inspired researchers with the idea of looking at topology optimization as a process of placing material in the most needed places. Due to the popularity of the finite element method, this approach was intensively studied by many researchers, and many subsequent approaches were developed in this process. These approaches include: SIMP, where the isotropic material is simplified with a penalization method (Bendsøe 1989, Zhou & Rozvany 1991, Mlejnek 1992); Evolutionary Structural optimization (Huang & Xie 2010*a*,*b*); the level set approach (Allaire et al. 2002, 2004); topology derivative (Sokolowski & Zochowski 1999); and the phase field method (Bourdin & Chambolle 2003).

Among all of these optimization approaches, SIMP remains the most widely used approach at the present time. Similar to the homogenisation method, material distribution in this approach is represented by a finite number of elements whose density can be varied during the optimization process, and the stiffness contributed by each element is determined by this element's density. However, the stiffness is not linearly related to the density, but is proportional to the p power of density (e.g. Eqn. (2.22)). This condition can effectively push the density variables to present a binary distribution, which leads to a penalty for the grey elements (i.e. elements with density between 0 and 1). Fig. 2.12 shows an example obtained with the SIMP 99-line algorithm (Sigmund 2001).

$$E = E_0 \rho^p \tag{2.22}$$

where E is the Young's modulus of one element, E_0 is the Young's modulus of the pre-defined material, ρ is the density of this material, and p is the penalty parameter.

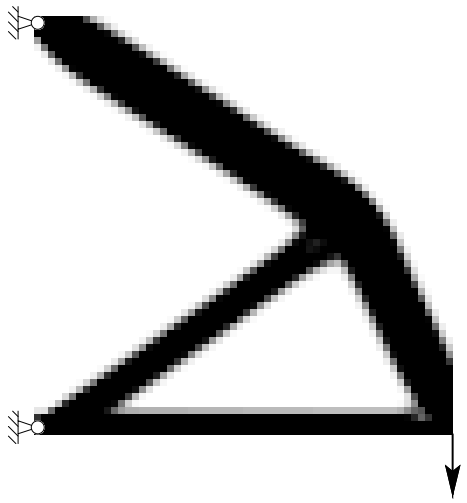

Figure 2.12: An optimized structure generated with the 99 line MATLAB script implementing the SIMP algorithm, where the command used is "top(50,50,0.3,3.0,1.5)" and the five parameters in the used command are design domain width, design domain height, volume fraction, penalty parameter p and filter diameter r_{min} respectively. (Sigmund 2001)

SIMP contains several parameters that can significantly affect the solution quality. First is the mentioned penalty parameter p. Usually, it is larger than 1 to act as a penalty, and the given recommendation is $p = 3$. The reason for the apparently magic effect of this value is discussed in Bendsøe & Sigmund (1999) and Amstutz (2011). The second one is r_{min}, which is the diameter of one element's filter region. By using the average density within this filter region, the so-called

checkerboard effect could then be eliminated (Sigmund 2001). The final important parameter is the numerical damping parameter η, which appears in the move limit calculation process (Sigmund 2001, page 121). The recommended value of η is 0.5. Increase in η leads to a larger step between iterations, which can cause numerical oscillation or a locally optimal result.

The continuum optimization approach is used in this thesis only for reproducing works of previous studies. The reason it is not chosen for building structure optimization because it usually requires a post-processing stage to transform the structure into a skeletal, or truss-like structure. Therefore, by directly using truss layout optimization, solutions can be obtained with less computational cost. More importantly, the continuum approach cannot guarantee a global optimal solution, and it can therefore sometimes output misleading results. Hence, in a situation where the global optimal solution is not known, the continuum approach is less reliable.

2.8 Transmissible load

Whilst in real design problems, the positions of wind loads, snow loads are dependent on the structure, optimization problems discussed in previous sections use loads with fixed positions, which potentially narrows the search area. To address this problem, (Fuchs & Moses 2000, Yang et al. 2005) proposed a approach for applying design-dependent loads. In this approach, instead of using a fixed position, loads are applied on a transmissible line. Hence in optimization solution, the optimal positions of the loads on their corresponding transmissible lines and the optimized structure are identified simultaneously.

2.8.1 Prager structure

Rozvany & Prager (1979), Wang & Dow (1982), Rozvany & Wang (1983*b*) considered transmissible loads in the context of topology optimization. These studies identified the funicular arch-grid structures which are sometimes called Prager structures. The approach employed introduced a virtual rigid bar along the transmissible line, which required that the virtual strains vanish along it. Consequently, the virtual rigid bars can transmit the load from any arbitrary point of application to the real structure. Additionally, these virtual rigid bars cause zero addition to the overall structural volume because they can carry the load with zero cross-sectional area. However,

this method was only applicable to Prager structure problems where only tension members or only compression members exist.

2.8.2 Rigid bar approach

Fuchs & Moses (2000) demonstrated that the rigid bar approach can be used to apply transmissible loads to more general cases (the detail formulation can be found in Section 3.4.2). This approach was then used by Fuchs & Moses (2000) with SIMP to identify the optimal structure that takes uniform load between simple supports, and the outcome is identical to the analytical solution of Prager's research. Yang et al. (2005) and Chiandussi et al. (2009) have implemented the rigid bar approach with evolutionary methods and the optimality criteria method respectively, and both have obtained similar optimization results to Fuchs & Moses (2000).

2.8.3 Migrating load approach

Darwich et al. (2010) incorporated an alternative equilibrium-based transmissible loads model (migrating load approach) in the classical plastic, linear programming (LP)-based, layout optimization formulation. In the formulation developed, LP variables (load variables) are introduced to represent potential loads applied at each node along the line of action of a given transmissible load. Constraints ensure that the sign and magnitude of the total load applied to all nodes within a group are the same as for the total applied load. The detail formulation of migrating load approach can be found in Section 3.4.1.

2.9 Lateral stability system

For a building structure, the lateral stability system is indispensable, due to the existence of wind, earthquakes and imperfections of the building itself. These effects are particularly important in the design of tall buildings and the requirement for lateral stability can govern the layout of the whole building. Consequently, many solutions exist to provide lateral stability for tall buildings; a detailed classification can be found in Gunel & Ilgin (2007). For the sake of clarity, three widely used lateral stability systems are introduced here:

Tubular system

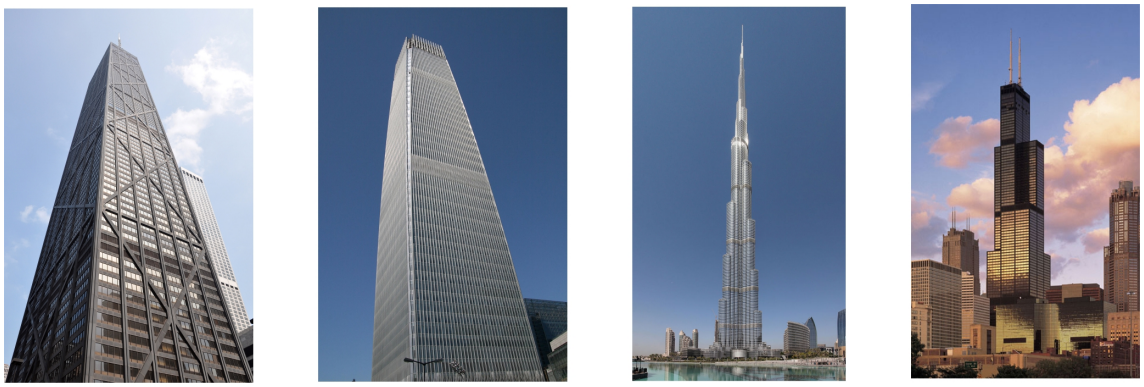

(a) (b) (c) (d)

Figure 2.13: Four tubular buildings: (a) John Hancock Building, Chicago (Jovianeye 2011) (b) China World Trade Center Tower III, Beijing (Holton 2008) (c) Burj Khalifa, Dubai (Donaldytong 2012) (d) Willis Tower, Chicago (Soakologist 1998)

Tubular systems are widely used in many tall buildings to provide lateral stability. The tubular system is defined by Fazlur Rahman Khan as:

"a three dimensional space structure composed of three, four, or possibly more frames, braced frames, or shear walls, joined at or near their edges to form a vertical tube-like structural system capable of resisting lateral forces in any direction by cantilevering from the foundation."(Ali 2001)

As this definition describes, a tubular system usually contains closely spaced columns on the perimeter of its exterior, which forms a hollow cantilever perpendicular to the ground, in order to provide stability against lateral loading from all directions.

The first example of the tube structure is the 43-storey Khan-designed DeWitt-Chestnut Apartments Building, built in 1963 in Chicago. After that, the tube structure underwent rapid development in the following decades. Consequently, there are many subsequent designs based on the classical tubular system, such as braced tube, tube in tube, bundled tube, and so on (Ali & Moon 2007). Currently, the tubular system has been used in many famous skyscapes such as the John Hancock Building in Chicago (e.g. Fig. 2.13a), the China World Trade Center Tower III in Beijing (e.g. Fig. 2.13b), the Burj Khalifa in Dubai (e.g. Fig. 2.13c), and the Willis Tower in Chicago (e.g. Fig. 2.13d).

Outrigger system

Other than the classical tubular buildings, a normal lateral stability system usually contains two parts: the core and perimeter structures. Whilst the core structure has a strong shear resistance and relatively low overturning resistance, the perimeter structure has large overturning resistance

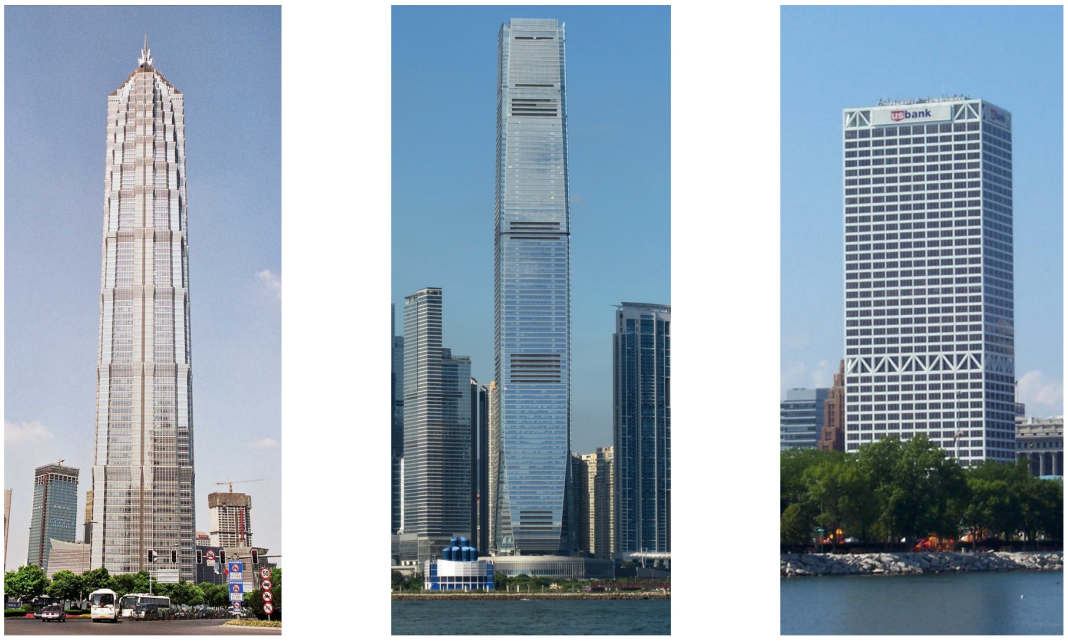

(a) (b) (c)

Figure 2.14: Three buildings using outrigger system: (a) Jin Mao Building, Shanghai (Airunp 2005); (b) International Commerce Centre, Hongkong (WiNG 2010); (c) U.S. Bank Center, Milwaukee (Sulfur 2006)

but is relatively weaker in terms of shear deformation control. Therefore, the two structures are usually both provided to resist overturning and shear deformation. However, the difference in deformation behaviour of the core and perimeter structures causes issues (e.g. in concrete structures, the difference in vertical member shortening will increase over time due to creep and shrinkage). Consequently, an outrigger bracing system has been developed to connect the core and perimeter structures through belt trusses, which leads to a greater lateral stability for tall buildings. The outrigger system is also a popular solution in providing lateral stability for tall buildings, and examples can be found in Fig. 2.14.

The performance of an outrigger system is affected by the location of outriggers throughout the height of the entire building. Lee & Tovar (2014) studied the optimal location of outriggers in tall buildings with the elastic optimization method. In this study, the truss bars in the beam and the floor are invariant pre-existing bars in the optimization problem, and the density of the truss bars in the outrigger is a design variable for the optimization problem. The value of this density is either 0 or 1, which leads to a controllable total number of outriggers. For this purpose, the penalty factor in SIMP is used to control the value of density. With the above approach, the optimal locations for a fixed-number of outriggers could be identified, and more importantly, it gave an example of how SIMP can be applied to discrete optimization to solve problems that involve binary variables.

Diagrid system

(a) (b) (c)

Figure 2.15: Three buildings using the diagrid bracing system: (a) 30 St Mary Axe, London (Guichard 2010); (b) Hearst Tower, New York (Alsandro 2006); (c) CCTV Headquarters, Beijing (Stojakovic 2013)

The diagrid bracing system is a recently developed, widely used, tall building lateral stability system. Compared with outrigger bracing, diagrid bracing can provide overturning and shear resistance by itself, and thus high core strength is not needed. Also, different from the tube system, columns on the exterior surface can be eliminated by allowing bracing members to take vertical loads. For this reason, diagrid bracing is highly functional, considering both aesthetic and efficiency aspects. Accordingly, diagrid bacing systems have attracted much interest from civil engineers, and many world-famous buildings have used this system in the past ten years. Examples of diagrid buildings can be found in Fig. 2.15.

Although the behaviour of a diagrid frame is very different to that of classical frame (e.g. with beams and columns), the design process for a diagrid building can be simplified with knowledge of structural optimization. For example, in the design of the Swiss Re Building, intended to be a symbolic diagrid bracing structure, a parametric optimization scheme was used to design the external form. Instead of exact connection positions, the external form was defined by a few parameters, and hence the complex geometric model could be rapidly generated (Foster 2005). Additionally, during the design of the CCTV headquarters, Beijing, China, an optimization process was used to modify the bracing pattern by adding or removing diagonals, subject to strength and stiffness requirements of a Level 1 earthquake analysis (Carroll et al. 2005).

2.9.1 Optimization of bracing system

The design of a tall building against lateral loading can be treated as a cantilever problem. As already mentioned, the cantilever problem was first studied by Michell (1904) (e.g. Fig. 2.8). Hemp (1973) re-considered this problem with different support conditions and obtained the optimal solution with an analytical approach. (e.g. Fig. 2.16a). Considering the complexity of the Hemp-Michell cantilever, Hemp (1973) further proposed a slightly less efficient solution with much simpler topology as shown in Fig. 2.16c. Following on from Hemp's work, the cantilever problem constrained within a half strip was studied by Graczykowski & Lewiński (2010) with an analytical approach, and the exact topology and volume were obtained for cases with different aspect ratios (e.g. Fig. 2.16b). Although the initial purpose of these studies was not bracing or tall building layout design, considering the similarity between these classical cantilevers and tall building bracing systems, these solutions are frequently obtained in many other bracing optimization studies.

Stromberg et al. (2011) investigated bracing topology using a continuum approach. With the consideration of fabrication issues, pattern gradation constraints were used in the optimization process. Simple and repeatable results were therefore obtained, and the importance of principal stress trajectories is emphasized. Additionally, three characteristics related to the shear and bending behaviour are noted through the analysis of the optimized structures. Following on from the previous study, Stromberg et al. (2012) introduced a beam/column member into the bracing design and identified the topology as in Fig. 2.16c. Due to the superior simplicity and efficiency of this topology, parametric studies have been carried out on this topology for different aspect ratios. It is worth noting that the effect of a column's stiffness on the optimal bracing topology has also been studied for one aspect ratio, and it has been found that the middle intersection point gradually moves from the 3/4 position to the 1/2 position as the column stiffness increases.

Different from Stromgberg's studies, Allahdadian et al. (2012) used dynamic loading in continuum topology optimization of multi-storey structures. In this study, cases with rigid and flexible beams were considered. The results obtained in cases with non-rigid beams were found to be similar to Stromberg bracing, while the results in cases with rigid beams were found to be similar to knee bracing structures.

Liang et al. (2000) assumed that for the lateral load cases and geometries investigated, the column

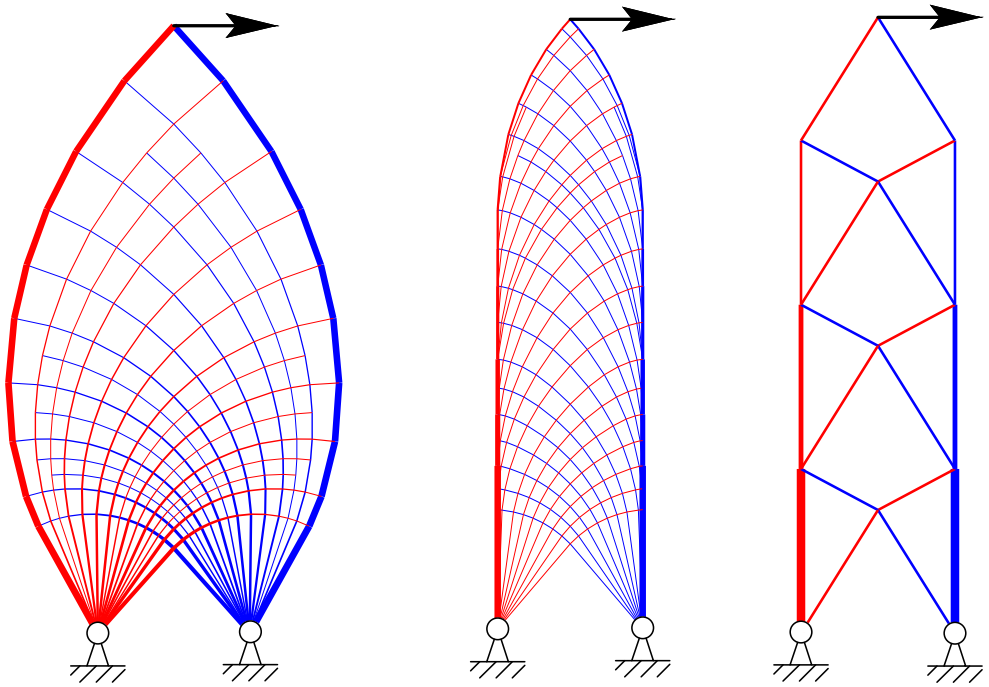

Figure 2.16: Three classical cantilever solutions, where red and blue lines respectively represent bars in tension and compression: (a) Michell-Hemp cantilever; (b) Michell-Hemp cantilever constrained within a half-strip; (c) Stromberg Bracing (Stromberg et al. 2012) .

and beam sizes determined from a gravity load analysis were adequate for the lateral case. Optimization based on this assumption led to new bracing structures different from Stromberg et al. (2012). This study was followed by (Baldock 2007), and more engineering-concerned (e.g. displacement control) and architecture-concerned (e.g. symmetry condition) constraints were involved in the optimization process. During his investigation, he pointed out limitations of ESO being a complex overall process and, more importantly, pointed out that the outcome will vary depending on the initial variable values, which means that these results cannot be considered as globally optimal.

Other optimization studies have been based on pre-defined structures. Burry et al. (2005) simultaneously applied lateral and gravity loads in a shape optimization problem for a pre-defined structure. However, the purpose was to improve the initially proposed design, and hence the final optimized result is very much like the initial design, apart from some minor details. Moon et al. (2007) and Moon (2008) optimized the stiffness of diagrid bracing systems, using the angles between members as variables. In this investigation, the optimal angle for a building with a specified storey number was identified, and the effect of the existence of corner columns was

also studied. Later, the performance of the diagrid structure was analysed by Moon (2012) with twisted, tilted, and freeform towers, considering different horizontal and vertical load cases.

2.10 Conclusions

The following conclusions have been obtained from the review of previous studies, and these identified problems will be addressed in the following chapters:

1. Although discrete truss layout optimization is suitable for the optimization of bracing truss structures, it appears not to have been used in previous studies for bracing structure optimization.

2. Currently there exist two transmissible load approaches. However, their respective effectiveness has not yet been critically investigated. Additionally, although wind load is naturally a kind of transmissible load, no previous study has treated it using transmissible load approaches.

3. Bracing members usually provide lateral stability through working together with column and beam members that take gravity loads. However, the interactions between bracing structure and column-beam frame structure appears not to have been previously studied in detail.

Chapter 3

On transmissible load formulations in topology optimization [i]

Preface

For building bracing design, the numerical techniques that are used in this thesis are layout optimization, geometry optimization and transmissible load approach. The former two are well developed techniques. However, currently there are two alternative approaches for the transmissible load (e.g. the migrating load approach and the rigid bar approach) and it has been identified in Tyas & Gilbert (2011) that these two approaches may produce different solutions for the same cases. Therefore, before the case study on bracing optimization, the difference in the formulations of the two approaches are investigated in this chapter through mathematical and numerical methods. It has been found that whilst migrating load approach is feasible for all situations, rigid bar approach is only feasible for some special cases. This occurs because the rigid bars that are used to transmit the loads onto the structure may form a part of the structure. Consequently, the rigid bar approach may leads to some incorrectly strengthened structures.

[i] The content of this chapter was originally prepared for a journal paper: Lu, H., Tyas, A., Gilbert, M. (2017), 'On transmissible load formulations in topology optimization', *Structural and multidisciplinary optimization*. Note that since this is a continuation of the Tyas & Gilbert (2011), part of this chapter is from Tyas & Gilbert (2011) (i.e. Section 3.2.2, Fig. 3.2, Fig. 3.3a, Fig. 3.4, Fig. 3.5a). Main contribution from the author is identification of the mathematical difference between the formulations of two previous formulations and reproduction of the results from previous studies for further numerical prove.

Abstract In the field of topology optimization, so-called *transmissible* (or 'design dependent') loads are sometimes used to avoid the form of the optimal structure being influenced by the locations of external applied loads, which are often not known *a priori*. Such loads are usually defined to act along specified lines of action, and have previously been represented in the problem formulation via constrained displacement (rigid bar) or equilibrium (migrating load) formulations. In this paper the range of applicability of each of these formulations is considered. It is demonstrated that the constrained displacement formulation as currently used should only be used in very special circumstances; otherwise incorrect or misleading topologies are likely to be identified.

3.1 Introduction

Whilst the field of topology optimization has a history stretching back well over a century, the problem of optimizing the position of applied loads in addition to structural layout has received relatively little attention. This is perhaps surprising, since in many cases the position at which external loads act cannot be precisely determined in advance, and will depend on the structural topology. Such loads have been termed *design dependent* by Yang et al. (2005), though the term *transmissible* is perhaps more illuminating (Fuchs & Moses 2000), as it highlights the requirement for the loads to be allowed to move through the design space to their most optimal points of application on the structure.

Transmissible loads appear to have been first considered in the context of topology optimization by Rozvany, Prager and co-workers (Rozvany & Prager 1979, Rozvany et al. 1982, Rozvany & Wang 1983*a*). The funicular arch-grid structures identified in these studies are sometimes referred to as *Prager-structures*. The approach employed required that the virtual strains vanish along the line of action of a transmissible load. This is equivalent to introducing a 'virtual' rigid bar along this line, which can transmit the load from any arbitrary point of application to the 'real' structure. Since this rigid bar can carry the load with zero cross-sectional area, it can be of arbitrary length without adding to the overall structural volume. However, it is important to realize that when using this approach a zero virtual strain requirement will also be imposed on the 'real' structure, and therefore has the potential to affect its topology. The method was used to demonstrate the optimality of Prager-structures for a range of problems when member stresses and strains were

constrained to be of one sign only, leading to funicular structures. However, similar constraints on the virtual displacement along the lines of action of transmissible loads have also been used in more recent finite element-based topology optimization studies (e.g. Fuchs & Moses (2000), Yang et al. (2005), Chiandussi et al. (2009)).

Gilbert et al. (2005) and Darwich et al. (2010) incorporated an alternative equilibrium based transmissible loads model (migrating load approach) in the classical plastic, linear programming (LP) based, layout optimization formulation. In the formulation developed, LP variables (load variables) are introduced to represent potential loads applied at each node present along the line of action of a given transmissible load. Constraints ensure that the sign and magnitude of the total load applied to all nodes within a group is the same as the total applied load.

The existence of these different formulations raises two questions: 1) Are these two approaches mathematically equivalent, and 2) if not, what do the differences mean for the efficacy of the two methods? We will demonstrate in this article that there is a simple but fundamental difference between the two approaches, meaning that the rigid bar formulation will typically lead to physically illogical solutions, whereas the migrating load approach results in correct solutions.

3.2 Comparison between rigid bar and migrating load approaches

3.2.1 Conceptual formulation

The conceptual formulations of the rigid bar and migrating load approaches are presented through a simple example which only contains six nodes Fig. 3.1. In this example, the left boundary is fixed in x and y direction. Load P could be transmitted to any nodes on the right boundary. In the optimized solution, the optimal point of the transmissible load P is the middle point.

The features of the two approaches can be described as follows.

For the rigid bar approach, as shown in Fig. 3.1b, the load is transmitted to the optimal point through loads generated in virtual, cost-free, rigid bars. It is important to note that due to these rigid bars, the virtual displacements are constant along the right boundary.

For the migrating load approach, the single external load P is replaced by three load variables, applied to the three nodes on the line of action of the external load. These three load variables are

controlled by sign and sum constrains (e.g. $\mathrm{P}_{1,2,3} \geq 0$ and $\sum_{i=1}^{3} \mathrm{P}_i = \mathrm{P}$). In situation presented in Fig. 3.1c, where the load is transmitted to the middle node, $\mathrm{P}_1 = \mathrm{P}_3 = 0$ and $\mathrm{P}_2 = \mathrm{P}$. There are no explicit constraints on the virtual displacements on the line of action of the transmissible loads.

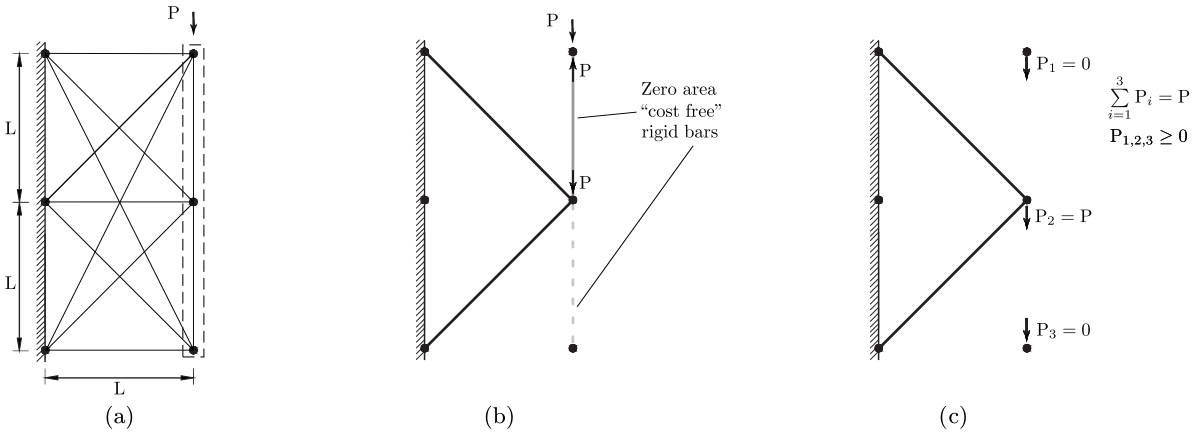

Figure 3.1: Rigid bar and migrating load approach for a problem involving six nodes: (a) the design problem and the trajectory of the transmissible load P; (b) solution obtained with rigid bar approach, where solid and dotted grey lines represent rigid bars have respectively non-zero and zero internal force; (c) possible solution obtained via migrating load approach, where P_1, P_2 and P_3 are the load variables and they must satisfy the sum and sign constraint in (c).

3.2.2 Mohr's circle analysis.

We first note the three general types of optimal structural layouts: (i) structurally 'rich' forms in which (generally orthogonal) truss bars are strained to their respective limits in tension and compression, (ii) similarly 'rich' forms but where all bars experience stresses in only one direction, and (iii) simpler flexure-less line or surface structures. These have been defined respectively as: (i) T-type, (ii) S-type and (iii) R-type structures (Rozvany (1997)). Rozvany & Wang (1983*a*) show how the rigid bar approach could successfully be used to identify R-type structures, but no rigorous assessment of the applicability of the method to the richer T-type and S-type structures appears to have been published in the literature.

As already noted, the rigid bar approach requires constant virtual displacements along the line of action of a transmissible load, which means the virtual strain equals to zero along the same line. For sake of simplicity we will assume henceforth, without loss of generality, that our problem is confined to 2-dimensions, and that the transmissible load acts in a direction normal to the x-axis, so that the y-virtual strain, ε_{yy} is zero.

From analysis of Mohr's Circle of strain with the requirement that $\varepsilon_{yy} = 0$, we obtain:

$$\varepsilon_{xx} = \varepsilon_1 + \varepsilon_2 \tag{3.1}$$

$$\gamma_{xy} = 2\sqrt{-\varepsilon_1\varepsilon_2} \tag{3.2}$$

$$\theta_p = \tan^{-1} \frac{-(\varepsilon_1 + \varepsilon_2)}{2\sqrt{-\varepsilon_1\varepsilon_2}} \pm \frac{\pi}{4} \tag{3.3}$$

where ε_{xx} is the x-virtual strain, $\varepsilon_{1,2}$ are the principal strains, γ_{xy} is the engineering shear strain and θ_p the angle between the trajectories of principal strain and the *x*-axis.

It is immediately apparent that the rigid bar approach can never be compatible with S-type structures. This is because the principal strains in such structures are of the same sign, and so no real values can be found for the shear strain or principal angle. (This is of course to be expected, since S-type structures intrinsically comprise bi-axial tension or compression fields).

For T-type structures, $\varepsilon_1 = \frac{1}{\sigma^+}$, $\varepsilon_2 = -\frac{1}{\sigma^-}$ and, where σ^+ and σ^- are the allowable stress in tension and compression respectively, furnishing:

$$\varepsilon_{xx}^T = \frac{\sigma^- - \sigma^+}{\sigma^+\sigma^-} \tag{3.4}$$

$$\gamma_{xy}^T = 2/\sqrt{\sigma^+\sigma^-} \tag{3.5}$$

$$\theta_p^T = \tan^{-1} \frac{\sigma^- - \sigma^+}{2\sqrt{\sigma^+\sigma^-}} \pm \frac{\pi}{4} \tag{3.6}$$

For the particular case of equal magnitudes of allowable tension and compression stress, these simplify to:

$$\varepsilon_{xx}^T = 0 \tag{3.7}$$

$$\gamma_{xy}^T = \frac{2}{\sigma} \tag{3.8}$$

$$\theta_p^T = \pm \frac{\pi}{4} \tag{3.9}$$

where $\sigma = (\sigma^+ + \sigma^-)/2$.

The constraints on the geometry imposed by (3.6) and (3.9) are particularly noteworthy results since they show that the rigid bar formulation is incompatible with T-type layouts apart for the unique case where the trajectories of principal strain are aligned at $\pm\frac{\pi}{4}$ to the line of the action of the transmissible load.

As for the migrating load approach, the present authors and their co-workers used this formulation for inclusion of load transmissibility (Gilbert et al. 2005, Darwich et al. 2007, 2010), and the results in the second and third articles show clearly that this approach is capable of producing a curvilinear T-type structure. Indeed, the structure presented in those articles (e.g. Fig. 3.2b) was later demonstrated by Tyas et al. (2010) to be globally optimal. It appears therefore that the numerical analysis used by Darwich et al. (2007, 2010) avoided the problems shown above to be inherent in the rigid bar approach. With this background, we now proceed to look more carefully at numerical examples.

3.3 Numerical examples

The suitability of migrating load and rigid bar approaches can be succinctly demonstrated through two numerical examples. In the following examples, we apply the migrating load approach to discrete optimization only and the rigid bar approach to both discrete and continuum optimization. The application of the rigid bar approach to contiuum problems aims at reproducing the work of Fuchs & Moses (2000), allowing us to interrogate their results in the light of the Mohr's circle analysis set out above. We use the SIMP based continuum formulation (Sigmund 2001) with the displacement constraints set out by Fuchs & Moses (2000) introduced using the method presented in Houlsby et al. (2000). We use the η_1 and η_2 parameters as described by Fuchs and Moses (2000). The adjustment of parameters in the continuum approach is similar to the original study (Fuchs & Moses 2000). As for the discrete optimization formulation, a post-possessing technique (He & Gilbert 2015) is used in Fig. 3.2 & Fig. 3.4 to produce a visually clearer solution.

3.3.1 Example 1 - uniform load between pinned supports

The first numerical example involves vertical loads uniformly distributed along a horizontal line and free to migrate along the vertical lines, and is supported by two pinned nodes at the left and right bottom corners. Sum of the vertical loads is 1 and a 100×100 grid is used for discrete optimization, but for visual clarity, only every fifth node is shown in Fig. 3.2a. As for continuum approach, 50×50 design domain size is used and the Young's Modulus is set to 1. Fig. 3.2b and Fig. 3.2c shows the result from discrete optimization with migrating load approach. The optimal form corresponds to the solution identified by Darwich et al. (2007, 2010) and later demonstrated

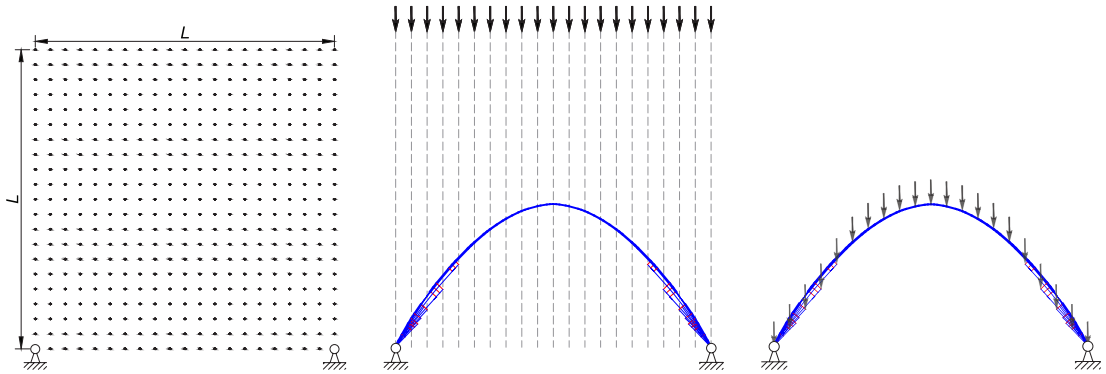

(a) (b) (c)

Figure 3.2: Migrating load approach: uniform load between pinned supports, where (a) is design domain description, (b) shows transmissible trajectory and result from discrete optimization and (c) shows final position of loads. Red bar takes tensile force and blue bar takes compressive force.

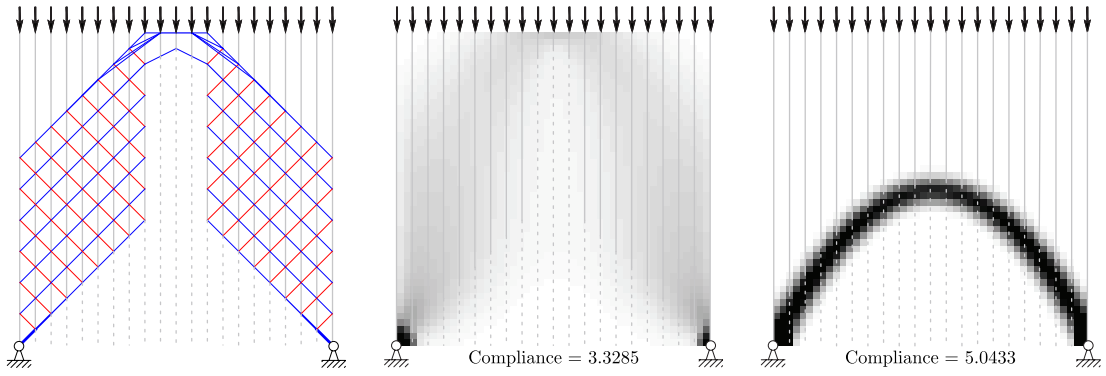

(a) (b) (c)

Figure 3.3: Rigid bar approach: uniform load between pinned supports, where (a) is discrete optimization result, (b) is early stage result of continuum optimization and (c) is final result of continuum optimization. Red, blue, grey solid, grey dotted lines represent, respectively, bars take tensile force, bars takes compressive force, rigid bars have non-zero internal force, rigid bars have zero internal force.

by Tyas et al. (2010) to be the globally optimal solution, including both rich T- and funicular R-regions.

Figure (3.3a) shows the optimal form for the same discrete problem when the rigid bar formulation is applied (here, displaying a 20x20 grid for visual clarity). This solution appears to comprise a central funicular R-region, spanning between two T-regions which are artificially braced by the presence of the zero-cost vertical rigid bars. As shown in Fig. 3.3b and Fig. 3.3c, the continuum approach outputs a similar result to the initial solution presented in the lower left image in Fig. 3.6 of Fuchs & Moses (2000). They suggested that in this solution, the optimal form (assumed to be a parabola) was obscured by "noise" which could be removed by the application of a filter parameter η_1. Fig. 3.3c shows, as Fuchs & Moses (2000) found, that the filtering does indeed reveal a parabolic solution. With the level of resolution of the mesh used in this study, this solution is indistinguishable from the true optimal form Fig. 3.2c.

3.3.2 Example 2 - Cantilever subject to uniform load

Figure (3.4a) illustrates the initial conditions of the second numerical case. The only difference between this and the previous example is the support condition; in this example, the structure is supported by a vertical line support symmetrical about the horizontal centre-line over a height equal to one-third of the horizontal extent of the design domain.

Figure 3.4b and 3.4c show the result for the migrating load formulation. Here, the optimal structural form follows that presented by Fig. 4.18 of Hemp (1973) , the so-called Hemp cantilever, with the load having been transmitted to be applied along the horizontal centre-line of the structure.

Figure 3.5a shows the discrete layout optimization result for this problem with the rigid bar formulation. It is clear that, without the assistance of the rigid bars, which can artificially stiffen the structure on each vertical line, this solution would be unstable. This highlights the fundamental problem of the rigid bar approach. The rigid bars are introduced into the problem definition order to facilitate transmission of applied loads onto the structure, and are not intended to form part of the structure. In Fig. 3.5a, however, rigid bars appear as load carrying members in the real structure.

Figure 3.5b shows the equivalent result from continuum optimization. As with the previous example, the initial, unfiltered continuum solution is similar in form to the discrete solution (

Fig. 3.5a). Application of the Fuchs & Moses (2000) filter to this solution results in the form shown in Fig. 3.5c, which bears little resemblance to the actual optimal form shown in Fig. 3.4c.

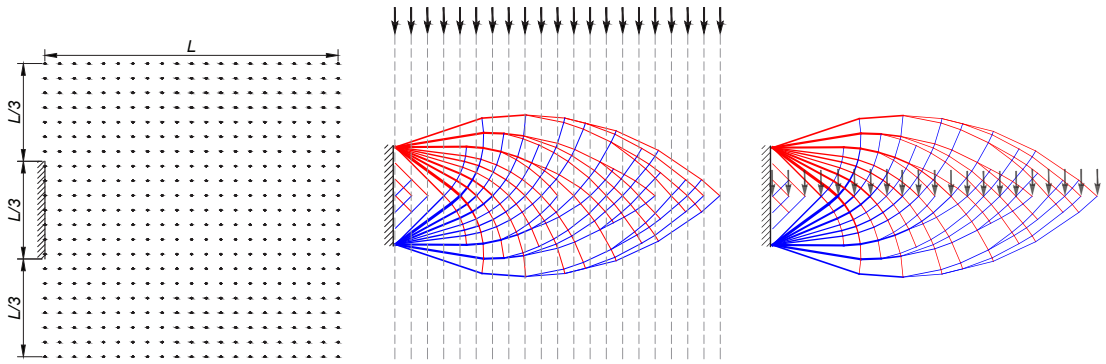

(a) (b) (c)

Figure 3.4: Migrating load approach: cantilever subject to uniform load, where (a) is design domain description, (b) shows transmissible trajectory and result from discrete optimization and (c) shows final position of loads. Red bar takes tensile force and blue bar takes compressive force.

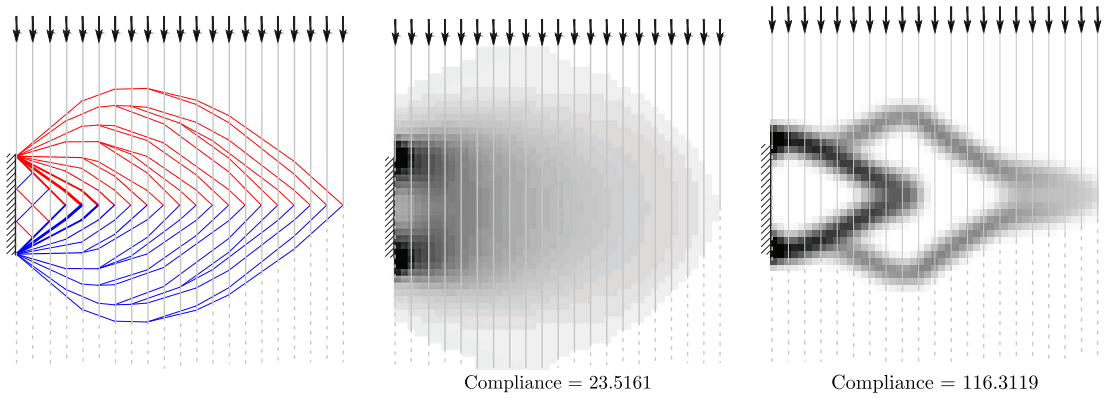

(a) (b) (c)

Figure 3.5: Rigid bar approach: cantilever subject to uniform load, where (a) is discrete optimization result, (b) is early stage result of continuum optimization and (c) is final result of continuum optimization. Red, blue, grey solid, grey dotted lines represent, respectively, bars take tensile force, bars takes compressive force, rigid bars have non-zero internal forces, rigid bars have zero internal forces.

3.3.3 Commentary

The example presented in Sections 3.3.1 and 3.3.2 demonstrate precisely the conclusion of the Mohr's Cirlce analysis: namely that, when the optimal form comprises curvilinear T-type structural regions, the rigid bar approach will produce structurally illogical forms which are artificially stiffened by the cost-free rigid bars. Comparison of the discrete and continuum rigid bar "optimal structures" suggests that, the unfiltered continuum solution does not comprise the correct solution over-written by noise. Instead, the unfiltered structure appears to be the correct

solution to a problem which does not correctly model the concept of transmissible loads. Filtering the results of Example 1 does lead to a structure (Fig. 3.3c) which broadly resembles the true optimal form (Fig. 3.2c). This is likely to be due to the fact that the T-type regions in the optimal structure are limited in extent. However, in the case of Example 2, the filtered result (Fig. 3.5c) bears little comparison to the true optimal form (Fig. 3.4c). It is also notable that the filtering increases the compliance of the structures in Example 1 and 2 by 52% and 395% respectively. This emphatically shows that the "filtering" is actually driving the solution to a fundamentally different structural form.

We emphasize that these issues only arises in the case of the rigid bars interacting with a curvilinear T-type structure. In the case of R-type (funicular) structures the issues do not occur since the structures comprise entirely line or surface elements. This is because, in R-type structures, external loads are resisted through internal axial forces only, and equilibrium dictates that the structural members cannot be co-axial with the line of action of the transmissible loads[ii]. The virtual rigid bars thus never form part of the real load carrying structure.

This can be demonstrated by re-visiting the problem set out in Section 3.3.1. Wang & Rozvany (1983) showed that when the ratio between compressive and tensile stress capacity is larger than 3 (e.g. $\sigma^-/\sigma^+ \geq 3$) , the optimal form is a funicular R-structure. This was supported by numerical results presented by Dawich et al (2010) which showed that as σ^-/σ^+ dropped below 3, T-region Hencky nets emerged adjacent to the supports. Thus, it should be expected that the rigid bar formulation will find the correct funicular structure for $\sigma^-/\sigma^+ \geq 3$, and inadmissible, artificially strengthened structures for lower values. The results in Fig. 3.6 show this to be the case.

It is worth noting that, whilst (as explained in Section 3.2.2) the rigid bar approach is unfeasible in regions where "curvilinear" T-type structures exist, there is one special T-type geometry which is compatible with the rigid bar formulation. For equal compressive and tensile stresses, Eqn. (3.9) shows that the rigid bar formulation will be admissible where the true optimal form comprises a rectilinear net oriented at $\pm 45^\circ$ to the line of action of the applied load. In the Hemp cantilever example, such a region exists in the triangular area immediately adjacent to the vertical support line; the rigid bar approach does indeed find the correct layout in this region (Fig. 3.5a).

[ii] An exception is when a support lies along the line of action of a transmissible load. This was discussed by Rozvany & Wang (1983*a*) who sensibly considered it to be of no practical significance as in this case the load can migrate directly to the support and no structure is required.

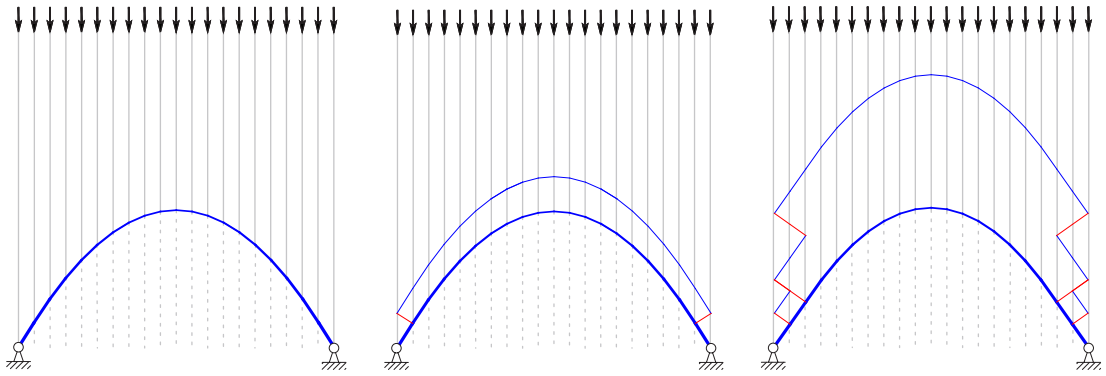

(a) (b) (c)

Figure 3.6: Rigid bar approach: uniform load between pinned supports, where (a) $\sigma^-/\sigma^+ = 3.33$, (b) $\sigma^-/\sigma^+ = 2.50$ and (c) $\sigma^-/\sigma^+ = 2.00$; where σ^- and σ^+ represents compressive and tensile stress capacity. Red, blue, grey solid, grey dotted lines represent, respectively, bars take tensile force, bars takes compressive force, rigid bars have non-zero internal forces, rigid bars have zero internal forces.

3.4 Formal mathematical status of the rigid bar and migrating load appraches

Having demonstrated the differences between the rigid bar and migrating load approaches from a Mohr's circle analysis, and by numerical examples, we now investigate the differences in the mathematical formulations of the two methods.

3.4.1 Dual theory based proof of the difference between migrating load and rigid bar approach

In Darwich et al. (2010) an equilibrium-based LP transmissible loads formulation (migrating load approach) for a design domain which contains n nodes and m members is stated as:

$$\min V = \mathbf{c}^{\mathrm{T}}\mathbf{q} \tag{3.10a}$$

subject to:

$$\mathbf{B}\mathbf{q} - \tilde{\mathbf{f}} = \mathbf{0} \tag{3.10b}$$

$$\mathbf{H}\tilde{\mathbf{f}} = \hat{\mathbf{f}} \tag{3.10c}$$

$$\mathbf{q} \geq \mathbf{0} \tag{3.10d}$$

$$\tilde{\mathbf{f}}_k \leq \mathbf{0} \text{ or } \tilde{\mathbf{f}}_k \geq \mathbf{0}\} \; k = 1....p \tag{3.10e}$$

Where $\mathbf{c}^{\mathrm{T}} = \{l_1/\sigma_1^+, -l_1/\sigma_1^-, ..., l_m/\sigma_m^+, -l_m/\sigma_m^-\}$, and l_i is the member length of member i, $\mathbf{B}$ is a suitable $2n \times 2m$ matrix containing direction cosines, $\mathbf{q^T} = \{q_1^+, -q_1^-, q_2^+, -q_2^-, ..., q_m^+, -q_m^-\}$, with q_i^+ and q_i being the tensile and compressive forces in member i, $\mathbf{H}$ is a $2p \times 2n$ matrix, and where p is the number of node groups to which external loads are applied, $\hat{\mathbf{f}}^{\mathrm{T}} = \{\hat{f}_1^x, \hat{f}_1^y, \hat{f}_2^x, \hat{f}_2^y ..., \hat{f}_p^x, \hat{f}_p^y\}$. The LP variables are the bar forces in $\mathbf{q}$ and the nodal loads in $\tilde{\mathbf{f}}$, where $\tilde{\mathbf{f}}^{\mathrm{T}} = \{\tilde{f}_1^x, \tilde{f}_1^y, \tilde{f}_2^x, \tilde{f}_2^y, ..., \tilde{f}_n^x, \tilde{f}_n^y\}$.

For sake of simplicity, we assume there is only one vertical transmissible load $\hat{f}$ and $\hat{f} \geq 0$. Hence the formulation becomes:

$$\min V = \mathbf{c}^{\mathrm{T}}\mathbf{q} \tag{3.11a}$$

subject to:

$$\mathbf{Bq} - \tilde{\mathbf{f}} = \mathbf{0} \tag{3.11b}$$

$$\mathbf{H}\tilde{\mathbf{f}} = \hat{f} \tag{3.11c}$$

$$\mathbf{q} \geq \mathbf{0} \tag{3.11d}$$

$$\tilde{\mathbf{f}} \geq \mathbf{0} \tag{3.11e}$$

Now, LP duality principles can be used to derive the dual formulations as follows:

$$\min W = u_{max}\hat{f} \tag{3.12a}$$

subject to:

$$\mathbf{B}^{\mathrm{T}}\mathbf{u} \leq \mathbf{c} \tag{3.12b}$$

$$u_{max} \leq \mathbf{u}_{trs}^y \tag{3.12c}$$

Where W is the work done by the applied loads, $\mathbf{u} = \{u_1^x, u_1^y, ..., u_n^x, u_n^y\}$, with u_j^x and u_j^y being the displacement in x and y direction of node j, u_{max} is the maximum displacement along the transmissible trajectory, $\mathbf{u}_{trs}^y = \{u_k^y, u_{k+1}^y, ..., u_{k+p-1}^y\}$ and u_k^y to u_{k+p-1}^y are the y-direction displacements of nodes located on the transmissible trajectory.

During the dual transformation, (3.12c) is a direct result caused by (3.11e). Hence, in

circumstances where (3.11e) is removed from (3.11), (3.12c) becomes:

$$u_{max} = \mathbf{u}^{y}_{trs} \tag{3.13}$$

As demonstrated by Fuchs & Moses (2000), (3.13) is the mathematical fundamental of rigid bar approach. Therefore, if (3.11e) is removed from migrating load approach, then immediately, it is equivalent to rigid bar approach. Hence the only difference between migrating load and rigid bar approach is (3.11e) (or (3.10e)), which are the constrains that control the sign of load variables.

3.4.2 Lagrangian function based proof of the difference between migrating load and rigid bar approach

(Notations in this section is independent of notations used previously.)

The conclusion of Section 3.4.1 also can be derived using the Lagrangian function. For the sake of completeness, we first note the mathematical derivation in Fuchs & Moses (2000). First, the transmissible load topology optimization was stated as:

$$\begin{aligned}\max_{\rho}\max_{p_{im}}\min_{u}\{\mathbf{u}'\mathbf{K}\mathbf{u}-\mathbf{p}'\mathbf{u}|\sum_{j}\rho_j V_j=\rho_0 V;\\ \sum_{m\in M}p_{im}-p_i=0, i\in\mathbf{I}\}\end{aligned} \tag{3.14}$$

where $\mathbf{K}$ is the stiffness matrix of the structure, $\mathbf{u}$ is the displacement vector, ρ_j is the element density of element j, V_j is the volume of element j, ρ_0 is a parameter which controls the amount of material available for the design, V is the total volume of the design domain, p_i is the applied load i with $i \in \mathbf{I}$ and each p_i can be split into p_{im}s with $m \in M$, and where M is the set of nodes located on the transmissible trajectory of p_i.

Equ (3.14) leaded to following Lagrangian function:

$$\begin{aligned}L(\boldsymbol{\rho},\lambda,\mathbf{u},p_{im},\mu_i) = (\mathbf{u}'\mathbf{K}\mathbf{u}-\mathbf{p}'\mathbf{u}) - \lambda(\rho_j V_j-\rho_0 V)\\ -\sum_{i\in\mathbf{I}}\mu_i(\sum_{m\in M}p_{im}-p_i)\end{aligned} \tag{3.15}$$

Equating the derivation of (3.15) with respect to p_{im} to zero gave:

$$u_{im} - \mu_i = 0, i \in \mathbf{I} \tag{3.16}$$

Equation (3.16) means that displacements of all nodes along the transmissible line are constant. Based on that conclusion, Fuchs & Moses (2000) suggested that "one could assume the existence of infinity stiff axial elements of zero mass along the line".

Based on Conclusion of Section 3.4.1, if we add the load variable sign control constrain ($p_{im}p_i \geq 0$) to (3.14), it yields:

$$\begin{aligned} \max_{\rho} \max_{p_{im}} \min_{u} \{ \mathbf{u}'\mathbf{K}\mathbf{u} - \mathbf{p}'\mathbf{u} | \sum_j \rho_j V_j = \rho_0 V; \\ \sum_{m \in M} p_{im} - p_i = 0; p_{im}p_i \geq 0, i \in \mathbf{I} \} \end{aligned} \tag{3.17}$$

Formulation (3.17) leads to following Lagrangian function:

$$\begin{aligned} L(\boldsymbol{\rho}, \lambda, \mathbf{u}, p_{im}, \mu_i) = (\mathbf{u}'\mathbf{K}\mathbf{u} - \mathbf{p}'\mathbf{u}) - \lambda(\rho_j V_j - \rho_0 V) \\ - \sum_{i \in \mathbf{I}} \mu_i (\sum_{m \in M} p_{im} - p_i) - \sum_{i \in \mathbf{I}, m \in M} \xi_{im}(p_{im}p_i - \varphi_{im}) \end{aligned} \tag{3.18}$$

Equating the derivation of (3.18) with respect to p_{im} to zero gives:

$$u_i m - \mu_i - \xi_{im} p_i = 0, i \in \mathbf{I} \tag{3.19}$$

This leads to a conclusion that, a slack variable, equal to $\xi_{im}p_i$, exists between μ_i and u_{im}. This conclusion is exactly the same as (3.12c), which means (3.17) is equivalent to the formulation for migrating load approach. This again proves that only difference between migrating load formulation (i.e. (3.17)) and rigid bar formulation (i.e. (3.14)) is $p_{im}p_i \geq 0$, which are the constrains that control the sign of load variables.

3.5 Conclusion

Two approaches to the modelling of load transmission through a design domain to the optimal point of application with a structure have been considered. It has been demonstrated that, there is a fundamental difference between the commonly used (kinematic) rigid bar formulation and the less used (equilibrium) migrating load approach. A simple strain analysis has demonstrated the limitations of the rigid bar approach, and shows that this is only usable where the actual optimal structure is a funicular, or a rectilinear net oriented at a specific angle to the line of the applied loads. Numerical results have demonstrated that, in other cases, the rigid bar approach will generate physically illogical forms, with the "optimal structure being artificially strengthened by the presence of the zero-cost rigid bars which form part of the structure itself. The application of filtering to structures found by the rigid bar approach has been shown to result in entirely different structural forms, accompanied by very large increases in compliance. Conversely, the migrating load approach does not suffer these limitations and produces numerical results which match know correct optimal forms. Finally, we have shown that the mathematical formulations for the migrating load and rigid bar formulations differ in one simple, but important way; the rigid bar formulation omits constraints on the signs of the load variables. In conclusion, our findings show that the rigid bar approach generally fails to identify correct optimal structural forms and should be used with caution, if at all.

3.6 Postscript

It has been identified that the rigid bar approach and the migrating load approach are mathematically different. The rigid bar approach implicitly assumes the presence of zero-cost load transfer members, and this assumption will usually lead to incorrectly strengthened structures. However, in certain circumstances, zero-cost members do actually exist. An example is the column-beam frames that have been designed for gravity loads and are not fully stressed when acting in bracing frames. Therefore, in the bracing frame design process, by treating column-beam frame as rigid bars could lead to efficient designs. Therefore, in the following chapters, which mainly focus on bracing layout optimization, Chapters 4 and 6 will take advantage of this idea to develop an enhanced understanding of the optimality of certain bracing systems.

Chapter 4

Optimal bracing systems in buildings: bracing pre-existing frames [i]

Abstract Bracing is commonly used to provide resistance to lateral forces in building structures. However, traditional bracing design approaches appear not to be underpinned by clear fundamental principles. Here, theoretically optimal arrangements of bracing members are sought for frames with pre-existing members, already designed to carry gravity loads. For sake of simplicity existing frame elements are assumed to be capable of carrying additional loads and three types of bracing are considered: tension only bracing, bracing intersecting only at the corners of the existing frame, and unconstrained optimal bracing, where bracing elements can intersect at any location. Layout optimization techniques are used to identify initial design solutions, against which the efficiency of other bracing layouts can be judged. These are then related to Michell trusses to obtain exact reference volumes, against which the efficiency of other bracing layouts can be judged. It is shown that tension only bracing is inefficient and that the optimal angle of intersection between pre-existing frame members and intersecting tension/compression bracing member pairs is 45°, something that can potentially be adopted as a basic principle when designing bracing for a pre-existing frame.

[i]The content of this chapter was originally prepared for a journal paper: Lu, H., Gilbert, M., Tyas, A. (2017), 'Optimal bracing systems in buildings: bracing pre-existing frames', *Structural and Multidisciplinary Optimization*

4.1 Introduction

The lateral restraint system is an indispensable part of any building. This is particularly true in a tall building structure, where the requirements for lateral strength and stiffness can govern the layout of the whole building. Consequently, the design of efficient bracing layouts to resist lateral wind loading is an area of active interest to structural engineers.

Optimization of bracing systems has often focussed on geometry or size optimization. For example, Moon et al. (2007) analysed diagrid bracing systems, using the angles between bracing members as parameters which were varied to optimize the lateral stiffness of the structure. Bobby et al. (2013) and Lee & Tovar (2014) optimized an outrigger bracing system by using binary variables to represent the existence of belt trusses; Sala & Candiani (2014) used the size optimization technique proposed by Baker (1990) to identify the optimal section sizes of a fixed topology bracing system whilst Tangaramvong & Tin-Loi (2015) used a discrete approach to optimize the bracing topology using a sparsely populated ground structure (only members connecting neighbouring nodes were considered). Others have used continuum optimization techniques (e.g. Liang et al. (2000), Allahdadian et al. (2012), Stromberg et al. (2012), Kingman et al. (2015)) or genetic algorithms (e.g. Baldock (2007), Yazdi & Sulong (2011), Richardson et al. (2013)). However, to date classical discrete layout optimization methods appear not to have been used to benchmark the efficiency of commonly used bracing systems.

The mathematical basis for the problem of finding the structural layout consuming the least volume of material was developed by Michell (1904). Whilst Michell's analytical approach provides a strong foundation for the field, it is seldom applied to practical structural design applications, partly because of the difficulty of identifying the optimal structure for specified loading and support conditions. However, the approach readily lends itself to numerical implementation, where the optimal layouts of discrete members are found from a 'ground structure', comprising all possible interconnections of discrete node points within a design space. Using linear programming (LP) techniques numerical layout optimization results can be found which closely approximate classical Michell forms for any given problem (Dorn et al. 1964, Hemp 1973); more recently the computational efficiency of this method was improved by Gilbert & Tyas (2003). Here, numerical layout optimization will be used to investigate the optimal bracing layout in various different scenarios.

Stromberg et al. (2012) and Liang et al. (2000) have considered the optimization of bracing systems within a beam/column frame represented by discrete beam members. Stromberg et al. (2012) optimized the bracing topology with different type connections between continuum and discrete beam elements and the effect of column stiffness on the optimal bracing layout was also considered. Liang et al. (2000) assumed that the beam/column members sized in a gravity load analysis would also be adequate for lateral load cases, and optimized the bracing topology for several bay aspect ratios. This raises two questions: (i) if the beams and columns designed for gravity loads have sufficient reserves of strength, such that they do not need to be resized to act as part of the lateral stability system, can general rules governing the optimal layout of bracing members be found? Also, (ii) if the structural system is optimized for both gravity and lateral load cases, and combinations thereof, what is the form of the optimal bracing system in this case? This study focuses on optimizing the layout of bracing elements within a pre-existing frame, where the members have already been designed to carry gravity loading, and are assumed to have the requisite additional reserves of strength to support lateral loads; the more holistic design problem, where the sizes of pre-existing frame members may need to be resized as a result of the forces generated in load cases involving lateral loads, other scenarios will be the subject of Chapter 5.

This chapter is organized as follows: Section 4.2 outlines the assumptions made with respect to loading and pre-existing frame performance; Section 4.3 describes the problem types considered and the numerical layout optimization method employed to obtain initial solutions; Sections 4.4 and 4.5 consider respectively single bay and multibay/storey building types, with exact analytical solutions derived for key problem types; finally conclusions from the study are drawn and the direction of future research is outlined in Section 4.6.

4.2 Assumptions

For the design of steel framed buildings, British Standard 5950-1:2000 suggests the following load combinations:

$$p_1 : 1.4G_{\mathrm{k}} + 1.6Q_{\mathrm{k}} \tag{4.1a}$$

$$p_2 : 1.0G_{\mathrm{k}} + 1.2Q_{\mathrm{k}} + 1.2W_{\mathrm{k}} \tag{4.1b}$$

$$p_3 : 1.0G_{\mathrm{k}} + 1.2Q_{\mathrm{k}} - 1.2W_{\mathrm{k}} \tag{4.1c}$$

where G_{k} is the characteristic permanent load, Q_{k} is the characteristic imposed load and W_{k} is the characteristic wind load.

Here, for simplicity the concept of Notional Horizontal Load (NHL) (a small lateral load which is applied as part of the main gravity load case (4.1a)) is ignored, and it is assumed that the bracing design is dominated by the wind load cases, (4.1b) and (4.1c).

From (4.1) it is clear that the maximum partial factor multipliers for gravity loads exist in load case (4.1a), and that the gravity load is decreased in load cases (4.1b) and (4.1c). Therefore, for the purpose of the studies herein, the following assumptions have been made:

- Assumption 1: The loads generated in the columns in load case (4.1b) and (4.1c) are always less than those resulting from load case (4.1a).
- Assumption 2: Vertical gravity loads are only carried by the columns in all load cases.
- Assumption 3: The sizes of pre-existing horizontal members (i.e. floor beams and/or slabs) are dominated by the gravity load case, (4.1a), and the axial loads induced in them by lateral load cases (4.1b) and (4.1c) are small in comparison.

Assumption 1 means that the sizes of the columns are not determined by the lateral load cases, and thus that the columns may be assumed to have infinite strength when designing for lateral loads. Assumption 2 is widely adopted in design practice, where columns are often first designed to resist gravity loads, with the design of bracing members to resist lateral loads coming later. Together these two assumptions mean that the vertical loads in load combination (4.1) will not affect the optimal layout of the bracing system, and the wind load (i.e. $1.5\mathrm{W_k}$) is governing. Assumption 3 means that the structural members forming the floors effectively possess infinite reserves of strength, and can distribute applied lateral loads to either side of the frame. With these three assumptions, the design of a bracing system for a frame already designed to carry gravity loads is considered, where the bracing need only resist lateral loads. This effectively replicates one step in the traditional design procedure for buildings (e.g. Brown et al. (2009) suggest that the sizes of beams and columns are first determined by considering gravity loads, with the sizes of bracing members then determined by considering lateral loads). A similar approach has also been used in previous bracing topology optimization studies; for example Mijar et al. (1998), Liang et al. (2000)

and Stromberg et al. (2012), who all take (or design) a column-beam frame capable of carrying gravity loads and then, considering only lateral loads, carry out bracing topology optimization.

4.3 Problem specification

4.3.1 Cases considered

Based on the assumptions made in Section 4.2, the general problem to be addressed here distils down to the simple problem shown in Fig. 4.1. This is a single storey frame bay subjected to a unit horizontal load P at the left top corner, with fixed pin supports at the bottom corners. For sake of simplicity the connections between members are treated as pin joints. Edge column and beam members are assumed to be pre-existing members which have infinite reserves of strength when functioning as part of a braced frame. Note that this can be viewed as removing the bending moment effect Ph from the problem and reducing it to one of finding the optimal bracing to resist the load in pure shear (e.g. see Stromberg et al. (2012)). It is also worth noting that Rozvany et al. (2006) studied the effect of including fully and partially stressed pre-existing members in an optimization by fixing member cross-sectional areas. In this numerical study, in order to account for the possibility that pre-existing members can also disappear from the final structure (i.e. have zero force), pre-existing members are treated as being composed of material of infinite strength.

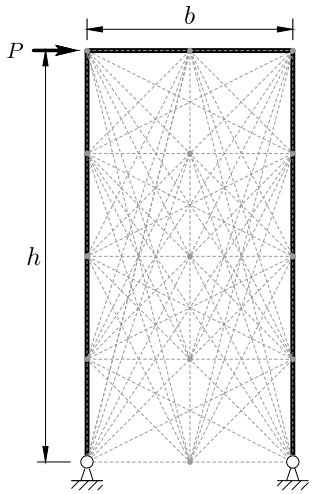

Figure 4.1: Bracing design case with pre-existing members around the edge of the bay, pinned supports at the bottom corners and a horizontal load at the top left corner. A 'ground structure' comprising interconnecting members (2×4 nodal division discretization shown, not including all connections for sake of clarity).

Two load cases involving horizontal loads of equal magnitude applied in opposite directions are

used to replicate real-world conditions, and to also ensure the resulting layout is symmetric. According to the superposition theory proposed by Hemp (1973), a two load case solution can be obtained by superposing the results from two design problems involving single load cases. Therefore, all design problems considered herein can be treated as single load case problems.

Three generic types of bracing systems are considered for various different aspect ratios ($h : b$ see Fig. 4.1):

- Case 1: Tension only bracing. This is frequently employed in practice as it obviates the need to take action to ensure compression members do not buckle. Numerically, this is implemented by making the compression stress capacity of bracing members infinitesimally small.

- Case 2: Bracing connected only at corners. Both tension and compression members are allowed to be present in the bracing system and the maximum tension stress is equal to the maximum compression stress. Numerically, bracing connected only at corners is implemented by removing the nodes along the perimeter of the design space, except at the corner points.

- Case 3: Optimal reference bracing. Both tension and compression members can be present in the bracing system and the maximum tension stress is equal to the maximum compression stress. Connections between bracing members and the beams or columns can exist at any location. The allowable stress of the bracing members is considered to be identical in both tension and compression. The resulting constraint-free bracing layout can be expected to be the most efficient of the three cases in terms of material consumption.

4.3.2 Single load case layout optimization formulation

The single load case layout optimization formulation for a two-dimensional problem can be stated as follows (after Dorn et al. (1964)):

$$\begin{aligned} &\text{min} && V = \mathbf{q}^T\mathbf{c} \\ &\text{subject to} && \mathbf{Bq} = \mathbf{f} \\ & && q_i^+, q_i^- \geq 0,\ i = 1, ..., m \end{aligned} \tag{4.2}$$

where there are m members and n nodes in the problem, and V represents the volume of the structure, $\mathbf{q}^T = \{q_1^+, q_1^-, ..., q_m^+, q_m^-\}$, $\mathbf{c}^T = \{l_1/\sigma_1^+, l_1/\sigma_1^-, ..., l_1/\sigma_m^+, l_1/\sigma_m^-\}$, where and $l_i, q_i^+, q_i^-, \sigma_i^+, \sigma_i^-$ represent, respectively, the length, tensile member force, compressive member force, tensile stress capacity and compressive stress capacity of member i. $\mathbf{B}$ is a $2n \times 2m$ equilibrium matrix and $\mathbf{f} = \{f_1^x, f_1^y, f_2^x, f_2^y, ..., f_n^x, f_n^y\}$, where f_j^x and f_j^y represent the component of load applied to node j in the x and y directions respectively. This problem is in a form suitable for solution using linear programming (LP).

The adaptive 'member adding' method proposed by Gilbert & Tyas (2003) is used to reduce the computational cost associated with solving problems; this involves solving a small initial problem involving sparse connectivity, and then iteratively adding further connections until a provably optimal solution is found. Additionally, to improve the quality of the optimized results, the geometry optimization rationalization procedure proposed by He & Gilbert (2015) is here used as a post-processing tool.

Finally, although formulation (4.2) is strictly speaking a 'plastic' formulation, the optimal layouts from plastic and elastic (minimum compliance) design optimization procedures are identical when only a single load case is involved.

4.3.3 Practical considerations

Some of the solutions generated by layout optimization are complex in form, leading to justifiable questions over their practical usefulness. However, as Cox (2014) suggested, in the field of structural design there is a need for reference solutions, against which alternatives can be judged (Cox pointed out that just as there is a limit on the theoretical thermal efficiency of a heat engine, set by the Carnot cycle, so there is a lower limit on the volume of material necessary to form a structure). Thus even a complex solution provides a useful reference against which alternative designs can be judged, where the latter may include simplified variants of the optimal reference form.

Also, many of the layouts presented in this paper contain long compression members and it might reasonably be suggested that buckling will limit the capacity of such elements in practice. However, for the purposes of this study the effect of member buckling under compressive load will be ignored. Whilst incorporating buckling may, in principle, lead to different optimal layouts,

there are two reasons for this omission. Firstly, as already stated, one goal of the study is to establish definite benchmarks for optimal layout and efficiency, against which real-world designs may be judged. The significance or otherwise of buckling effects in a given scenario depends to a great extent on specific design decisions, and this emphasizes the need for benchmarks to properly assess the effects of these decisions. Secondly, previous work by two of the present authors (Tyas et al. 2005) has indicated that the reduction in the strength of real steel members due to member buckling is rarely significant when suitable member cross-sections are used. This latter study considered standard circular hollow structural steel sections, widely available in the UK, and showed that a near-linear relationship held between member cross-sectional area and the required compression capacity for a given unrestrained length. Euler buckling was significant only for very long, and/or very lightly loaded members, whereas, '...at most combinations of load and length, there exists a member which can effectively utilize the majority of its compressive crushing strength and minimise the effect of Euler buckling'. Also buckling can often be addressed by either selecting a suitable member cross-section in the detailed design stage, and/or by providing lateral restraint at intermediate locations (e.g. at floors), though this is likely to be more difficult in the case of small buildings, with lightly loaded members.

4.4 Optimized single bay bracing designs

Optimized bracing layouts and associated volumes for each of the three cases described in Sections 4.3.1 are shown for a range of aspect ratios in Fig. 4.2a to Fig. 4.2c. The volumes of these frames are also presented in Fig. 4.3. Note that although the optimized layouts were initially obtained numerically, using the approach described in Section 4.3.1, the volumes of the simple layouts (e.g. those involving diagonal bracing) can be obtained analytically via simple calculation. Also, it is shown in Section 4.4.2 & 4.4.3 that the more complex layouts are closely related to Michell cantilevers for which known analytical solutions exist. For this reason exact analytical volumes are shown in Fig. 4.2.

4.4.1 Case 1: Tension only bracing

It is evident from Fig. 4.2a that tension only bracing leads to very simple optimized layouts. It is also evident from Fig. 4.3 that tension only bracing requires at least double the volume of material

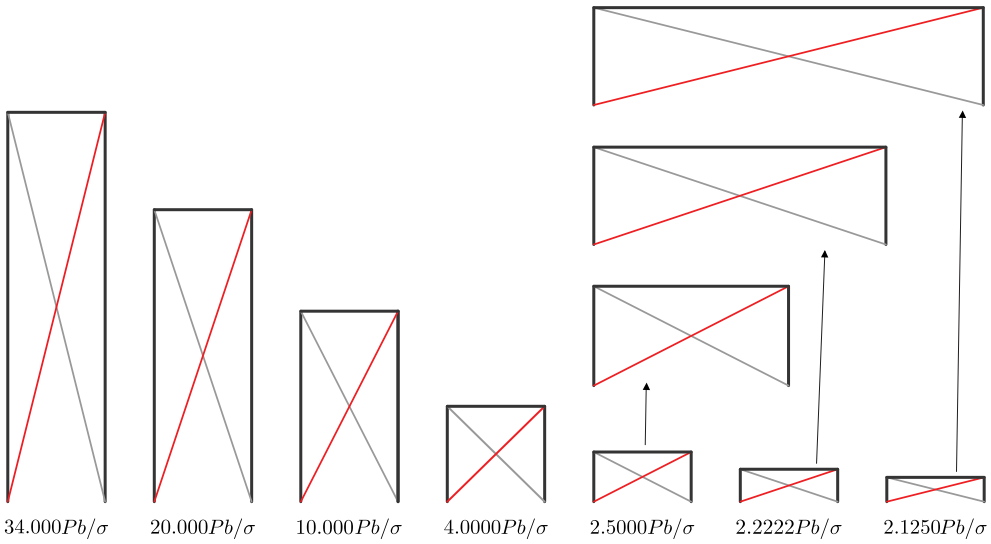

(a)

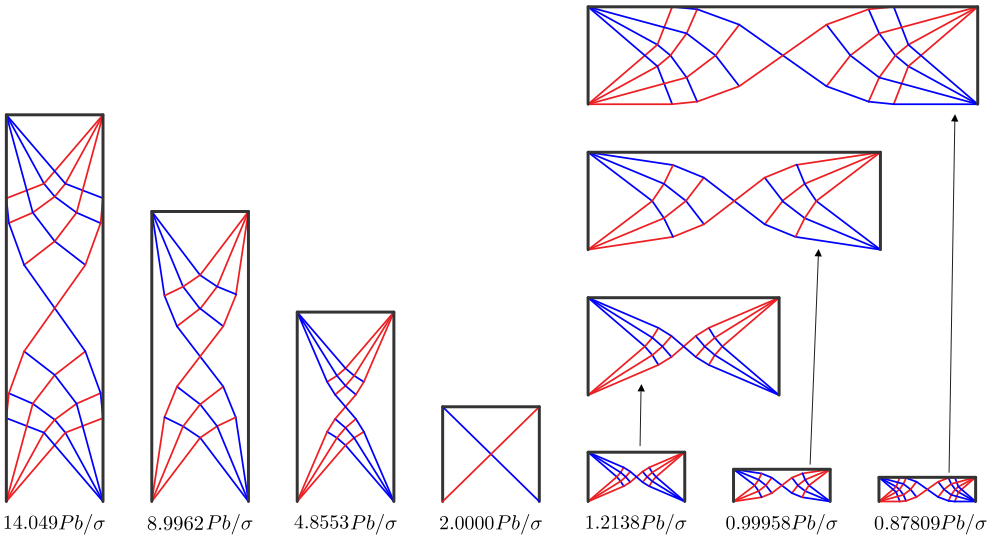

(b)

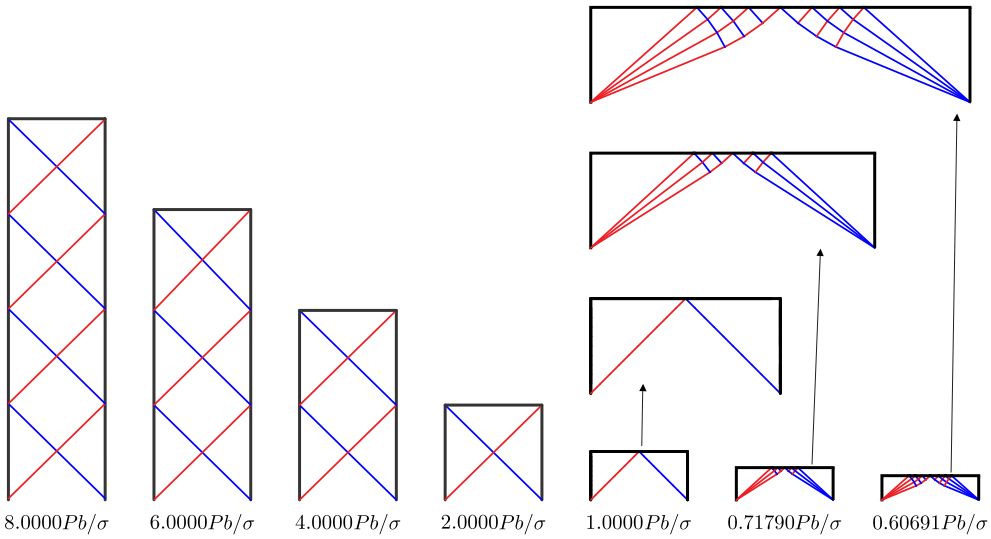

(c)

Figure 4.2: Optimized bracing layouts for various h:b aspect ratios (4:1, 3:1, 2:1, 1:1, 1:2, 1:3 & 1:4): (a) Case 1 - tension only bracing; (b) Case 2 - bracing connected only at corners; (c) Case 3 - optimal reference bracing. The corresponding analytical volume is indicated below each layout, where P is the magnitude of the horizontal load applied at the top left corner of the design domain, of breadth b and height h, and σ is the limiting tensile strength. Element color key: red = tensile, blue = compressive, grey = zero force, black = pre-existing (assuming left to right loading).

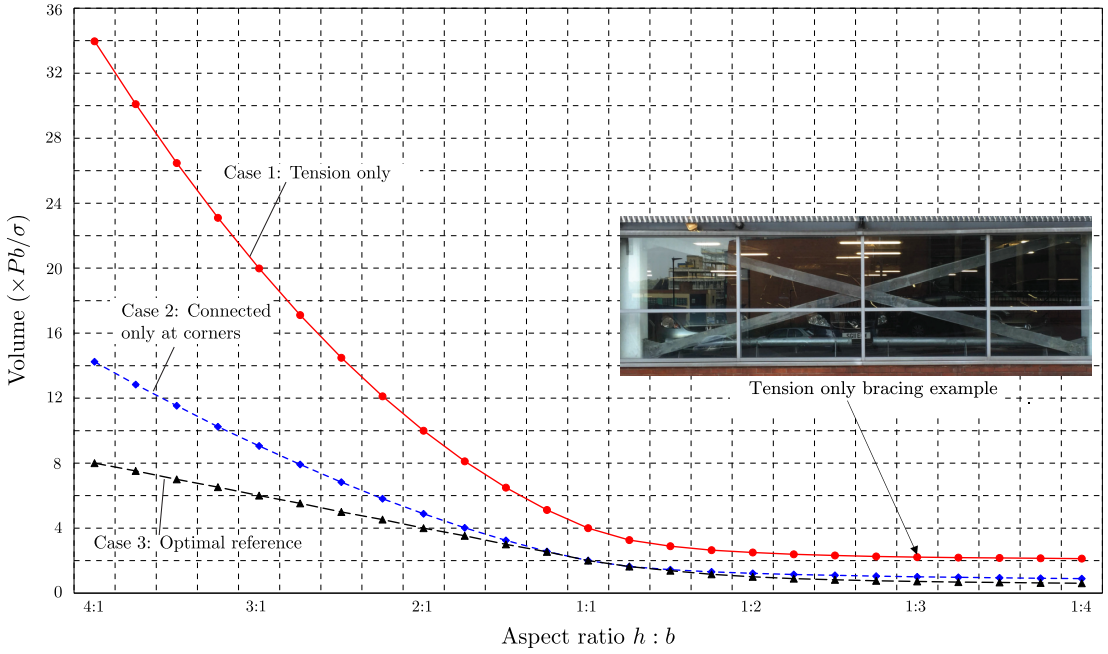

Figure 4.3: Volume comparison for the three bracing cases considered (where P is the magnitude of the horizontal load applied at the top left corner of the design domain, of breadth b and height h, and σ is the limiting tensile strength)

required by any other kind of bracing. This is because only one of the two inclined members carries a force when a horizontal load is applied. Thus, since the lateral load direction can be reversed, at least twice the volume of material must be consumed as when standard tension / compression bracing is used, assuming that the allowable stresses are equal in tension and compression. The issue of buckling must obviously be considered, but often this can be addressed by modifying the shape of the cross section and/or providing sufficient lateral restraint. The use of tension only bracing is therefore not a good choice when material savings are of paramount importance.

4.4.2 Case 2: Bracing connected only at corners

The optimized bracing layouts for Case 2, shown on Fig. 4.2b, are in most cases quite complex. It is also evident that their forms resemble Michell cantilevers. This observation gives rise to the following hypothesis:

Hypothesis 1: The optimized result for the case with connections only at corners is a combination of two adjacent Michell cantilevers, contained within a laterally restricted design space (so-called Michell cantilevers in a half strip).

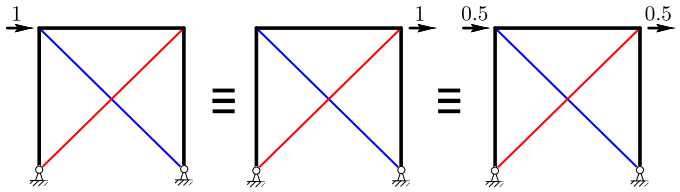

Figure 4.4: Ability of a pre-existing beam member with infinite reserves of strength to make an external load 'transmissible' (i.e. each of the above cases is equivalent)

The exact volume of a Michell cantilever in a half strip has been obtained using analytical methods by Graczykowski & Lewiński (2010). To explain the relationship between Case 2 and a Michell cantilever, first consider the influence of the infinite strength (i.e. rigid) pre-existing members. Fuchs & Moses (2000) demonstrated that a rigid member transforms any external load applied along its line of action into a 'transmissible load'. Therefore, a horizontal load applied at the end of a pre-existing beam with infinite reserves of strength can be transmitted to any other point along the beam, as illustrated in Fig. 4.4. Given this, a relationship between Case 2 and a Michell cantilever problem can be established, as indicated in Fig. 4.5. This gives rise to the following relation:

Relation 1: The volume of the optimal Case 2 layout for a problem with an aspect ratio $h : b$*, where* $h : b \geq 1$*, is twice the volume of a Michell cantilever of aspect ratio* $\frac{h}{2} : b$ *(though the latter is subjected to a loading at the centreline).*

A similar logic can also be applied for low aspect ratio cases, leading to the following relation:

Relation 2: The volume of the optimal Case 2 layout for a problem with an aspect ratio $h : b$*, where* $h : b \leq 1$*, is* $\frac{2h}{b}$ *times the volume of a Michell cantilever of aspect ratio* $h : \frac{b}{2}$ *(though the latter is subjected to a loading at the centreline).*

Therefore, using Relation 1 and 2, exact analytical solutions can be obtained for bracing problems, with numerical values for these solutions taken e.g. from Graczykowski & Lewiński (2010).

Whilst it has been demonstrated that the layouts shown in Fig. 4.2b are the combination of two constrained Michell cantilevers, an unconstrained Michell-Hemp cantilever (Hemp 1973) could alternatively be used. Fig. 4.6 shows the outcome when an expanded design domain is used, in this case using an aspect ratio of 10:1. Although unlikely to be of practical relevance, it is

of interest that the bracing volume is in this case reduced by 20.6% from the restricted domain equivalent.

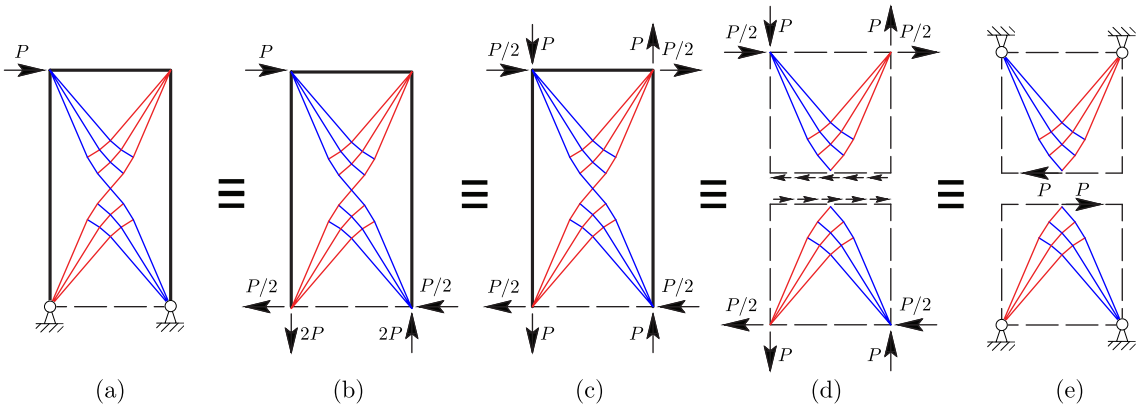

Figure 4.5: Demonstrating the equivalence between Case 2 (bracing only connected at corners) and a Hemp-Michell cantilever: (a) starting problem, in this case with a frame with a 2:1 aspect ratio; (b) base supports replaced by reaction forces; (c) corner forces replaced by equivalent loads (since forces can be distributed arbitrarily along rigid members); (d) design domain divided along line of antisymmetry; (e) corner loads replaced by supports and appropriate forces added along line of division.

4.4.3 Case 3: Optimal reference bracing

In Case 3 bracing members are free to intersect pre-existing members at any location around the perimeter of the design space, as shown in Fig. 4.2c.

An important feature of the layouts obtained is stated in Property 1:

Property 1: If a pre-existing member with infinite reserves of strength actively carries load, then the optimal intersection angle between this and intersecting tension/compression member pairs will be $45°$.

This property can easily be verified with the aid of a Mohr's circle analysis, as shown in Fig. 4.7. (It can also be observed that the angle between bracing members in tension and compression in the Mohr's circle is $180°$, or $90°$ in practice, a characteristic of an optimal Michell structure.) This presupposes that tension and compression members are simultaneously intersecting a given point on the pre-existing member, or, from an optimization theory point of view that a T-region exists within the building envelope (see e.g. Rozvany et al. (1995)). (Alternatively if a situation arises where there is only an intersecting tension or compression member (i.e. an R^+ or R^--region) then

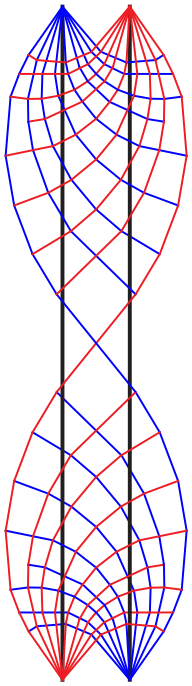

Figure 4.6: Optimized layout for Case 2 (connections only at corners) when the bracing elements are allowed to extend beyond the lines of the columns

the Mohr's circle analysis indicates that the maximum angle of intersection is $45°$.)

For low aspect ratio cases it is evident that the optimal bracing layout resembles standard knee bracing, as shown in Fig. 4.8. However, some of the layouts shown in Fig. 4.2c are rather more complex; see the 1:3 and 1:4 aspect ratio layouts. In Table (4.1) the bracing volumes are compared with the volumes of standard knee bracing; this suggests that standard knee bracing is very efficient, becoming only slightly less so as the intersection angle between the bracing members and the pre-existing frame members deviates markedly from $45°$.

It can also be observed that the more complex layouts found for low aspect ratios have similarities with the layouts of Michell cantilevers. Thus, following a similar process to that outlined in Fig. 4.5, a relationship between these layouts and the corresponding Michell cantilever truss can be established, as shown on Fig. 4.9. This leads to the following relation:

Relation 3: The volume of the optimal Case 3 layout for a problem with an aspect ratio $h : b$*, where* $h : b \leq 1$*, is* $\frac{2h}{b}$ *times the volume of a Michell cantilever of aspect ratio* $\frac{b}{2} : 2h$ *(though the latter is subjected to a loading at the centreline).*

Using Relation 3, analytical solutions can be obtained for the Case 3 low aspect ratio cases, with

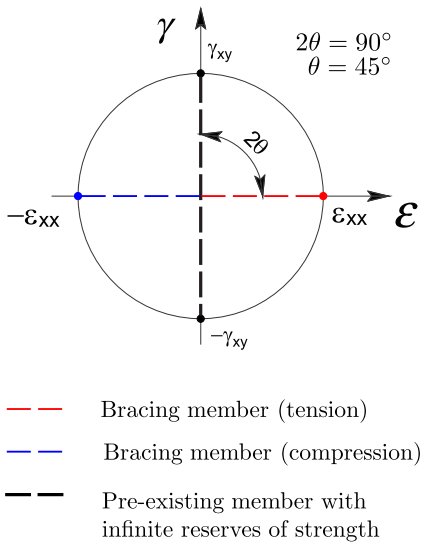

Figure 4.7: Use of a Mohr's circle analysis to demonstrate that $45°$ is the optimal intersection angle between a pre-existing beam/column and an optimal tension/compression bracing member pairs. (An optimal bracing member follows the direction of principal strain (Hemp 1973), whilst the strain in a pre-existing member is zero due to its infinite strength. Thus the subtended angle between such members will be $90°$ on the circle, or $45°$ in reality.)

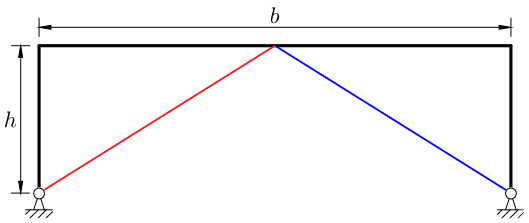

Figure 4.8: A standard knee bracing layout

Table 4.1: Comparison between optimal reference bracing (Case 3) and standard knee bracing volumes (where P is the magnitude of the horizontal load applied at the top left corner of the design domain, of breadth b and height h, and σ is the limiting tensile strength).

Aspect ratio (h:b) (Angle between knee bracing members)	1:2 (45°)	1:3 (33.7°)	1:4 (26.6°)
Volume of Case 3 optimal bracing ($\times Pb/\sigma$)	1.00	0.71790	0.60691
Volume of standard knee bracing ($\times Pb/\sigma$)	1.00	0.72222	0.62500
Difference (%)	0	0.60175	2.9806

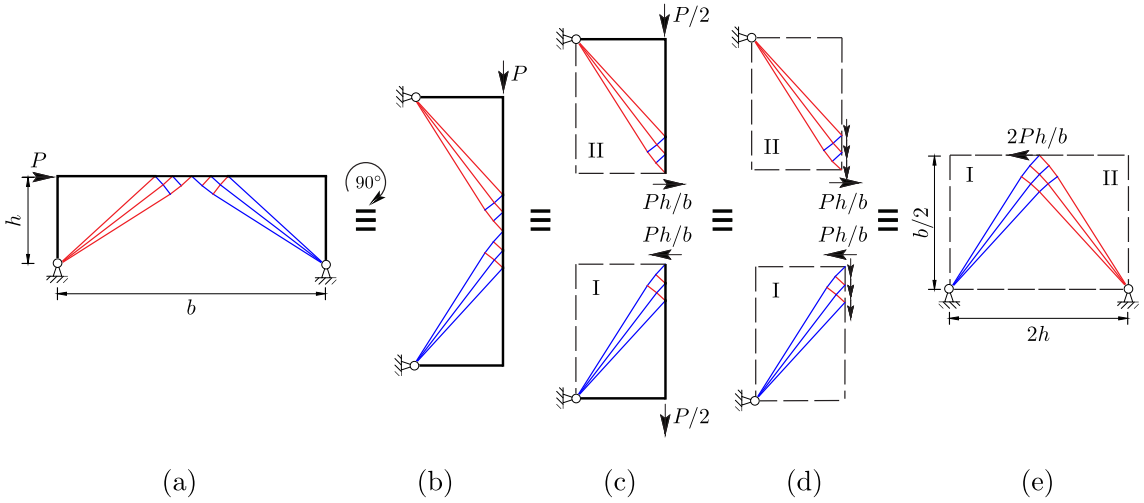

Figure 4.9: Demonstrating the equivalence between Case 3 (optimal reference bracing) and Hemp-Michell cantilever solutions: (a) starting problem, in this case using frame with 1:3 aspect ratio; (b) rotate the problem by 90° clockwise; (c) design domain divided into Structure I & II along the line of antisymmetry; (d) point loads are replaced by distributed loads (since forces can be distributed arbitrarily along rigid members); (e) Structure I & II are combined into a Michell cantilever.

numerical values for these solutions taken e.g. from Graczykowski & Lewiński (2010).

4.5 Multi-storey / multi-bay buildings

Bracing members may cross several stories in multi-storey buildings (Moon et al. 2007). In such a building each floor-slab can be considered as a pre-existing member. Therefore, in this section the focus is on considering the contribution of additional intermediate beams and columns. (Also, an intermediate pin support is added to the bottom of each intermediate column.)

Firstly, it is observed that for Cases 1, 2 and 3 all layouts revert to cross bracing once intermediate beams and columns are added. Therefore, for sake of clarity, only results for a 4:1 aspect ratio structure is considered further, as shown in Fig. 4.10a.

Since there are intermediate connections available across the height of the multiple storey building, Case 2 & 3 become identical, with the volume of the bracing structure shown in Fig. 4.10a being equal to $8.00Pb/\ \sigma$ in both cases. However, the volume of the Case 1 (tension only bracing) structure is still double the volume of the corresponding Case 2 & 3 (tension / compression bracing) structures, for the reason given in Section 4.4.1.

It is worth noting that the cross bracing layout shown in Fig. 4.10a is not the only optimal solution since there are many variants of this layout that satisfy Property 1 (see Section 4.4.3); thus

Fig. 4.10c shows an equivalent optimal solution. Additionally, it should be noted that although the results shown in Fig. 4.10 relate to the case when horizontal loads are applied only to the top of the building, due to the existence of Property 1, structures similar to Fig. 4.10c are found when loading is applied uniformly throughout the building height, with the density of the bracing net depending on the spacing between columns and beams. It can also be observed that these solutions resemble the braced tube structures that have been used in practice (e.g. see Fig. 4.10b & Fig. 4.10d). However, although 45° diagonal bracing is optimal if the assumptions stated in this paper are adopted, if bracing members are allowed to also take vertical gravity loads the optimal angle is likely to change somewhat (as is evident on Fig. 4.10b & Fig. 4.10d, where angles of less than 45° to the vertical have been adopted in practice). This suggests that there is an opportunity to develop an alternative holistic optimization approach involving multiple load cases (i.e. gravity and lateral) for the design of new buildings, though in this case it must be borne in mind that a side effect will be a lack of clarity on what constitutes 'bracing', since diagonal members may be designed to be active in both gravity only and lateral load cases.

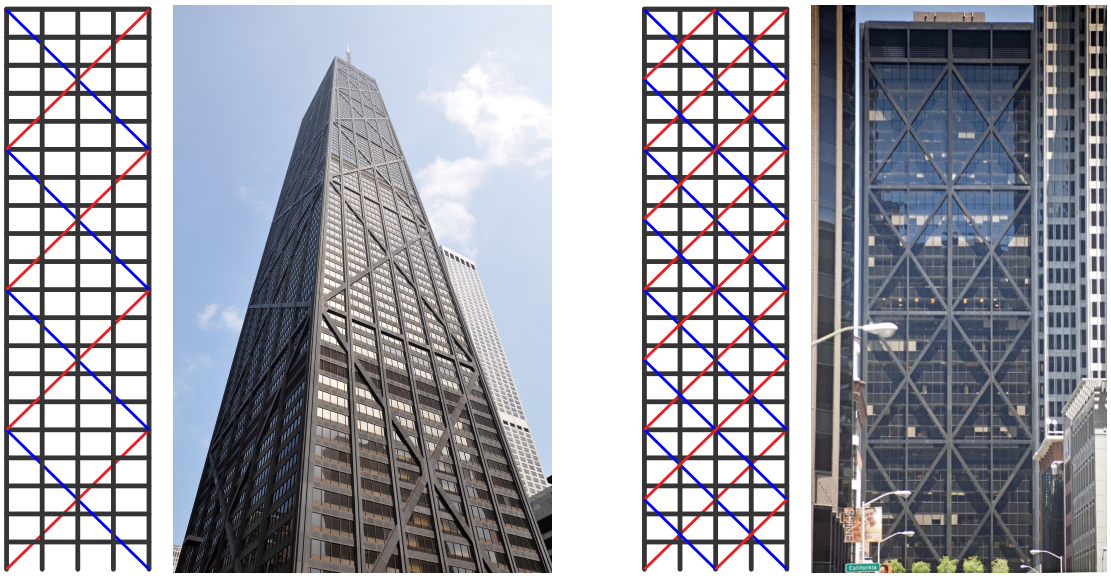

(a) (b) (c) (d)

Figure 4.10: Comparison of optimal bracing layouts in multi-storey frames and sample braced tube structures constructed in practice: (a) the optimal layout for a 4:1 aspect ratio case with intermediate pre-existing beams and columns; (b) John Hancock Center in Chicago, a braced tube structure similar to (a); (c) an alternative optimal layout with the same volume as (a); (d) One Maritime Plaza in San Francisco, a braced tube structure qualitatively similar to (c). Element color key: red = tensile, blue = compressive, black = pre-existing (assuming Case 2 or 3 bracing and left to right loading). Note however that the angles in (b) and (d) differ from the 45° found to be optimal when bracing a pre-existing frame.

4.6 Conclusions

In this paper, theoretically optimal layouts of bracing systems designed for pre-existing building frames have been identified. For the sake of simplicity, it has been assumed that pre-existing members designed for gravity loading will have sufficient reserves of strength to accommodate the additional forces that result from lateral loads. Three different cases have been considered:

- Case 1: Bracing systems comprising tension only members have been demonstrated to be inefficient from a theoretical standpoint. Replacing tension only bracing with tension/compression bracing will save at least 50% of the material needed if the limiting tensile and compressive material strengths are equal (i.e. assuming that buckling does not reduce the maximum compressive stress that can be sustained).

- Case 2: When bracing is only allowed to connect at the corners of the pre-existing frame it is shown that the optimal layout takes the form of two adjacent Michell cantilevers. This allows exact reference volumes to be obtained, against which the efficiency of other bracing layouts can be judged.

- Case 3: When bracing is allowed to connect pre-existing frame members at any location it is shown that intersecting tension/compression bracing member pairs meet each pre-existing member at 45° in the optimal layouts. It is also shown that traditional cross bracing and knee bracing are very efficient from a theoretical standpoint.

In the case of multi-storey frames, layouts involving diagonal cross-bracing, with braces meeting pre-existing members at 45°, are shown to be most efficient. Also it is evident that the theoretically optimal layouts identified herein quite closely resemble those which have been employed in braced tube building frames in practice. However, the exact reference solutions derived herein are only strictly applicable when bracing a pre-existing frame; the more general holistic frame design case, where all framing elements are optimized simultaneously, under the action of multiple load cases, is the subject of Chapter 5.

Chapter 5

Optimal bracing systems in buildings: holistic design [i]

Abstract In this study the holistic bracing design problem is considered, in which the layout of all principal members in a building structure are sought. Multiple load cases arising from the requirements of a commonly used structural design code are used to illustrate the methodology. It is found that the optimal layouts obtained differ from those obtained in Chapter 4, when bracing was sought for a pre-existing frame. It is also demonstrated that a parameter related to the difference in vertical and horizontal loads applied in different load cases is a key factor determining the optimal layout of frame members. Simple benchmark problems and a practical building design example are used to illustrate the concepts explored.

5.1 Introduction

Ensuring adequate resistance to lateral loads is central to the design of any building. When designing a building, structural engineers normally rely on codes of practice, which generally require that several separate load cases are considered. Often the load case which involves application of the maximum lateral load includes design gravity loads which are not at their maximum value. This is because it is considered improbable that maximum gravity loads will coincide with, say, maximum wind loads. As a result, in many bracing optimization studies, it is

[i] The content of this chapter was originally prepared for a journal paper: Lu, H., Gilbert, M., Tyas, A. (2017), 'Optimal bracing systems in buildings: holistic design', *Structural and multidisciplinary optimization*

assumed that the sizes of the main columns and beams in the structural frame are determined by consideration of gravity load cases (only), and that these members will have sufficient strength to play their required roles in resisting horizontal loads without needing to be resized; this scenario is considered in more detail in Chapter 4. There are consequently relatively few examples of what may be termed 'holistic' optimization of the structural frame, in which all load cases are considered when selecting all members forming the frame of a building. This runs contrary to recent practice in the field of structural engineering, where, for example, diagrid exoskeleton frames are increasingly being used to resist both vertical and lateral loads (see detail in Section 2.9).

Considering previous research involving holistic optimization of frames, Burry et al. (2005) simultaneously apply lateral and gravity loading in a shape optimization problem for a pre-defined structure, whilst Moon et al. (2007) consider diagrid bracing systems, using the angles between bracing members as parameters which are varied in order to optimize the lateral stiffness of the structure. In addition to these academic studies, optimization has been used in the practical design of landmark structures. For example in the design of the diagrid structure for the Swiss Re ('Gherkin') building in London, a parametric optimization scheme was used to design the external form to resist gravity and wind loading. Instead of using prescribed joint positions, the external form was defined by a small number of parameters, enabling a complex geometric model to be manipulated rapidly (Foster 2005). For the design of the visually striking CCTV headquarters building in Beijing, an iterative optimization process was used in the design of the bracing, adding or removing diagonals to meet the strength and stiffness requirements associated with a Level 1 earthquake (Carroll et al. 2008).

Whilst these studies have yielded interesting findings, it appears that no rigorous academic studies of the holistic frame layout design problem have been conducted to date. Addressing this is the main driver for the present study. Both theoretical and numerical layout optimization approaches are used to identify optimal framing systems capable of withstanding gravity loads only and also combined gravity plus lateral loading scenarios.

5.2 Consideration of multiple load cases

In Chapter 4, pre-existing members of the frame (i.e. beams and columns which have already been designed to resist gravity loads) are assumed to have infinite reserves of strength, and do not need to be resized to play an active role in the bracing system. However, this may not always be a valid, conservative, assumption. For example, it is possible in the case of a tall, slender, frame that the design of the columns may be partly determined by the loads induced in them by the lateral load. Additionally, decoupling the different load cases in this way may mean that more optimal holistic designs are missed. Therefore in this chapter, all main load cases are considered in the optimization.

As stated in Chapter 4, for the design of steel framed buildings, British Standard 5950-1:2000 suggests the following load combinations:

$$p_1 : 1.4G_{\mathrm{k}} + 1.6Q_{\mathrm{k}} \tag{5.1a}$$

$$p_2 : 1.0G_{\mathrm{k}} + 1.2Q_{\mathrm{k}} + 1.2W_{\mathrm{k}} \tag{5.1b}$$

$$p_3 : 1.0G_{\mathrm{k}} + 1.2Q_{\mathrm{k}} - 1.2W_{\mathrm{k}} \tag{5.1c}$$

where G_{k} is the characteristic permanent load, Q_{k} is the characteristic imposed load and W_{k} is the characteristic wind load. (For sake of simplicity notional horizontal forces are neglected.)

To tackle the resulting design problem three assumptions were introduced in Chapter 4:

- Assumption 1: The loads generated in the columns in load case (5.1b) and (5.1c) are always less than those resulting from load case (5.1a).
- Assumption 2: Vertical gravity loads are only carried by the columns in all load cases.
- Assumption 3: The sizes of pre-existing horizontal members (i.e. floor beams and/or slabs) are dominated by the gravity load case, (5.1a), and the axial loads induced in them by lateral load cases (5.1b) and (5.1c) are small in comparison.

In this chapter, all of these assumptions are removed. This means that vertical loads can be resisted

by any frame member, and the sizes of the column members may be partly governed by the lateral load cases.

5.2.1 Parameter governing the optimal layout, ΔV_{norm}

Using the British Standard load cases (5.1) and with Assumptions 1, 2 and 3 removed, a parameter governing the optimal layout can be identified. To establish this, Rozvany's work on optimization with multiple load cases (Rozvany et al. 2014) and the superposition method of Rozvany & Hill (1978) will be used.

Figure (5.1a) shows a graphical depiction of the load cases (5.1). Here V is the vertical load in load cases (5.1b) and (5.1c) (i.e. $1.0G_{\text{k}} + 1.2Q_{\text{k}}$) and ΔV is the additional vertical load in load case (5.1a) (i.e. $0.4G_{\text{k}}+0.4Q_{\text{k}}$). ΔH is used to represent the difference in horizontal load between the gravity and lateral load cases. Since the horizontal loads in the first load case are equal to zero, $\Delta H = H$.

The optimized solution to the problem shown in Fig. 5.1a can be obtained using the superposition approach put forward by Rozvany & Hill (1978). However, this approach requires there to be 2^n load cases, with n being a positive integer. Following Rozvany et al. (2014), a fourth, dummy load case p_4 can be introduced, comprising vertical loads $V-\Delta V$. According to Property 3 in Rozvany et al. (2014), since $\Delta V > 0$, the optimized result for the problems shown in Fig. 5.1a and Fig. 5.1b must be identical. Providing the problem shown in Fig. 5.1b satisfies the specific conditions of the superposition approach, then the optimized solution may be obtained by superimposing the optimized results of four single component load cases $\overline{p}_1$ to $\overline{p}_4$; see Fig. 5.1c. Derivation of the component load cases $\overline{p}_1$ to $\overline{p}_4$ is presented in Appendix I of current chapter.

Using the superposition approach, the optimum structure for all four load cases can be obtained by superimposing the optimal layouts for each of the four individual component load cases. Referring to Fig. 5.1c, it is obvious that the optimal layout for load case $\overline{p}_1$ will be vertical columns running along the outer edges of the domain. Also, it is obvious that the optimal layout for load case $\overline{p}_4$ will comprise no members at all (since there are no applied loads). Therefore, the optimal bracing layout can be obtained simply by superimposing the optimal layouts arising from load cases $\overline{p_2}$ and $\overline{p_3}$. As these latter layouts depend only on ΔV and ΔH, a new parameter $\Delta V_{\text{norm}} = \Delta V/\Delta H$ can be introduced as the parameter that controls the form of the optimal layout. Table (5.1) shows

a sample calculation of ΔV_{norm}. To verify the correctness of the superposition approach, solutions were also obtained for sample problems using the standard multiple load case LP formulation, as shown on Fig. 5.2 (details of the formulation are given in Appendix II of current chapter).

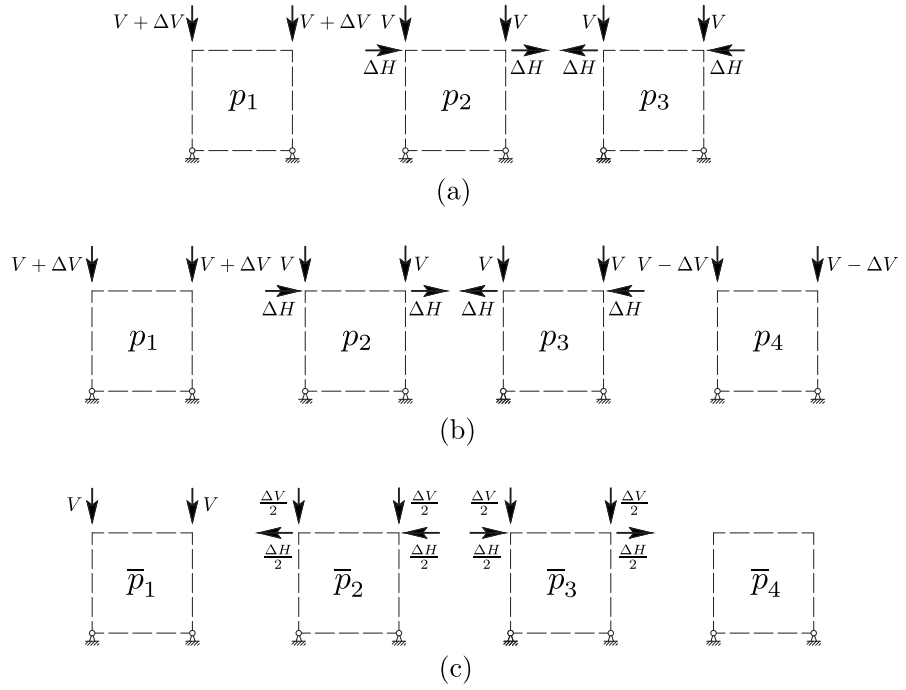

Figure 5.1: Use of superposition approach to derive the optimization result of multiple load cases: (a) three load cases based on British Standard load case combination, where $V = 1.0G_{\text{k}} + 1.2Q_{\text{k}}$, $\Delta V = 0.4G_{\text{k}} + 0.4Q_{\text{k}}$, $\Delta H = 1.2W_{\text{k}}$, where G_{k}, Q_{k} and W_{k} are, respectively, characteristic permanent, imposed and wind loads; (b) as (a) but with additional dummy load case added to enable superposition principle to be applied; (c) using superposition, the solution to (b) can be obtained by superimposing the individual results from four single load case problems, $\overline{p}_1$ to $\overline{p}_4$.

Table 5.1: Calculation example of parameter ΔV_{norm}, where p_i represents the ith load case.

Load case	Load type	Load magnitude
p_1	Vertical load	400 kN
	Horizontal load	0 kN
p_2	Vertical load	200 kN
	Horizontal load	100 kN
	ΔV_{norm}	$(400-200)/(100-0) = 2$

The finding that there is a parameter ΔV_{norm} which governs the optimal layout is significant. Since different design codes stipulate that different combinations of loads are involved in the various load cases to be considered, this indicates that the optimal layout will be strongly influenced by the choice of design code. This fact is unlikely to have been anticipated by the code writers.

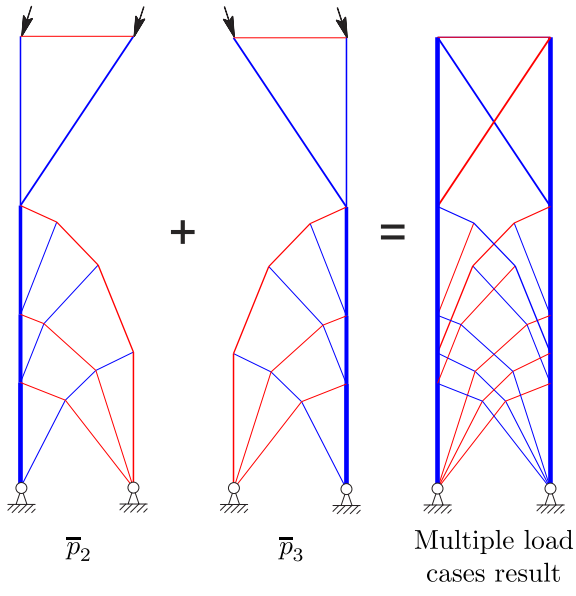

(a)

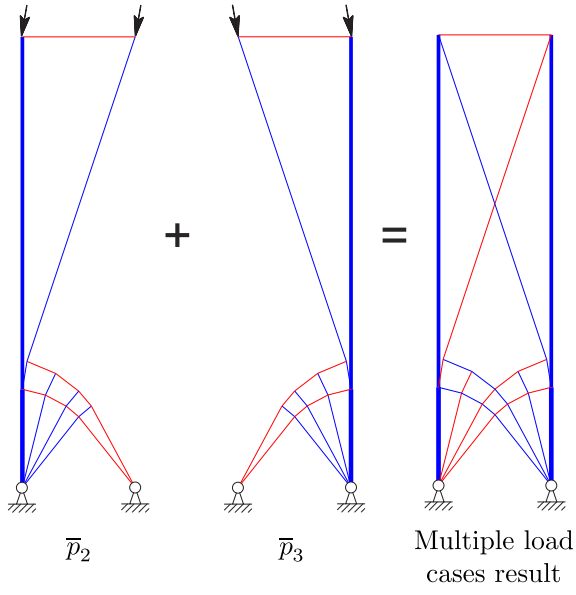

(b)

Figure 5.2: Numerical verification of superposition approach using layout and geometry optimization: (a) example with $\Delta V_{\text{norm}} = 3$; (b) example with $\Delta V_{\text{norm}} = 6$, where ΔV_{norm} is the parameter governing layout for multiple load case problems. On the left hand side are optimized results from single component load cases $\overline{p}_2$ and $\overline{p}_3$, see Fig. 5.1c, and on the right hand side are multiple load case results. Red and blue bars represent, respectively, members taking tensile and compressive forces. For the multiple load case results the force distribution shown corresponds to the load case with horizontal loads acting from left to right.

5.3 Examples: simple single and multi-storey braced frames

In this section, examples of the relationships between ΔV_{norm} and the optimal layout are presented for two types of braced bay, one with loading applied only at the top corners of the design domain, and the other with the frame split into square vertical bays with loading at each 'floor' level. The

numerical multiple loading layout optimization approach described in Appendix II is used.

5.3.1 Problem definition

Figure (5.3) shows the design domain and load and support conditions for the cases considered in this study. For sake of simplicity, the aspect ratio of the design domain of all cases has been fixed to 4:1. Table (5.2) presents the values of the load parameter V and H in Fig. 5.3. In the study V is kept constant but the horizontal load H is varied, replicating a changing external environment. For the vertical load V defined by the British Standard the ratio of the vertical load in the gravity and wind load cases can be denoted c, where:

$$c = \frac{1.4G_{\mathrm{k}} + 1.6Q_{\mathrm{k}}}{1.0G_{\mathrm{k}} + 1.2Q_{\mathrm{k}}} = 1.33 + \frac{0.07G_{\mathrm{k}}}{1.0G_{\mathrm{k}} + 1.2Q_{\mathrm{k}}} \tag{5.2}$$

Therefore, from Eqn. (5.2), it is clear that $c_{min} = 1.33$ when $G_{\mathrm{k}} = 0$ and $c_{max} = 1.40$ when $Q_{\mathrm{k}} = 0$. This means that the horizontal load H equals $\frac{(c-1)P}{\Delta V_{\mathrm{norm}}}$ and $-\frac{(c-1)P}{\Delta V_{\mathrm{norm}}}$ in load cases p_2 and p_3 respectively. For the examples documented, c has been taken as 1.35, though with checks later undertaken using c = 1.33 and c = 1.40 to verify that the main findings were largely unaffected by this choice.

The volumes of the optimized layouts are compared to two other layouts: standard cross bracing and the modified layout identified by Stromberg et al. (2012).

5.3.2 Optimal layout results

Figures 5.4 and 5.5 show the optimal layouts and corresponding normalized volumes for the single and multi-storey frames described in Section 5.3.1. Note that simple (pinned) frame connections have been assumed in the models. Also note that, as indicated in Table (5.2), a high value of ΔV_{norm} is associated with a low value of lateral load H.

Firstly, as expected, the optimized bracing can be observed to always be more efficient (i.e. to consume less material) than both standard cross bracing and Stromberg bracing. However, the differences between the normalized volumes of the different layouts are comparatively small (maximum difference is 7%). This is partly because the normalized volume includes both the

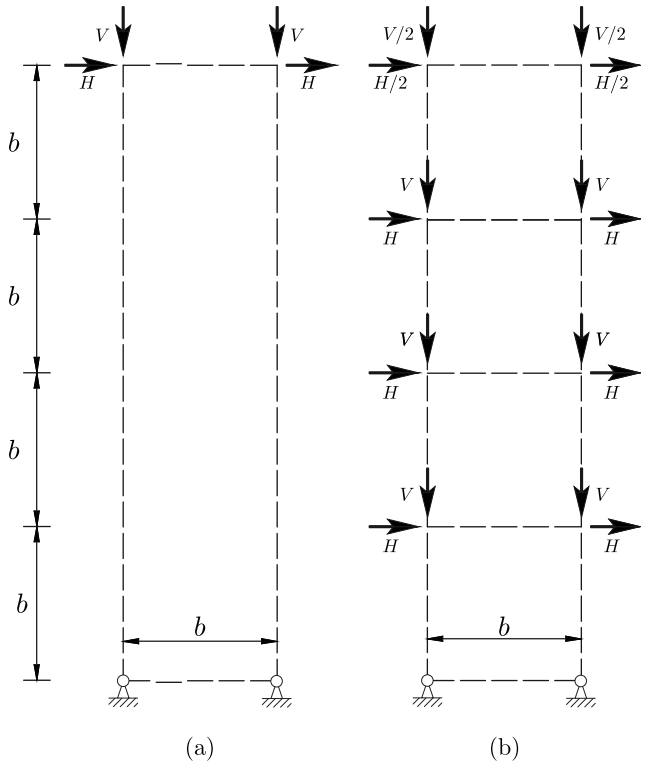

Figure 5.3: Loads for single- and multi-storey bracing layout optimization study: (a) single-storey cases; (b) multiple-storey cases; values of V and H are given in Table 3.

volume of vertical columns and the volume of interconnecting bracing elements.

Secondly, it is clear that as ΔV_{norm} increases, the optimized layouts tend to include highly inclined members to transmit the applied vertical loading more directly towards the supports. This finding is at variance with the finding in Chapter 4 that there should be a 45° intersection angle between columns and bracing members, since this only applies if the columns are assumed to have infinite reserves of strength, which is not the case here.

Thirdly, it is clear that whilst Stromberg bracing is more efficient than standard cross bracing when ΔV_{norm} is low, the situation is reversed when ΔV_{norm} is high. This is a result of the fact that the shallow inclined members of the Stromberg bracing layout are most suitable for cases when horizontal loads are significant. In such cases it can be observed that Stromberg bracing has a much simpler layout than the optimized layouts, but the associated volume is only slightly higher. This suggests that Stromberg bracing provides a practical layout.

Table 5.2: Load values of V and H in different load cases, where p_i represents the ith load case; P is a unit load; c is a loading coefficient, assumed to be 1.35 based on British Standard 5950-1:2000 load case combinations, see Eqn. (1); ΔV_{norm} is the parameter governing layout for multiple load case problems (load positions are shown in Fig. 5.3).

Load case	Load type	Load magnitude
p_1	V	$c \cdot P$
	H	0
p_2	V	P
	H	$\frac{(c-1)P}{\Delta V_{\text{norm}}}$
p_3	V	P
	H	$-\frac{(c-1)P}{\Delta V_{\text{norm}}}$

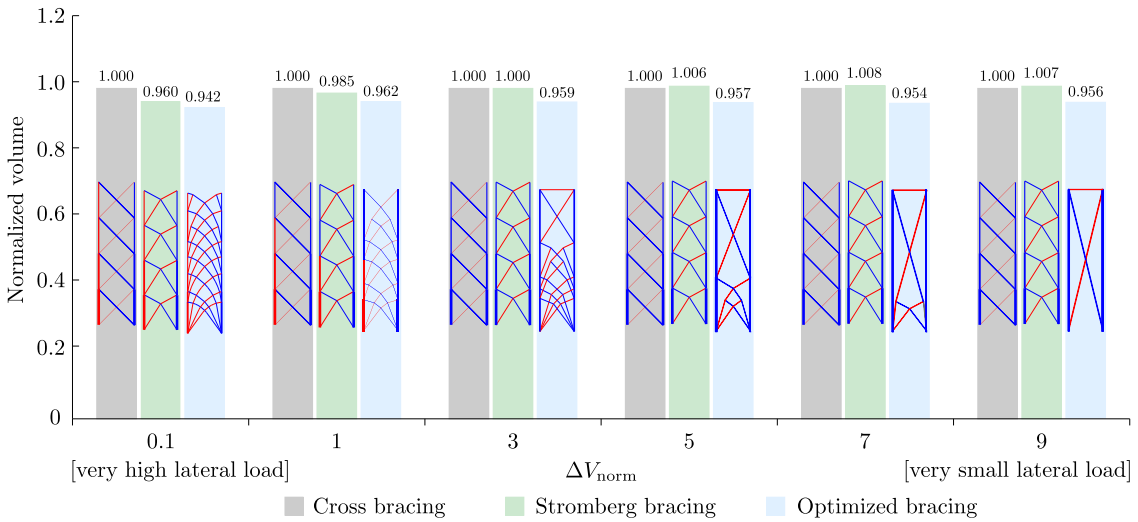

Figure 5.4: Volume comparison and optimized layout results for a single-storey frame based on British Standard loading with $c = 1.35$ and $\Delta V_{\text{norm}} = (0.4G_{\text{k}} + 0.4Q_{\text{k}})/(1.2W_{\text{k}})$, where c is the ratio of the vertical load between load cases (i.e. $(1.4G_{\text{k}} + 1.6Q_{\text{k}})/(1.0G_{\text{k}} + 1.2Q_{\text{k}})$); all the volumes are normalized against the volumes of standard cross bracing systems; red and blue bars represent, respectively, members taking tensile and compressive forces when horizontal loads are applied from left to right.

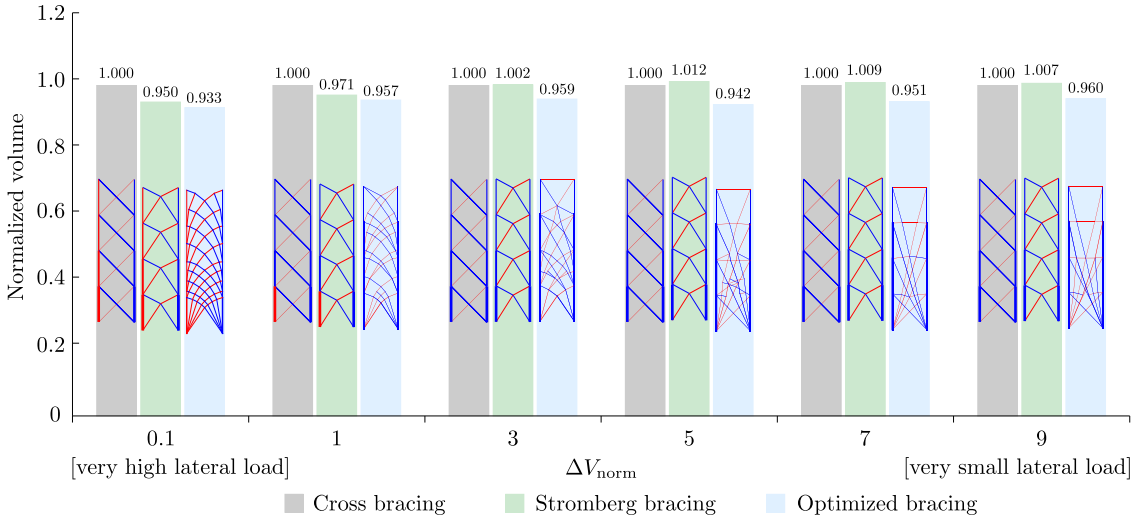

Figure 5.5: Volume comparison and optimized layout results of multi-storey cases based on British Standard loading with $c = 1.35$ and $\Delta V_{\text{norm}} = (0.4G_{\text{k}} + 0.4Q_{\text{k}})/(1.2W_{\text{k}})$, where c is the ratio in vertical load between load cases (e.g. $(1.4G_{\text{k}} + 1.6Q_{\text{k}})/(1.0G_{\text{k}} + 1.2Q_{\text{k}})$); all the volumes are normalized against the volumes of standard cross bracing systems;red, blue bars represent, respectively, members taking tensile and compressive forces in the load case which includes horizontal loads from left to right.

5.4 Bracing design of a small office building

Here the optimization of the frame of a four-storey steel frame structure for a small office building is considered. In this case ΔV_{norm} equals 0.68 and 2.33 for the major and minor wind directions respectively.

Figure 5.6 shows details of the building. Lateral stability of the frame is provided by the presence of braced bays through the full height of the frame (Fig. 5.6 shows a typical plan above ground floor level). Actions applied to this structure are shown in Table (5.3). Load cases for a braced bay are based on British Standard loads, defined in Eqn. (5.1). For sake of simplicity only the wind load case acting normal to the long side of the building, and the design of the bracing resisting this load is considered in the design. The steel has a yield stress of 355MPa in both tension and compression and an elastic modulus of 205GPa.

The optimized bracing design is shown in Fig. 5.7a. To permit comparison, a conventional design is shown in Fig. 5.7c, depicting the bracing layout presented by Brettle & Brown (2009). An intermediate optimized design, which is obtained in optimization with horizontal beams, is also shown in Fig. 5.7b.

To achieve the conventional design shown in Fig. 5.7c, Brettle & Brown (2009) kept the sizes of all columns and bracing members constant throughout the height of the frame, even though the

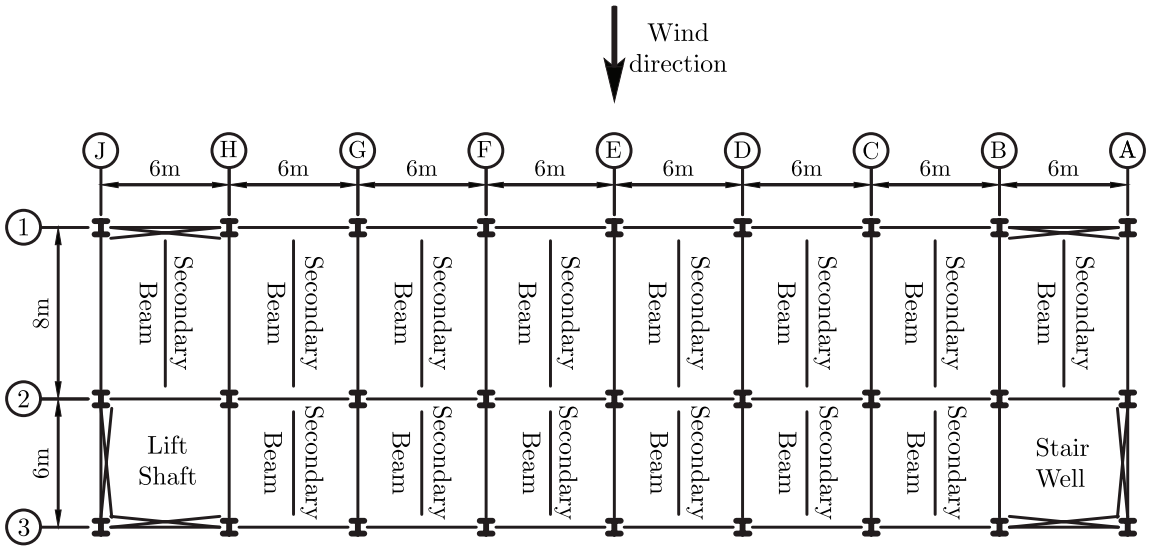

Figure 5.6: Plan of a typical small office building, after Brettle & Brown (2009)

Table 5.3: Characteristic actions on the small office building

	Actions on roof	Actions on floors
Permanent action	0.9kN/m^2	3.7kN/m^2
Variable action	0.6kN/m^2	3.3kN/m^2
Wind action	89.5kN	187.1kN

forces in the members reduce significantly from ground to top floor. This kind of rationalization is common in practice. However, to remove the associated inefficiency, and hence to provide a fair comparison with the optimized layouts, here the members were resized, with the chosen sections being the most efficient H-section column and circular hollow sections available in the UK (Tata Steel Europe Limited 2016). The horizontal beams used in the conventional design were then also used as pre-existing members in the intermediate optimized design shown in Fig. 5.7b.

To realize the optimized designs shown in Fig. 5.7a and Fig. 5.7b a two-stage process was adopted. Firstly, layout optimization and geometry optimization were used to find the optimal layout of the braced bay (the 6m wide four-storey right hand bay shown in Fig. 5.6) and associated volume of required material (these were 0.0900m^3 and 0.0976m^3 for the layouts shown in Fig. 5.7a and Fig. 5.7b respectively, compared with 0.1032m^3 for the layout shown in Fig. 5.7c). Secondly, in a post-optimization rationalization step the column and inclined bracing members were each assigned the most efficient Tata Steel section to transmit the required load, taking account of member buckling effects in compression members as necessary. The total steel masses of the resulting optimized bracing systems are shown in Fig. 5.7. The structure shown in Fig. 5.7a

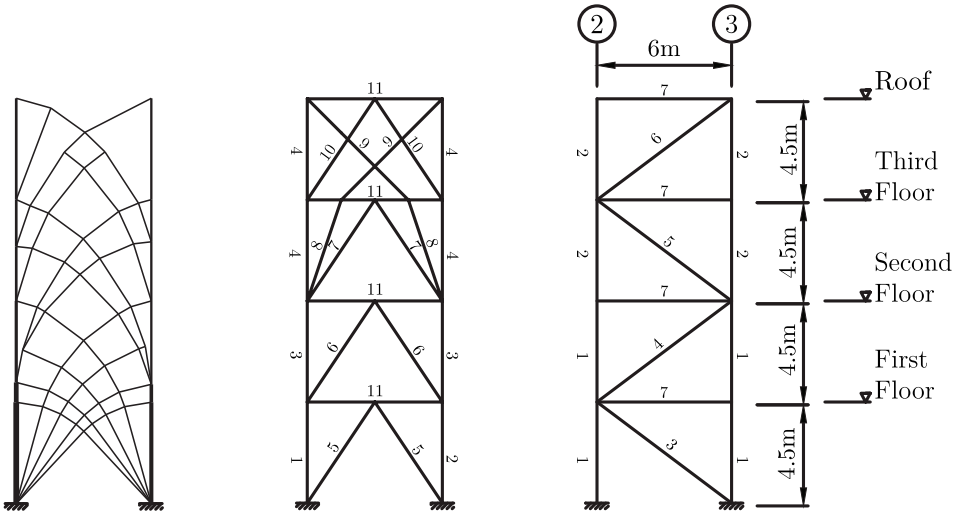

1	UKC 203 × 203 × 52
2	UKC 203 × 203 × 46
3	UKC 152 × 152 × 37
4	UKC 152 × 152 × 23
5	CHS 168.3 × 8.0
6	CHS 168.3 × 5.0
7	CHS 139.7 × 5.0
8	CHS 76.1 × 2.9
9	CHS 60.3 × 2.6
10	CHS 48.3 × 2.6
11	UKB 203× 133 × 25

(d)

1	UKC 203 × 203 × 46
2	UKC 152 × 152 × 23
3	CHS 219.1×8.0
4	CHS 219.1×5.6
5	CHS 193.7×5.0
6	CHS 139×3.6
7	UKB 203 × 133 × 25

(e)

Figure 5.7: Different braced bay designs for a typical small office building: (a) optimized bracing design; (b) optimized deisign with pre-existing beams; (c) conventional braced bay; (d) sections chosen for the structure shown in (b), with buckling effects considered; (e) sections chosen for the structure in (c), with buckling effects considered. Note that the selected bay could be found in Fig. 5.6 using reference points in this graph.

has the lowest mass, representing a 32% material saving compared to the conventional design shown in Fig. 5.7c (this is greater than the reduction prior to rationalization, of 13%, which in turn exceeds the reductions found previously due to the comparative inefficiency of the layout shown in Fig. 5.7c).

In addition to the strength of the bracing system, the stiffness of the frame must also be checked. Linear elastic static analyses were therefore conducted as a post-processing step for the three cases, considering load case (5.1b). The tip displacements for the designs shown in Fig. 5.7a, (5.7b) and (5.7c) were found to be 55.1mm, 44.5mm and 57.7mm respectively, which all satisfy the design code requirements (for details see Appendix III).

Compared to the optimized design shown in Fig. 5.7a, the intermediate optimized structure containing pre-existing beams (Fig. 5.7b) has a simpler layout and is thus likely to be easier to construct in practice; Fig. 5.8a shows a visualization of how this could look in reality.

5.5 Conclusions

In this paper layout optimization has been used to identify efficient bracing systems for building frames. Whereas Chapter 4 considered bracing for frames containing pre-existing members, in this chapter a holistic optimization strategy in which the sizes and locations of all members are sought has been adopted. The following conclusions can be drawn:

- The optimal layouts obtained using the holistic strategy differ from those obtained when seeking to brace a frame comprising pre-existing members (as considered in Chapter 4).
- For the simple holistic design problems involving square bays, the optimal layouts obtained were only slightly more efficient than the layouts incorporating 45° cross-bracing or Stromberg bracing (max. difference = 7%).
- When one of the applied load cases involves no lateral load, the optimal layout was found to be controlled by a parameter ΔV_{norm}, where $\Delta V_{\text{norm}} = \Delta V / \Delta H$ and ΔV and ΔH represent respectively the differences in vertical and horizontal load between the load cases.
- Since different design codes stipulate different combinations of loads in the various load cases considered, this indicates that the optimal layout will be influenced by the choice of

Figure 5.8: Visualization of small office building employing optimized bracing structure shown in Fig. 5.7b

design code. This outcome is unlikely to have been anticipated by the code writers.

- The bracing layout presented by Stromberg et al. (2012) has been found to be very efficient in cases where the horizontal load dominates (e.g. $\Delta V_{\text{norm}} < 3$). However, standard cross bracing becomes more efficient when the vertical load dominates (e.g. $\Delta V_{\text{norm}} \geq 3$).

- Adopting a holistic design strategy, in which non-vertical members are allowed to carry gravity loads as well as act as bracing members, appears to be most worthwhile in cases where the vertical load dominates (e.g. $\Delta V_{\text{norm}} \geq 5$).

- Layout optimization has been applied to the design of the frame of a small four storey office building comprising rectangular bays. This led to an unconventional frame layout and a reduction in the volume of material required compared with the conventional layout considered (13% prior to rationalization).

Appendix I : Application of principle of superposition

A superposition approach may be used to obtain the optimization solution for multiple load cases via superimposing the optimization solutions of certain single component load cases. Hemp (1973) first demonstrated that this approach could be applied to two arbitrary multiple load cases and it was later expanded by Rozvany & Hill (1978) to be suitable for more than two load cases. Nevertheless, in situations with more than two load cases, certain conditions need to be fulfilled for the superposition approach of Rozvany & Hill (1978) to be valid. Rozvany and Hill's method involves the replacement of the actual load cases with associated "component" load cases. In situation with four alternative load cases (e.g. p_1, p_2, p_3 and p_4), there exist four component load cases in superposition approach (e.g. $\overline{p}_1$, $\overline{p}_2$, $\overline{p}_3$ and $\overline{p}_4$) and each of them could be obtained based on the original four alternative load cases using Eqn. (5.3).

$$\overline{\mathbf{p}} = \frac{1}{4} \begin{bmatrix} 1 & 1 & 1 & 1 \\ 1 & -1 & 1 & -1 \\ 1 & 1 & -1 & -1 \\ 1 & -1 & -1 & 1 \end{bmatrix} \mathbf{p}, \tag{5.3}$$

where $\overline{\mathbf{p}} = \{\overline{p}_1, \overline{p}_2, ..., \overline{p}_n\}$ is the vector of component load cases; $\mathbf{p} = \{p_1, p_2, ..., p_n\}$ is the

vector of alternative load cases.

Rozvany & Hill (1978) demonstrate that, if one of several specific conditions is met at every point in the design domain, then the superposition approach is feasible. For sake of simplicity, two necessary conditions are set out here for the case of four actual load cases.

Condition 1 requires that, at an arbitrary point in the design domain, the sum of the maximum and minimum stresses from the four load cases is not less than the sum of the stresses from the other two load cases (e.g. (5.4)).

$$|q_1| + |q_4| \geq |q_2| + |q_3| \tag{5.4}$$

where q_i is the stress at an arbitrary position within the design domain under ith load case ; $\max_i|q_i| = |q_1|$ and $\min_i|q_i| = |q_4|$ after subscript arrangement.

Condition 2 requires, at any arbitrary point in the design domain, the stress generated by at least one of the component load cases is zero.

Given the method to obtain component load cases and the conditions for superpositon approach, proving the superposition approach is feasible for case shown in Fig. 5.1b can be divided into two parts. Firstly, consider an arbitrary point at any location within the design domain, except the two vertical edges. It is clear that under component load case $\overline{p}_1$ in Fig. 5.1c, at all such points the stresses equal to zero. Secondly, for an arbitrary point at the left vertical edges on two sides, consider the four load cases shown in Fig. 5.1b, stress of this point resulted by the four load cases (e.g. q_1, q_2, q_3 and q_4) have the following relation:

$$\begin{aligned} &q_1 \propto V + \Delta V \qquad q_2 \propto V - \Delta B \\ &q_3 \propto V + \Delta B \qquad q_4 \propto V - \Delta V \\ &\text{where } \Delta B \text{ is the stress change caused by the bending} \\ &\text{effect of } \Delta H \text{ on the design domain.} \end{aligned} \tag{5.5}$$

In case shown in Fig. 5.1, ΔV and ΔB are relatively small compared to V, therefore $V - \Delta B > 0$ and $V - \Delta V > 0$. It is thus clear that $|q_1| + |q_4| = |q_2| + |q_3|$, which means that points in the left edge fulfils Condition 1. This argument clearly applies equally to the right edge. Consequently, one of the two conditions applies at each and every point in the design domain, and thus the

superposition approach is feasible to be used in case shown in Fig. 5.1b to derive the optimized result.

Appendix II : Multiple load case plastic layout optimization formulation

The LP plastic truss layout optimization problem formulation for problems involving multiple load cases can be written as:

$$\begin{aligned} &\text{min} && V = \mathbf{l^T a} \\ &\text{subject to} && \mathbf{B q}^\alpha = \mathbf{f}^\alpha \\ & && \mathbf{a} \geq 0 \\ & && a_i \geq \{q_i^+/\sigma_i^+ + q_i^-/\sigma_i^-\}^\alpha \\ & && \{q_i^+\}^\alpha, \{q_i^-\}^\alpha \geq 0 \end{aligned} \tag{5.6}$$

where $\alpha = 1, 2, ..., M$ and $i = 1, 2, ..., m$; and M, m, n represent, respectively, the number of load cases, members and nodes of the design problem; V represents total structure volume, $\mathbf{a} = \{a_1, a_2, ..., a_i\}$, $\mathbf{l} = \{l_1, l_2, ..., l_i\}$, $\mathbf{B}$ is a suitable $(2n \times 2m)$ equilibrium matrix, $\mathbf{q^T} = \{q_1^+, -q_1^-, ..., q_m^+, -q_m^-\}$, $\mathbf{f}^\alpha$ is the load case vector, where $\mathbf{f}^\alpha = \{f_1^x, f_1^y, ..., f_n^x, f_n^y\}^\alpha$; and $a_i, l_i, q_i^+, q_i^-, \sigma_i^+, \sigma_i^-$ represent, respectively, the cross section area, length, tensile force, compressive force, tensile stress capacity and compressive stress capacity of member i and also $\{f_j^x\}^\alpha$ and $\{f_j^y\}^\alpha$ represent, respectively, the x and y direction component load applied on node j in load case α.

The adaptive member adding method for multiple load case problem proposed by Pritchard et al. (2005) has been employed to reduce the computational cost and the geometry optimization rationalization scheme propose by He & Gilbert (2015) has been used to simplify the resulting layouts shown herein.

Appendix III : Influence of second order effects

One main function of bracing is to control the second order effects induced by lateral displacements. Here the practical design example described in Section 5.4 will be considered.

Eurocode 3 (1993) uses a parameter α_{cr} to account for second order effects. An approximate formula for α_{cr} is shown in Eqn. (5.7). Eurocode 3 stipulates that, using an elastic analysis, if $\alpha_{cr} > 10$, then second order effects can be neglected. If $3 > \alpha_{cr} > 10$, then the amplification factor given in Eqn. (5.8) must be applied to the horizontal load. If $\alpha_{cr} < 3$, then a global second order effect analysis must be carried out.

$$\alpha_{\text{cr}} = \left(\frac{H_{\text{Ed}}}{V_{\text{Ed}}}\right)\left(\frac{h}{\delta_{\text{H,Ed}}}\right) \tag{5.7}$$

$$\text{Amplification factor} = \frac{\alpha_{\text{cr}}}{\alpha_{\text{cr}} - 1} \tag{5.8}$$

where H_{Ed} is the total horizontal reaction at the bottom of the storey, V_{Ed} is the total design vertical load applied on the storey, h is storey height and $\delta_{\text{H,Ed}}$ is the horizontal displacement at the top of the storey, relative to the bottom, calculated using an elastic analysis.

For each structure shown in Fig. 5.7 values for α_{cr} can be obtained for each storey and the minimum of these found. The minimum α_{cr} values for Fig. 5.7a, Fig. 5.7b and Fig. 5.7c were found to be 19.20, 27.55 and 23.47 respectively. Since all these values are larger than 10, then, according to Eurocode 3, second order effects can be neglected.

In some circumstances α_{cr} may drop below 10. In this case the amplification factor shown in Eqn. (5.8) can be employed during the layout optimization process to obtain an acceptable design.

Chapter 6

Bracing topology optimization with transmissible loads

6.1 Introduction

Whilst wind loading is treated as position-fixed loading in all the scenarios of Chapters 4 and 5, in reality, the acting positions of wind loads are effectively dependent on the shape of the structure (e.g. Fig (6.1)). Hence, using fixed-position loading rules out some feasible solutions before the optimization begins (since the solutions of layout optimization are highly sensitive to the loading positions). To address this problem, the transmissible load technique introduced in Chapter 3 will be used in this chapter for layout optimization. By doing so, the optimization search range can be expanded, and the building's external shape and the bracing structure can be simultaneously identified during the optimization.

6.2 Approaches and assumptions

Chapter 3 introduces and compares two transmissible load approaches: migrating load and rigid bar approach. The conclusion is that whilst the migrating load approach can be used in general cases, the rigid bar approach, because of its limitations, can only be used in situations where certain conditions are met. The key limitation of the rigid bar approach centres on the concept of "virtual" rigid bars, introduced into the optimization formulation as a means of allowing the

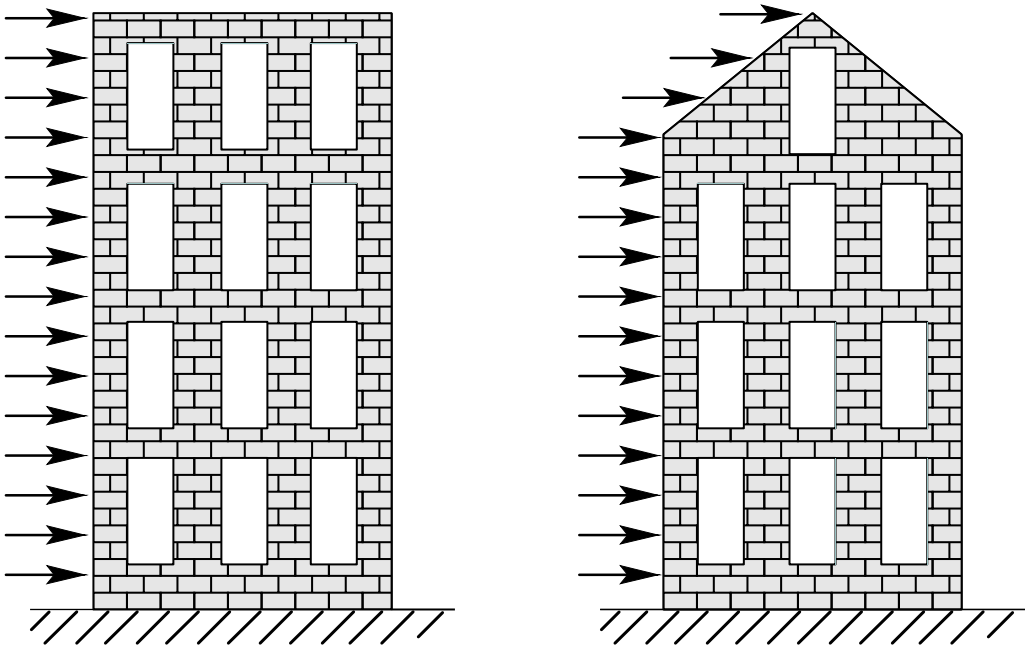

Figure 6.1: Two examples show that acting positions of the wind loads are dependent on the structure shape.

transfer of load from an arbitrary application point to the optimal point of interaction with the "real" structure. The problem identified in Chapter 3 is the danger of these virtual bars artificially stiffening and strengthening the real structure. It was shown in Chapter 3 that, in general, the concept of virtual rigid bars is safe to use as a load transfer mechanism only if the true optimal structural form is either an R-field catenary, or a T-field where the optimal trajectories of the tension and compression members are oriented at $\pm 45^{\circ}$ to the rigid bars.

However, there are circumstances where effectively rigid "real" bars are present in a structure and can be used as zero-cost elements to transfer load from an arbitrary point of application to the optimal point of interaction with the structure. One such type of real rigid bar is a floor plate in a framed building. The floor plates are typically designed for maximum factored gravity loads, and when wind load cases are considered, the factored loads applied to the floor members are significantly lower. This means that, when wind loading is considered in conjunction with less-than-maximum factored gravity loads (see, e.g. Eqn. (4.1)), the floor members are likely to have very large reserves of strength and can therefore act as "cost-free" axial load members to transfer the wind load from the point of application at the perimeter of the building to the optimal location of interaction with the bracing system. Consequently, the rigid bars in the optimisation formulation are actually real members and the problem with the rigid bar formulation identified in Chapter 3 is eliminated. Similar assumption has been used in previous studies, for example, Allahdadian et al.

(2012) considered bracing optimization of a multi-storey building with rigid intervening beams. In addition, floor beams and/or slabs are also treated as un-designable rigid members in the external envelope optimization of Bobby et al. (2013). Besides the assumption for horizontal members, it is also worth noting that the vertical loads are not considered in this chapter, since the current target is simultaneously optimizing the building envelope and inside bracing structure and vertical load cannot be known before the building shape is determined.

6.3 2D Single load case optimization

Figure 6.2 shows the bracing design case of this study. This is a typical 40-storey office building with 4m storey height and 10m storey width. Each floor is treated as a horizontal pre-existing rigid member with infinite strength. Since the obtainedHorizontal loads are assumed to be applied at 40m, 80m, 120m, and 160m height position of the two side boundaries. The magnitude of the wind loading is estimated using examples in Brettle & Brown (2009). The maximum tension and compression stress used for the bracing members are both 275MPa.

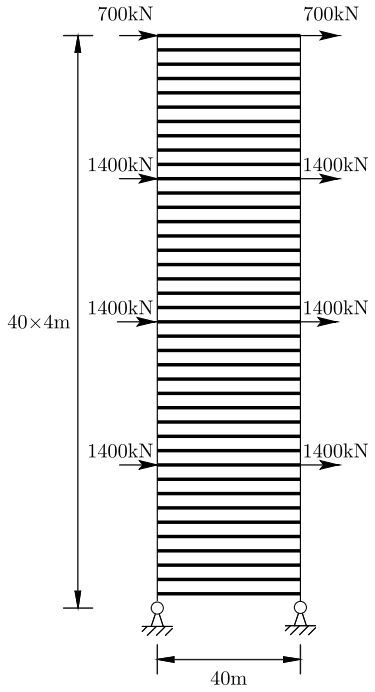

Figure 6.2: Case description, where bold lines represent pre-existing beams.

Four different cases are studied for this 40-storey building:

(1) Case 1: Bracing optimized with rigid floor members

(2) Case 2: Bracing optimized without rigid floor members

(3) Case 3: Fixed topology - Stromberg bracing

(4) Case 4: Fixed topology - Cross bracing

Considering that the main function of the bracing system is to control lateral displacement, an elastic analysis would consequently be involved in the optimization process. It is worth noting that Sved (1954) proved that the optimal topology would be identical for optimization with strength criteria and stiffness criteria in single load case situation. Therefore, if a structure optimized under strength criteria does not achieve the required stiffness, one could multiply all of the sections of the optimized structure with an amplification factor to achieve the required stiffness.

Hence, the optimization process includes four steps: (1) Layout optimization is used to identify the optimal topology and section size; (2) For Cases 1 & 2 only, geometry optimization is used based on the layout optimization results to identify more rational results; (3) The optimized structures were put into an elastic analysis to obtain the maximum lateral displacements; (4) According to the lateral displacements data and the suggested displacement limit (Renuka & Kumar 2015), a factor is chosen to amplify all of the members in these four cases.

The optimization results are shown in Fig. 6.3, where the volumes and displacement data are results after amplification. Note that under a suggested lateral drift limit H/500 (Renuka & Kumar 2015), an amplification factor equal to 7 is chosen for all the members.

The structure shown in Fig. 6.3a exhibits many similarities to that presented in Fig. 3.5a. The current solution is constrained by the horizontal limits set upon the design domain, and, of course, here, the rigid bars are either real floor members (within the structure) or transferring the wind load from the outer perimeter of the design domain to the catenary members at the uppermost outside edge of the structure. The Michell bracing shown in Fig. 6.3b is less efficient (e.g. 6.67% more material than Fig. 6.3a) and it does not have a repetitive pattern at every floor. Stromberg (e.g. Fig. 6.3c) and Cross bracing (e.g. Fig. 6.3d) have much simpler topology, but their volumes are respectively 9.11% and 15.4% higher than Fig. 6.3a.

Additionally, it has been noticed that the perimeter shape of Fig. 6.3a is very different from the other results. This happens since the top wind loads are transmitted through rigid members to the middle position. In this situation, one could choose to treat the rigid bars as 'virtual' members,

which are only used for numerical load transmission. Consequently, a building with optimized exterior shape could be obtained. Alternatively, these rigid members could also be treated as real floor members, which makes the bracing shown in Fig. 6.3a also suitable for rectangular-shaped buildings.

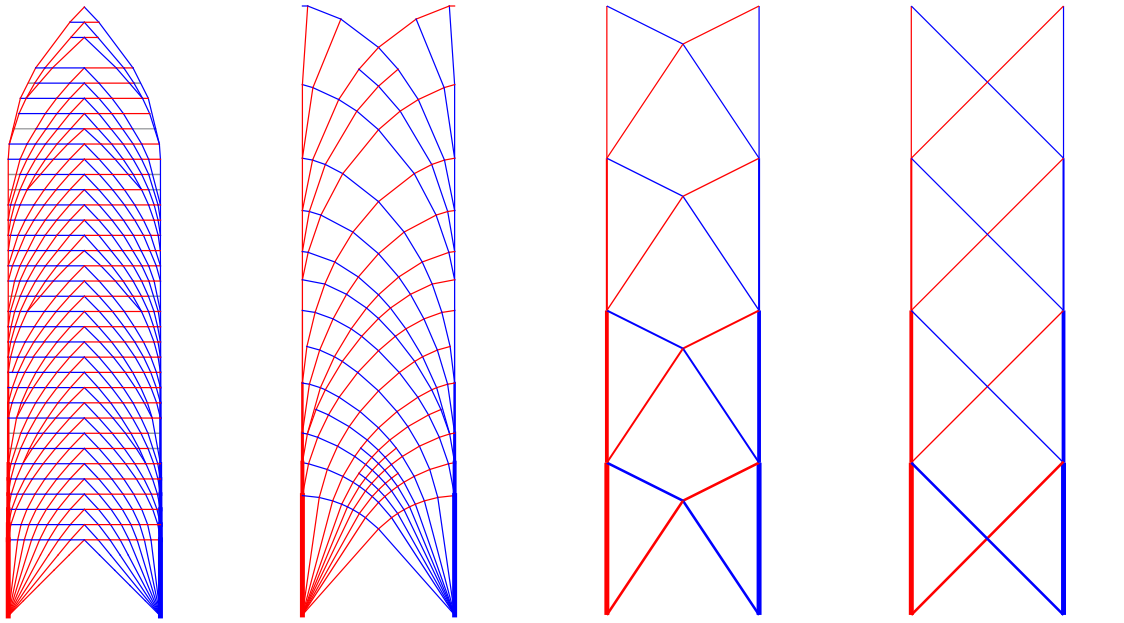

Volume=93.814m^3
Tip displacement=0.16586m
(a)

Volume=100.09m^3
Tip displacement=0.17230m
(b)

Volume=102.365m^3
Tip displacement=0.17629m
(c)

Volume=108.32m^3
Tip displacement=0.18403m
(d)

Figure 6.3: Results of 2D bracing optimization: (a) Case 1: Bracing optimized with rigid floor members; (b) Case 2: Bracing optimized without rigid floor members; (c) Case 3: Fixed topology - Stromberg bracing; (d) Case 4: Fixed topology - Cross bracing; red, blue and grey lines represent bars in tension, compression and takes no forces respectively, when horizontal loads are applied from left to right

6.3.1 Relation between topology simplicity and rigid floor number

In Fig. 6.3a it can be seen that, along the central vertical axis of the structure, the tension and compression bracing members intersect with the rigid bar at $\pm 45°$, as required for a T-field by the Mohr's circle analysis set out in Section 4.4.3. At all other horizontal positions, only a single tension or compression member intersects. This does not in fact contract the 45° rule set out in Section 4.4.3 because here, the structure comprises an R-field and the 45° rule does not apply. This can be shown by consideration of a Mohr's circle analysis when one of the principal strains is not at the limiting value, which is discussed in detail in Section 8.2 and Fig. 8.4.

In addition to strengthening & stiffening the optimum structure, the inclusion of the effectively

rigid floor members in the optimisation analysis also greatly simplifies the optimal topology compared to the "optimal" Michell structure without the floor members Fig. 6.3a & b. However, even though the lateral loads are applied at every tenth floor, the rigid-member optimised solution effectively ties in every floor into a repetitive bracing system. This repetitive system takes advantage of the presence of every rigid floor member, tying all the floors into a stiff, strong bracing frame. Thus, the penalty that is paid for the lighter, stiffer structure is the presence of considerably more bracing members than are required in the Stromberg or X-bracing solutions Fig. 6.3c & d.

To investigate the potential for reducing this number of bracing members, alternative layout optimisations were conducted, where the bracing members were allowed to connect to only every second, fifth or tenth rigid floor (Fig. 6.4). It can be observed that with the increase of the number of the rigid floors, the number of repetitions of the structure is reduced, but the repetitive structure gradually becomes complicated. Consequently, the desired simple structure may appear when the number of rigid floors is not too large nor too small.

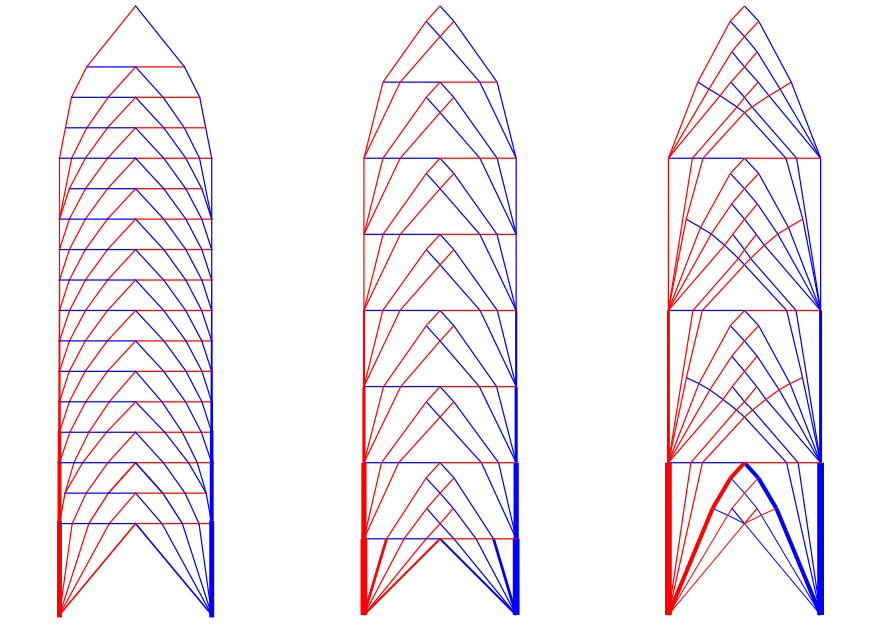

Figure 6.4: Results of 2D bracing optimization with different number of pre-existing beams: (a) 20 pre-existing beams across the height, (b) 8 pre-existing beams across the height, (c) 4 pre-existing beams across the height; red and blue lines represent bars in tension and compression respectively, when horizontal loads are applied from left to right.

6.3.2 Implication of single load case result

The single load case result could be used in situations when the wind load comes from one major direction; an example is shown in Fig. 6.5. Note that for this kind of building if braced faces are only added at two sides of the building, the lateral drift may be higher than the requirement in the middle position across the width. In this situation, more braced surfaces may be added across the building width to control the lateral displacement, which is similar to adding intermediate supports to a simply supported beam. In the example shown in Fig. 6.5, one additional braced face is added in the centre of the building.

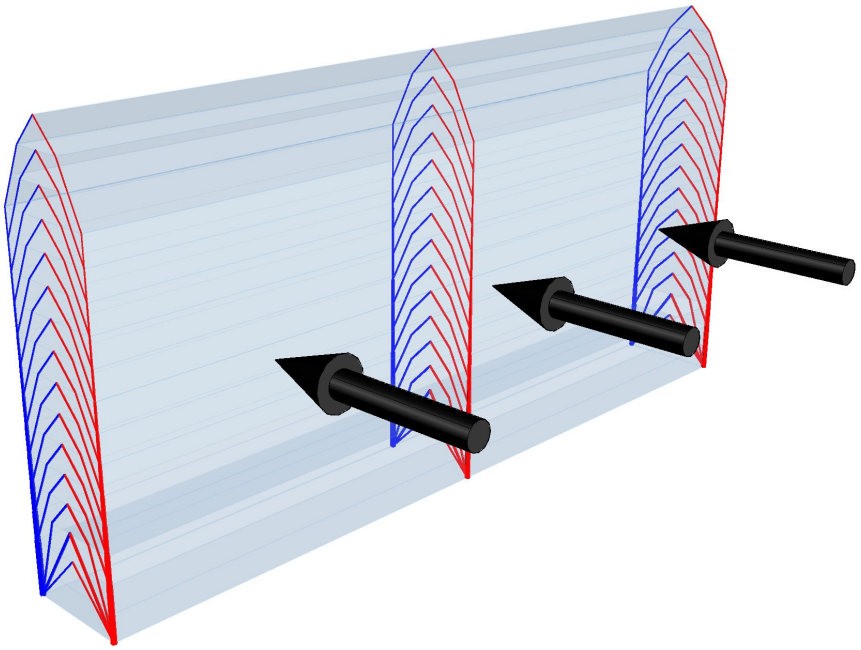

Figure 6.5: Single load case result implementation example, where the building needs to take wind load from one major direction; red and blue lines respectively represent bars in tension and compression.

6.4 3D multiple load case optimization

The example shown in Section 6.3 presents optimization results in the single load case situation. Nevertheless, tall buildings in reality usually need to take wind load from different directions. Therefore, the 3D bracing design case with multiple alternative load case are also studied in this section. The investigated case is shown in Fig. 6.6. This is the same as the cases in Section 6.3: this is a 40-storey building with 4m storey height. Since a 3D design domain is used, the storey size is correspondingly set to 40m $\times$40m. It has already been demonstrated in Section 6.3.1 that

bracing complexity is related to the number of the rigid floors. Therefore, as in Fig. 6.4a, every other floor is treated as a rigid floor for the load transmission. As shown in Fig. 6.6, two load cases that include wind load in, respectively, the x and y direction, are applied at the 40m, 80m, 120m, and 160m height position of this building. Pin supports are added along the four external boundaries of the bottom surface. The maximum tension and compression stress used for the bracing member are both 275MPa.

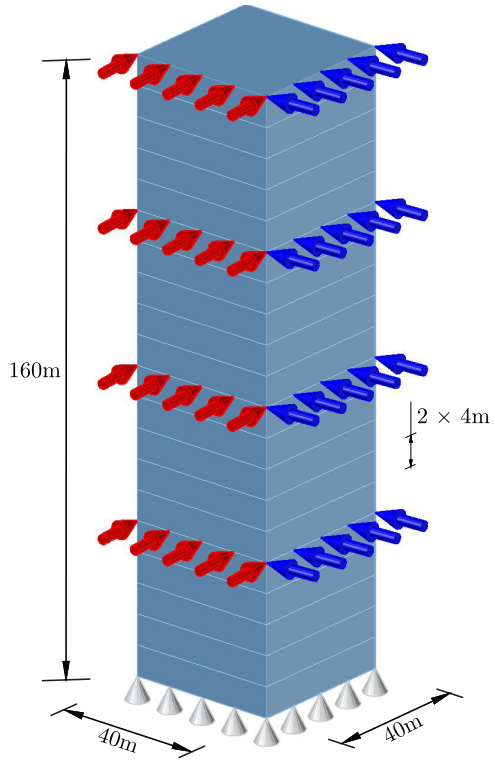

Figure 6.6: 3D Case description, where red and blue arrows represent loads in load case 1 and 2.

Based on these general conditions, two different cases are studied:

(1) Case 5: Bracing member could exist anywhere within the cuboid design domain

(2) Case 6: Bracing members can only exist at the external surface of the design domain.

In this section, only layout optimization is used to identify the optimized structure. Nevertheless, since in this case there are only two multiple load cases, the superposition approach described in Section 2.6.5 is used to reduce the computational cost. Additionally, by analysing the results from the single-component load cases, a better understanding of the optimized structure for multiple load cases could potentially be achieved. It is worth noting that in the superposition approach, the same rigid floor members need to be added to each of the component load cases to obtain correct solutions. The relationships between two multiple load cases and component load cases

are established in Fig. 6.8a and Fig. 6.9b.

The optimized results are shown in Fig. 6.7. It can be observed that the optimized results for both cases are simple and rational. For Case 5, all of the bracing members locate on the diagonal of the structure, which leads to usable space located in the four triangular regions of the building (i.e. Fig. 6.7a). The results from Component load cases 1 and 2 are similar to the 2D results, where all the bracing members intersect with rigid floor member at 45° in the centre line. In addition, it can be observed that in each component load case, bracing members appear at the diagonal only. Therefore, as shown in Fig. 6.8a, it can be derived that all the horizontal loads are transmitted through the rigid members to the floor central position. It is also worth noting that this is similar to the results shown in Fig. 6.3a and Fig. 6.4a. A part of the top rigid floor members are treated as 'virtual' members that are used for numerical load transmission only, which leads to a pyramid-like exterior shape on the top of the optimized structure. Alternatively, these rigid floor members can be treated as real members to make the bracing topology shown in Fig. 6.7a fit for a cuboid building.

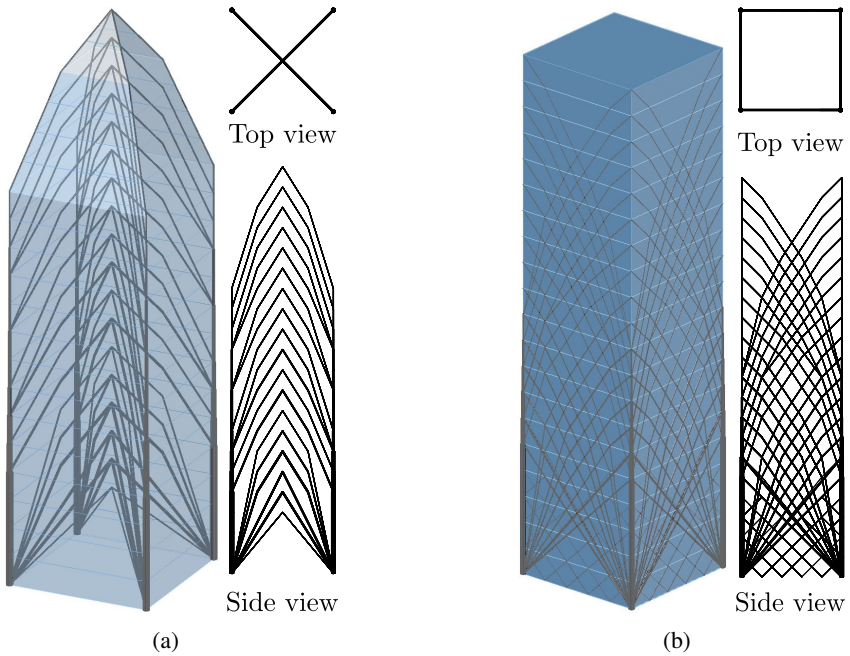

Figure 6.7: Results from the 3D bracing optimization cases: (a) Case 5 - bracing member could exist anywhere within the cuboid design domain; (b) Case 6 - bracing members can only exist at the external surface of the design domain.

The results of Case 5 have 14.3% less material than Case 6, but the bracing member distribution in Case 6 is more suitable for the current exoskeleton structure. Since bracing members could exist only at the external surface, in the results of component load cases, the horizontal loads are

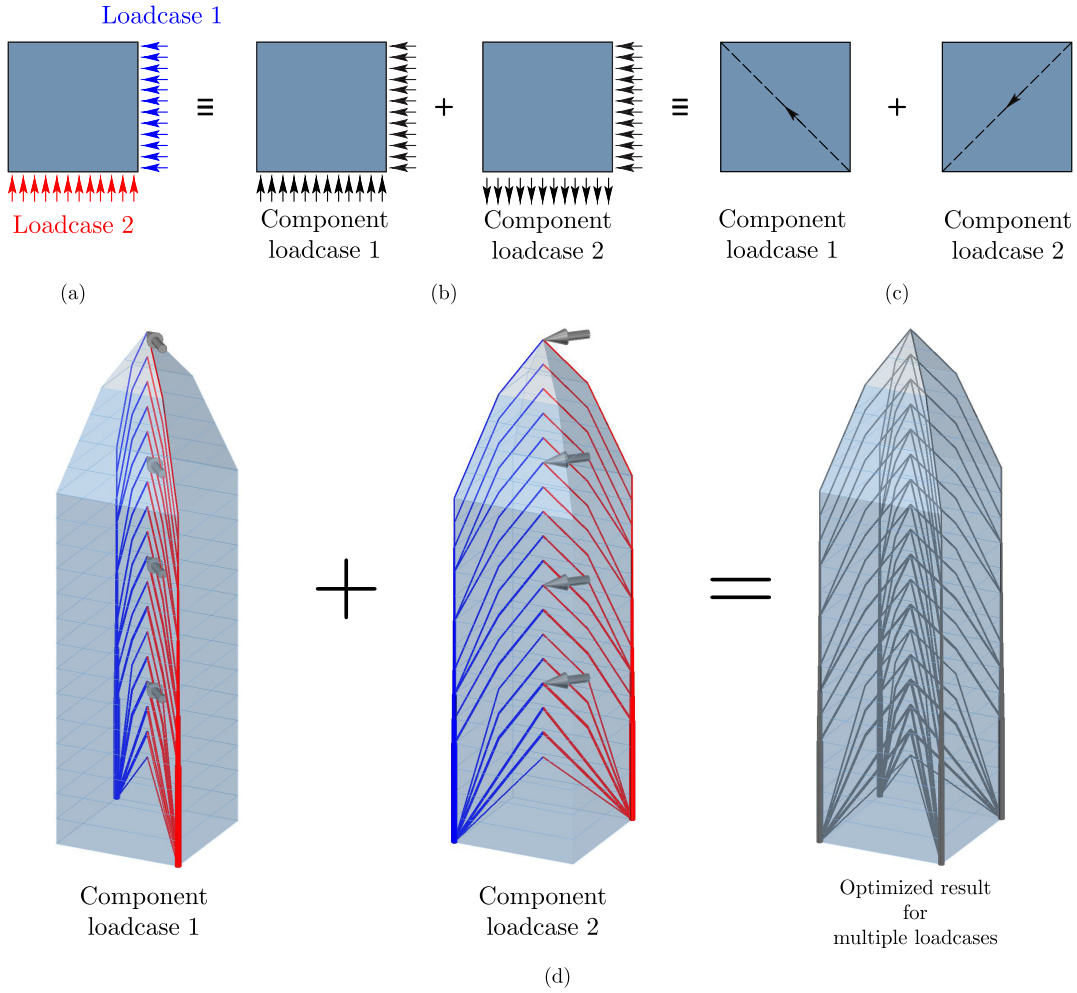

Figure 6.8: Relation between original load cases and component load cases in Case 5 where a bracing member could exist anywhere within the cuboid design domain: (a) top view graph of the original load cases on the building; (b) top view graph of the component load cases; (c) top view graph of the final acting positions of the transmissible loads in the component load cases; (d) numerical results of the component load cases; red and blue lines respectively represent bars in tension and compression.

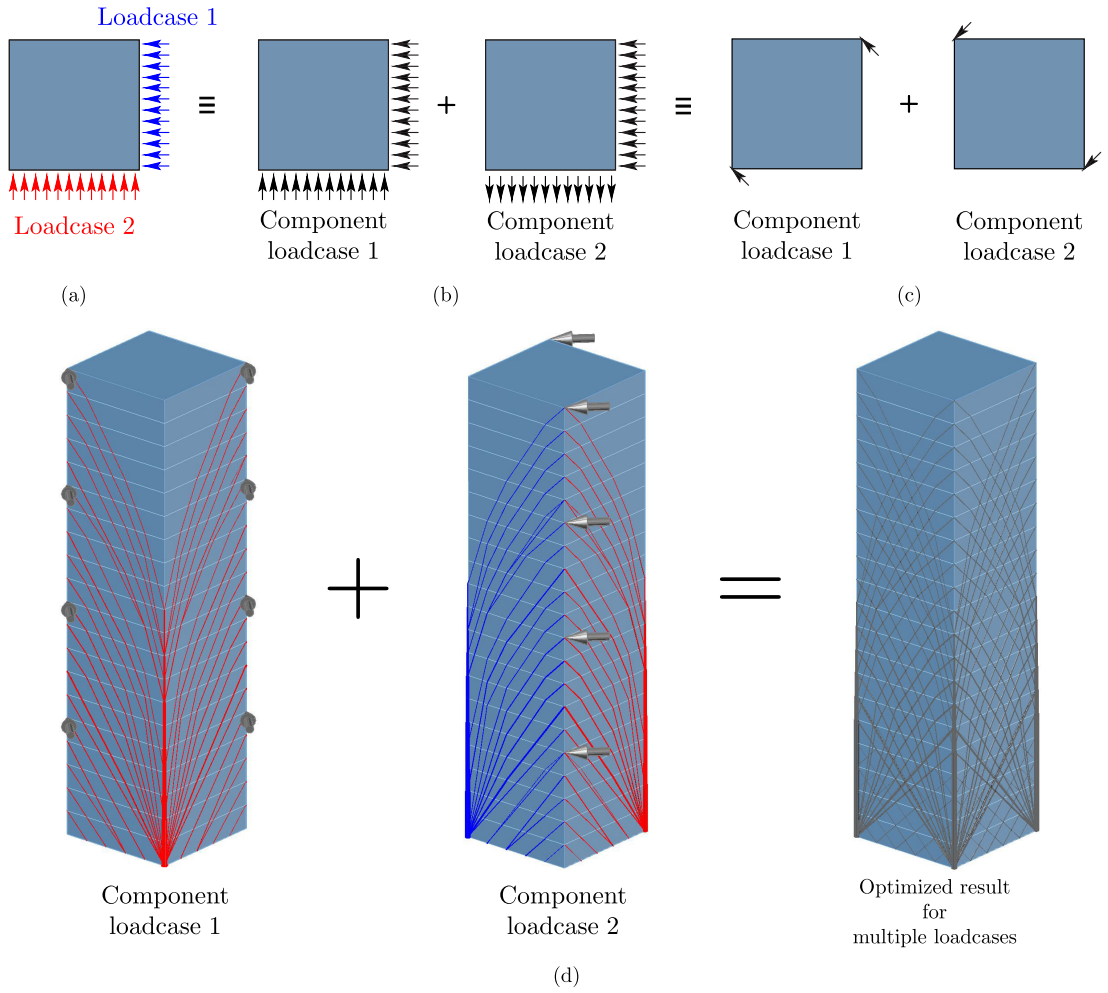

Figure 6.9: Relation between original load cases and component load cases in Case 6 where bracing members could only exist at the external surface of the design domain: (a) top view graph of the original load cases on the building; (b) top view graph of the component load cases; (c) top view graph of the final acting positions of the transmissible loads in the component load cases; (d) numerical results of the component load cases.

transmitted through rigid floor members to the corner positions (e.g. Fig. 6.9a). Consequently, similar results to Fig. 6.3a can be observed in the result of Component load case 2 in Fig. 6.9d, through the bracing members exist in two mutually perpendicular planes. Additionally, it can be observed that identical topology to the result of Component load case 2 can be obtained by rotating the optimized result of Component load case 1 in 90° around the z axis. Therefore, the structures in each side of Fig. 6.7b are identical to each other, which further reduced its construction difficulty.

Beghini et al. (2014) suggest that for a structure under lateral loading, the top half is dominated by shear effect, while the bottom half is dominated by bending effect. This principle could also be observed in the optimized results of Case 6. It has been found that in the bottom position of Fig. 6.7b bracing members intersect with each other at 90 degrees, which means that they do not interact with the rigid plate that is used to transmit horizontal shear force. Additionally, it has been observed that the corner column only exists in the bottom half of Fig. 6.7b. Moon et al. (2007) once studied the effect of keeping and removing the corner columns in diagrid bracing structures. The result shown in Fig. 6.7b suggest that placing corner columns in a region where the bending effect dominates will contribute to structural efficiency.

6.5 Conclusion

This chapter studies the optimized bracing topology with transmissible load technique. The following conclusions have been obtained:

(1): A simple and efficient structure has been identified in the 2D single load case. It could be used in situations where lateral loads are coming from one major direction (i.e. Fig. 6.5).

(2): Under the assumption of pre-existing beams, the simplicity of the optimized structures is related to the number of pre-existing beams across the height of the design domain. However, either too many or too few pre-existing beams will both lead to an increase in structure complexity. An intermediate number of pre-existing beams leads to the most rational structures.

(3): In the 3D optimization cases with multiple load cases, two structures are identified using different constraints. One of them allows structure members to exist only in the external surface of the building, and the other allows structure members to exist anywhere within the design domain. The logic of the optimization results is demonstrated using the superposition approach. The former

leads to a less efficient structure, but its topology is more practically acceptable than the latter result. These optimization results could be chosen for use based on the practical requirements of real scenarios.

Chapter 7

Layout optimization formulation for combined structure of trusses and frames

7.1 Introduction

When designing a steel-framed building, both truss bracing structures and moment resisting frames have been widely used to provide lateral stability. Layout optimization of the former has been investigated in previous chapters. However, the optimal structure of a moment resisting frame or the optimal combination of trusses and frames is still unknown. In a previous study, a similar grillage problem has been considered by Prager (1974). In this study, only the moment resistance is considered as a variable for each member, and the axial force is not involved. The objective in a typical grillage design problem is to find the minimum total moment resistance, rather than to find the minimum volume. Therefore, although moment is considered in the grillage problem, from a mathematical perspective, it is still very similar to the truss layout optimization problem. Liang et al. (2000), Stromberg et al. (2012) used moment-resisting elements (beams) in bracing design cases. However, the positions of these beams are fixed, and therefore they are not a part of the topology optimization. To date, in previous literature, there exists no method for the combined layout optimization of trusses and frames. Therefore, a new approach for moment resisting frame layout optimization is necessary and this chapter is an attempt to address this problem.

7.1.1 Optimization formulation

In truss layout optimization, a structural member's cross-sectional area is designed to take axial force only. Nevertheless, in moment resisting frame optimization, a member should have the capability to take axial force, shear force, and moment. Consequently, the optimization problem changes from a linear problem to a non-linear problem since one member's moment resistance is non-linearly related to its cross-sectional area. However, solving a non-linear problem is more computationally expensive than solving a linear problem. Therefore, the challenge of this problem lies in developing a robust and efficient optimization approach. To achieve this, the usual development approach is to find the non-linear formulation first and then make assumptions to simplify the algorithm. Therefore, the non-linear formulation for the frame optimization is considered first.

Revising the truss optimization formulation, it contains three main components: (1) Objective function, which is the relation between total volume and cross section area of each member; (2) Equilibrium function, which guarantees that the applied load is transmitted through an optimized structure into supports; (3) Strength criteria, which establish the relation between internal force and cross section area for each member.

$$\min \quad V = \mathbf{l^T a} \tag{7.1a}$$

$$\text{subject to} \quad \mathbf{Bq} = \mathbf{f} \tag{7.1b}$$

$$a_i = g(m_i^a, m_i^b, f_i, l_i) \tag{7.1c}$$

Where m_i^a, m_i^b, f_i and l_i are as defined in Fig. 7.1.

Figure 7.1: Force components of a beam

These three constituents are the sufficient and necessary components of a truss optimization

problem. Since the truss and frame layout optimization approaches are both based on the ground structure approach, these three aspects are also sufficient and necessary components of a frame optimization formulation. Therefore, firstly, for the objective function, it stays the same as the truss optimization since for each member the relation $V = la$ remains unchanged. Secondly, for the equilibrium function, additional force components m_{A} and m_{B} need to be added to the vector $\mathbf{q}$ to represent the moments at two ends (e.g. Fig. 7.1). Due to this change, the equilibrium matrix $\mathbf{B}$ also needs to be modified correspondingly.

The last part is strength criteria. Whilst in truss optimization, all the cross-sectional area is used to take the axial force, in rigid optimization it also needs to take moment and shear force. Hence, the stress distribution within a cross section needs to be considered first. For this purpose, it is first assumed that *a square section is used for all members in the optimization* (e.g. Fig. 7.2a). Based on this assumption, consider the situation where a member simultaneously takes bending moment and compression force; the corresponding normal stress distribution can be obtained as in Fig. 7.2b. From the stress distribution, it is clear that axial force is taken by the mid-part area (e.g. a_{N}) and moment is taken by the area on the top and bottom sides (e.g. a_{M}). Therefore, the stresses caused by axial force can be obtained with Eqn. (7.2). Assuming that the one with larger absolute value in m_a and m_b will be used in the bending stress calculation of the whole bar, the equation for bending stress (e.g. σ_{M}) is obtained as Eqn. (7.2b).

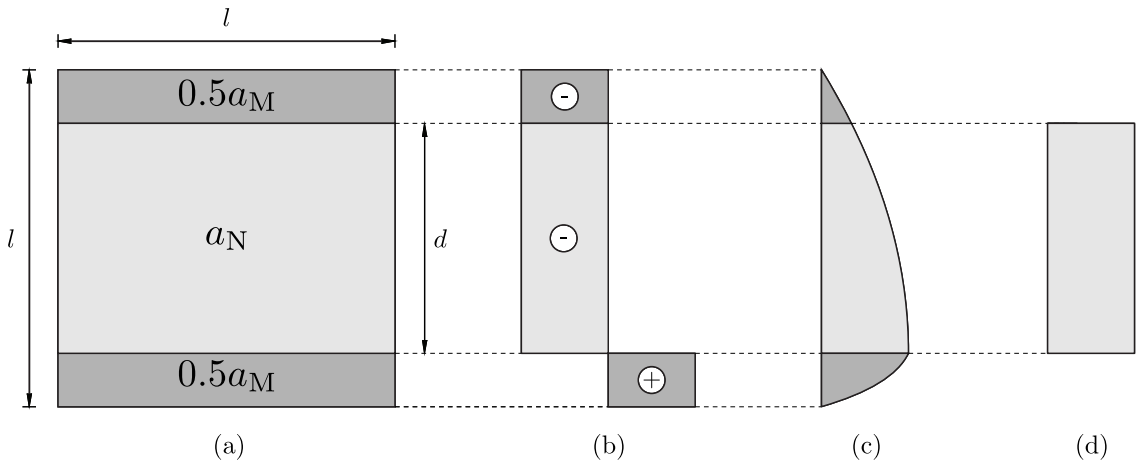

Figure 7.2: Force distribution within a square section: (a) within a square section, the top and bottom area a_{M} is used to take moment and a_{N} is used to take axial force; (b) normal stress distribution within the section; (c) shear stress distribution within the section; (d) modified shear stress distribution within the section.

$$\sigma_{\mathrm{N}} = \frac{f}{a_{\mathrm{N}}} \tag{7.2a}$$

$$\sigma_{\mathrm{M}} = \frac{\max(|m_a|, |m_b|)}{Z_{\mathrm{M}}} \tag{7.2b}$$

where Z_{M} is the plastic section modulus of a_{M}, σ_{M} is the bending stress, and σ_{N} is the normal stress caused by axial force.

From Eqn. (7.2b), it is clear that the plastic section modulus Z_{M} is a necessary parameter for σ_{M}. Hence, based on the cross section assumption shown in Fig. 7.2a, Z_{M} is obtained as Eqn. (7.3).

$$Z_{\mathrm{M}} = \frac{1}{4} a_{\mathrm{M}} (l + d) \tag{7.3}$$

From Fig. 7.2a, it is clear that

$$l = \sqrt{a_{\mathrm{N}} + a_{\mathrm{M}}} \tag{7.4a}$$

$$d = \frac{a_{\mathrm{N}}}{l} = \frac{a_{\mathrm{N}}}{\sqrt{a_{\mathrm{N}} + a_{\mathrm{M}}}} \tag{7.4b}$$

Therefore, combining Eqn. (7.4) and Eqn. (7.3) yields:

$$Z_{\mathrm{M}} = \frac{1}{4} a_{\mathrm{M}} (\sqrt{a_{\mathrm{N}} + a_{\mathrm{M}}} + \frac{a_{\mathrm{N}}}{\sqrt{a_{\mathrm{N}} + a_{\mathrm{M}}}}) \tag{7.5}$$

In most situations, bending is accompanied by shear force. As shown in Fig. 7.2c, shear stress is mainly concentrated on the middle part of the section in reality. Therefore, for the sake of simplicity, it is assumed that shear stress is evenly distributed in a_{N} (e.g. Fig. 7.2d). Consequently, shear stress τ may be obtained as Eqn. (7.6).

$$\tau = \frac{m_a + m_b}{l a_{\mathrm{N}}} \tag{7.6}$$

The middle part a_{N} takes axial force and shear force. Therefore, based on the yield criteria of von Mises, the following constraint needs to be satisfied for each member:

$$\sigma_{\mathrm{N}}^2 + 3\tau^2 \leq \sigma_{\mathrm{max}}^2 \tag{7.7}$$

Gathering all of the above information, the rigid joint optimization formulation becomes:

$$\begin{aligned}
\min \quad & V = \mathbf{l^T a} && \text{(7.8a)}\\
\text{subject to} \quad & \mathbf{Bq} = \mathbf{f} && \text{(7.8b)}\\
& \sigma_i^m = \frac{\max(|m_i^a|, |m_i^b|)}{\frac{1}{4}a_i^{\mathrm{M}}(\sqrt{a_i^{\mathrm{N}} + a_i^{\mathrm{M}}} + \frac{a_i^{\mathrm{N}}}{\sqrt{a_i^{\mathrm{N}} + a_i^{\mathrm{M}}}})} && \text{(7.8c)}\\
& \sigma_i^n = \frac{q_i}{a_i^n} && \text{(7.8d)}\\
& \tau_i = \frac{m_i^a + m_i^b}{l_i a_i^n} && \text{(7.8e)}\\
& \sigma_{\mathrm{max}} \geq \sigma_i^m && \text{(7.8f)}\\
& \sigma_{\mathrm{max}}^2 \geq (\sigma_i^n)^2 + 3\tau_i^2 && \text{(7.8g)}
\end{aligned}$$

where $i = 1, 2, ..., n$ and n represents total bar number of the optimization problem.

In this formulation, Eqn. (7.8c) and (7.8g) are non-linear constraints. Whilst (7.8g) is a conic quadratic function (e.g. a typical convex function), (7.8c) is a non-convex function that would require significant computational cost. Consequently, linearisation of Eqn. (7.8c) would yield significant reduction in computational cost. For this purpose, instead of using Eqn. (7.5), Z_{M} is approximated by its first-order expansion:

$$Z_{\mathrm{M}}(a_{\mathrm{N}}^{\mathrm{new}}, a_{\mathrm{M}}^{\mathrm{new}}) \approx Z_{\mathrm{M}}(a_{\mathrm{N}}^{\mathrm{old}}, a_{\mathrm{M}}^{\mathrm{old}}) + \frac{\partial Z_{\mathrm{M}}}{\partial a_{\mathrm{M}}}(a_{\mathrm{M}}^{\mathrm{new}} - a_{\mathrm{M}}^{\mathrm{old}}) + \frac{\partial Z_{\mathrm{N}}}{\partial a_{\mathrm{N}}}(a_{\mathrm{N}}^{\mathrm{new}} - a_{\mathrm{N}}^{\mathrm{old}}) \tag{7.9}$$

The approximate equation (7.9) could be simplified to:

$$Z_{\mathrm{M}}(a_{\mathrm{N}}^{\mathrm{new}}, a_{\mathrm{M}}^{\mathrm{new}}) \approx Z_0 + \frac{\partial Z_{\mathrm{M}}}{\partial a_{\mathrm{M}}} a_{\mathrm{M}}^{\mathrm{new}} + \frac{\partial Z_{\mathrm{N}}}{\partial a_{\mathrm{N}}} a_{\mathrm{N}}^{\mathrm{new}} \tag{7.10}$$

where

$$Z_0 = Z_{\mathrm{M}}(a_{\mathrm{N}}^{\mathrm{old}}, a_{\mathrm{M}}^{\mathrm{old}}) - \frac{\partial Z_{\mathrm{M}}}{\partial a_{\mathrm{M}}} a_{\mathrm{M}}^{\mathrm{old}} - \frac{\partial Z_{\mathrm{N}}}{\partial a_{\mathrm{N}}} a_{\mathrm{N}}^{\mathrm{old}} \tag{7.11}$$

Based on Eqn. (7.5), it can be obtained that:

$$\frac{\partial Z_{\mathrm{M}}}{\partial a_{\mathrm{M}}} = \frac{4a_{\mathrm{N}}^2 + 3a_{\mathrm{M}}^2 + 6a_{\mathrm{N}}a_{\mathrm{M}}}{8\sqrt{(a_{\mathrm{N}} + a_{\mathrm{M}})^3}} \tag{7.12a}$$

$$\frac{\partial Z_{\mathrm{N}}}{\partial a_{\mathrm{N}}} = \frac{3a_{\mathrm{M}}^2 + 2a_{\mathrm{N}}a_{\mathrm{M}}}{8\sqrt{(a_{\mathrm{N}} + a_{\mathrm{M}})^3}} \tag{7.12b}$$

$$Z_0 = -\frac{a_{\mathrm{M}}^2 + a_{\mathrm{N}}a_{\mathrm{M}}}{8\sqrt{a_{\mathrm{N}} + a_{\mathrm{M}}}} \tag{7.12c}$$

In the optimization, the values of $\frac{\partial Z_{\mathrm{M}}}{\partial a_{\mathrm{M}}}$, $\frac{\partial Z_{\mathrm{N}}}{\partial a_{\mathrm{N}}}$, and Z_0 are given a relatively large value in the first step, and in the subsequent steps, their value would be calculated using Eqn. (7.12). With this iterative scheme, in each step the problem that needs to be solved is a conic optimization problem that requires low computational cost. For the sake of completeness, the formulation for this conic problem is shown in Eqn. (7.13).

$$\min V = \mathbf{l}^{\mathbf{T}}(\mathbf{a}_{\mathrm{N}} + \mathbf{a}_{\mathrm{M}}) \tag{7.13a}$$

$$\text{s. t.} \tag{7.13b}$$

$$\mathbf{Bq} = \mathbf{f} \tag{7.13c}$$

$$\left.\begin{aligned} &|m_{1i}| \le \sigma_0(Z_{0i} + \tfrac{\partial Z}{\partial a_{\mathrm{N}i}}a_{\mathrm{N}i} + \tfrac{\partial Z}{\partial a_{\mathrm{M}i}}a_{\mathrm{M}i}) \\ &|m_{2i}| \le \sigma_0(Z_{0i} + \tfrac{\partial Z}{\partial a_{\mathrm{N}i}}a_{\mathrm{N}i} + \tfrac{\partial Z}{\partial a_{\mathrm{M}i}}a_{\mathrm{M}i}) \\ &v_{\mathrm{N}i} = \tfrac{1}{l}(m_{1i} + m_{2i}) \\ &(a_{\mathrm{N}i}\sigma_0)^2 \ge (q_i)^2 + 3v_{\mathrm{N}i}^2 \\ &a_{\mathrm{N}i} \ge 0 \\ &a_{\mathrm{M}i} \ge 0 \end{aligned}\right\} i = 1, 2, ..., n \tag{7.13d}$$

7.1.2 Numerical examples - Moment load

In the previous truss optimization approach, only force load could be applied to a layout optimization problem. Nevertheless, as the moment resisting capability is introduced in frame optimization, moment load could be applied to the optimization problem, as well. Therefore, this section shows several numerical results related to moment load.

As Fig. 7.3 shows, the cases studied in this section are a square design domain with four sides fixed

in x, y and rotation displacement and one moment load applied in the middle. Figs. (7.3a), (7.3b), and (7.3c) show three cases with different moment load magnitudes. From the results, it can be observed that moment-resisting beams only appear in the middle position, which directly connects to the loading position. Hence, the moment load is transmitted through the beams to the nearby nodes. This effectively turns a moment load into several force loads with different directions, and then these forces are transmitted through a Michell cantilever to the closest support on the side. Since there are four supports that have the same smallest distance to the middle loading point, two of them have been used in this case to take the load, which causes the symmetrical topology in Fig. 7.3. It is worth noting that in other cases with different loading magnitude, structures connecting to all the four supports are also found.

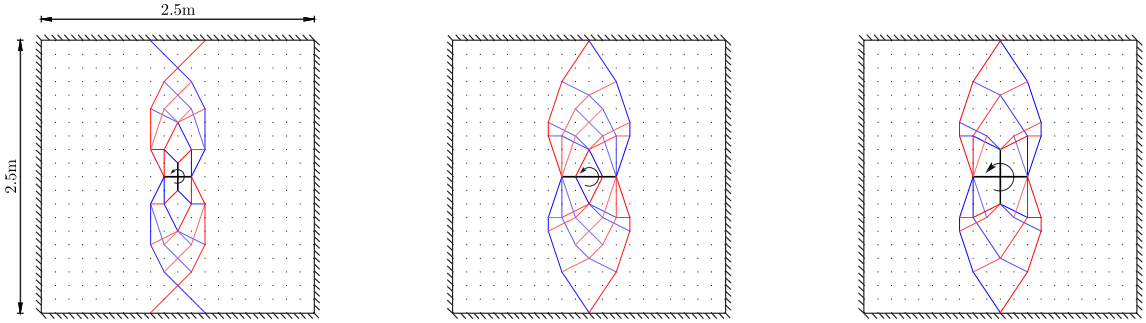

Figure 7.3: Cases with different in-plane moment load at the centre where the load magnitude for (a) 500kNm; (b) 2000kNm; (c) 4000kNm; red, blue and black lines represent members take tensile axial force, compressive axial force and bending moment.

It is worth noting that the three cases in Fig. 7.3 have the same design domain, support condition, and loading position, and only differ in loading magnitude. In previous truss optimizations, this setting should lead to an optimized solution with the same topologies having different volumes. However, in rigid optimization, the optimized topologies are also different. This happens because for a specific member, its plastic modulus Z is non-linearly related to its cross-sectional area. Therefore, the general benefit of using moment-resisting beams increases as the cross section area increases. Consequently, in situations with relatively large loading values (e.g. Fig. 7.3c), more beams appeared in the optimized solution for load transmission.

In theory, length of beam members gradually increases as the loading magnitude increase. However, continuum does not exist in discrete approach. Therefore, when the loading magnitude is relatively small, beam members are only used to connect the center node and the most neighbouring nodes (i.e. Fig. 7.3a). When the loading magnitude is relatively large, beam

members are used to connect the center node and the secondly neighbouring nodes (i.e. Fig. 7.3b & c). Therefore, it can be obtained that the optimized results in the moment load cases are highly dependent on the density of the node grid.

7.1.3 Numerical examples - bracing design under restricted design domain

In previous truss optimization, the optimized results are efficient, but they usually require relatively more space. In contrast, moment-resisting frames are less efficient but could provide sufficient usable space. Hence, these two structures are usually combined to guarantee the stability and usability of a structure. This combined structure could not be studied with previous truss optimization, where members can take only axial force. Therefore, the optimal combination structure is investigated in this section using a frame optimization approach.

As Fig. 7.4 shows, the cases studied in this section are two-storey braced frames. Two bottom corners of the design domain are fixed in x, y and rotation displacement, and lateral loads are applied at 10m and 20m height position at the two sides. The aspect ratio of the design domain is h:w=2:1, and holes have been added to the design domain to control usable space.

From the results, it is clear that structure efficiency is decreased as the hole size increases. The horizontal beams in Fig. 7.4a are replaced by truss structures somewhat similar to Michells cantilever in the other two cases and this yields 33.2% and 43.2% material reduction for Fig. 7.4b and Fig. 7.4b. Moreover, it can be observed in Fig. 7.4b that in each of the truss structures, the top and bottom horizontal bar take forces with different signs. This means that a truss structure is used to provide the moment resistance against lateral load. In addition, if we treat the horizontal truss structures in Fig. 7.4b and Fig. 7.4c as two giant beams, it can be observed that the horizontal members on the top and bottom of the giant beams disappear at the centre, where shear is the dominating effect.

As shown above, in 2D cases, rigid joint optimization could be used to identify the optimal combination between truss and beam structure and conduct investigation in structure material and space efficiency. These applications could readily be expanded to 3D cases. Nevertheless, in 3D cases, rigid joint optimization is potentially more useful since some space structures like grid shells require moment resistance to be stable.

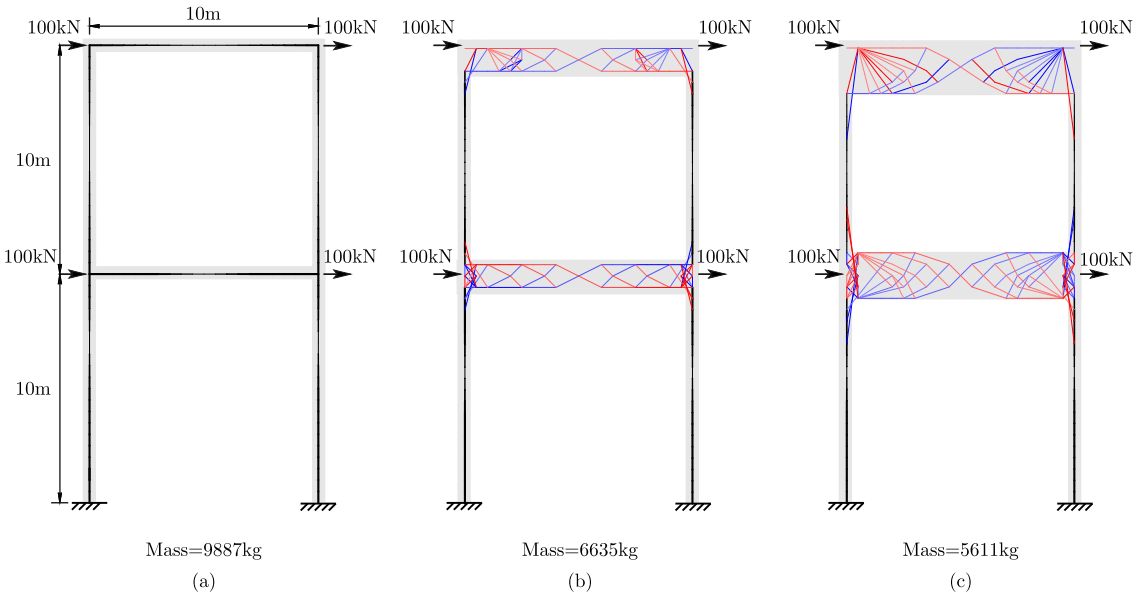

Figure 7.4: Cases with different design domain spaces: (a) only one layer of nodes located in the grey area; (b) one layer of nodes located on the two sides and 1.5m design space for the top and middle horizontal areas; (c) one layer of nodes located on the two sides and 3m design space for the top and middle horizontal areas.

7.2 Frame optimization formulation with multiple load cases

Section 7.1 demonstrated the formulation for frame optimization in the single load case. Nevertheless, it is clear from previous content that the multiple load case is a necessary consideration for structure layout optimization. Therefore, the frame layout optimization formulation with multiple load cases is discussed in this section.

Hemp (1973) suggested in optimization with multiple load cases that *"each member should be stressed to the limit σ_T or $-\sigma_C$ for at least one system of force"*. This means that for each member, its cross-sectional area is dominated by one load case, and that the stresses caused by other load cases must be equal to or less than the stress limit. Given this, we could consider a simple example for a square cross section in a scenario with two multiple load cases.

Figure 7.5 shows that for the same cross section under different load cases, the proportion of a_{M} and a_{N} is different. In this case, some part of a_{N} that is used to take axial force and shear force in load case 1 have been used to take moment in load case 2. However, the total cross-sectional area is unchanged. Therefore, we need an additional variable a and the constraint (7.14) to take this fact into consideration. Note that in reality, the cross section remains the same for different load cases,

and the stress magnitude within this section may vary. However, in the optimization formulation, in order to maintain it as a convex problem, the stresses caused by different load cases are equal to the stress limit, and the required areas of different load cases may vary. Therefore, (7.14) shows a greater than or equal to relation instead of an exclusively equal relation.

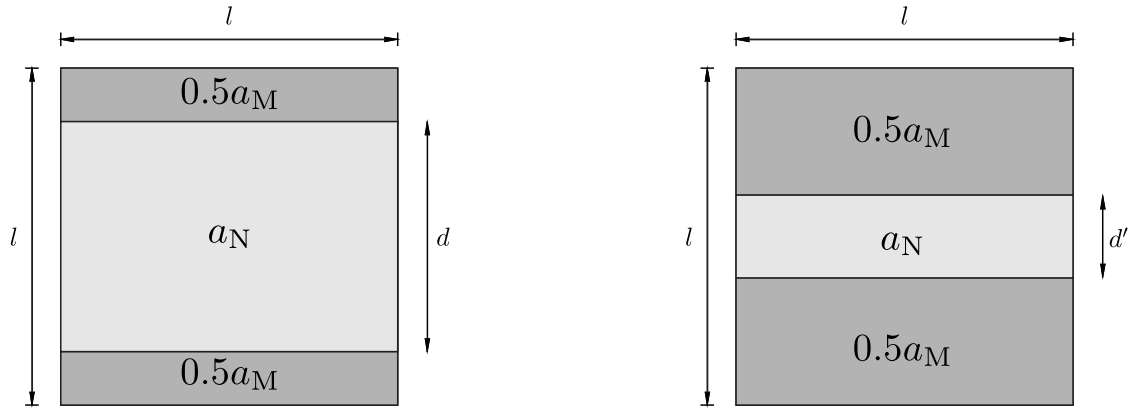

Figure 7.5: Example of a single member's cross-sectional area in two load cases, where a_{M} is the area used to take moment and a_{N} is the area used to take axial and shear force.

$$a \geq \{a_{\mathrm{M}} + a_{\mathrm{N}}\}^{\alpha}, \qquad \alpha = 1, 2, ..., m \tag{7.14}$$

where *m* represents the number of the load cases.

As previously demonstrated, one member's cross-sectional area is dominated by one or several major load cases, and the required areas for other minor load cases may be less than the total area. Consequently, when the areas for a minor load case are considered, the area parameters $\{a_{\mathrm{M}}\}^{\alpha}$ and $\{a_{\mathrm{N}}\}^{\alpha}$ may take any feasible values between the required value (e.g. lower boundary) and the total area value (e.g. upper boundary). Therefore, instead of directly using the values of $\{a_{\mathrm{M}}\}^{\alpha}$ and $\{a_{\mathrm{N}}\}^{\alpha}$ in the first-order approximation equation (i.e. $Z = Z_0 + \frac{\partial Z}{\partial a_{\mathrm{N}}} a_{\mathrm{N}} + \frac{\partial Z}{\partial a_{\mathrm{M}}} a_{\mathrm{M}}$), one should re-calculate $\{a_{\mathrm{M}}\}^{\alpha}$ and $\{a_{\mathrm{N}}\}^{\alpha}$ based on the axial force and moment values produced by the concerned load case.

Summarizing all of the above considerations on multiple-load cases, the following formulation

can be obtained for frame layout optimization of n members and m multiple-load cases.

$$\min V = \mathbf{l^T a} \tag{7.15a}$$

$$\text{s. t.} \tag{7.15b}$$

$$\mathbf{Bq} = \mathbf{f} \tag{7.15c}$$

$$\left.\begin{array}{l} a_i \geq a_{\mathrm{M}i}^{\alpha} + a_{\mathrm{N}i}^{\alpha} \\ |m_{1i}^{\alpha}| \leq \sigma_0 (Z_{0i}^{\alpha} + \frac{\partial Z^{\alpha}}{\partial a_{\mathrm{N}i}^{\alpha}} a_{\mathrm{N}i}^{\alpha} + \frac{\partial Z^{\alpha}}{\partial a_{\mathrm{M}i}^{\alpha}} a_{\mathrm{M}i}^{\alpha}) \\ |m_{2i}^{\alpha}| \leq \sigma_0 (Z_{0i}^{\alpha} + \frac{\partial Z^{\alpha}}{\partial a_{\mathrm{N}i}^{\alpha}} a_{\mathrm{N}i}^{\alpha} + \frac{\partial Z^{\alpha}}{\partial a_{\mathrm{M}i}^{\alpha}} a_{\mathrm{M}i}^{\alpha}) \\ v_{\mathrm{N}i}^{\alpha} = \frac{1}{l}(m_{1i}^{\alpha} + m_{2i}^{\alpha}) \\ (a_{\mathrm{N}i}^{\alpha}\sigma_0)^2 \geq (q_i^{\alpha})^2 + 3(v_{\mathrm{N}i}^{\alpha})^2 \\ a_i \geq 0, a_{\mathrm{N}i}^{\alpha} \geq 0, a_{\mathrm{M}i}^{\alpha} \geq 0 \end{array}\right\} \begin{array}{l} i = 1, 2, ..., n \\ \alpha = 1, 2, ..., m \end{array} \tag{7.15d}$$

7.3 Use of an I section in frame optimization algorithm

The formulation in Section 7.1 is based on solid square sections. Nevertheless, since the 2D problem only involves moment in one direction, the I section is a better choice for moment-resisting purposes. For this reason, the property of the I section is investigated in this section.

A typical I section is presented in Fig. 7.6a. Based on the size parameters shown in this graph, the formulation for the cross-sectional area a and full plastic modulus Z can be obtained as:

$$a = t_{\mathrm{w}} d + 2 w t_{\mathrm{f}} \tag{7.16}$$

$$Z = w t_f (d + t_f) + 0.25 t_w d^2 \tag{7.17}$$

From Eqn. (7.16) and (7.17), it can be determined that in a situation with a constant cross-sectional area a, Z could reach an infinitely large value if t_w is infinitely small and d is infinitely large. Obviously, this could not happen in reality because the capacity of one section is dominated by local buckling effects if its t_w is very small. Therefore, according to Eurocode 3, to guarantee that one section's full plastic moment capacity is larger than its local buckling moment capacity, this section needs to be at least class 2, which means that its sizes need to satisfy the size conditions

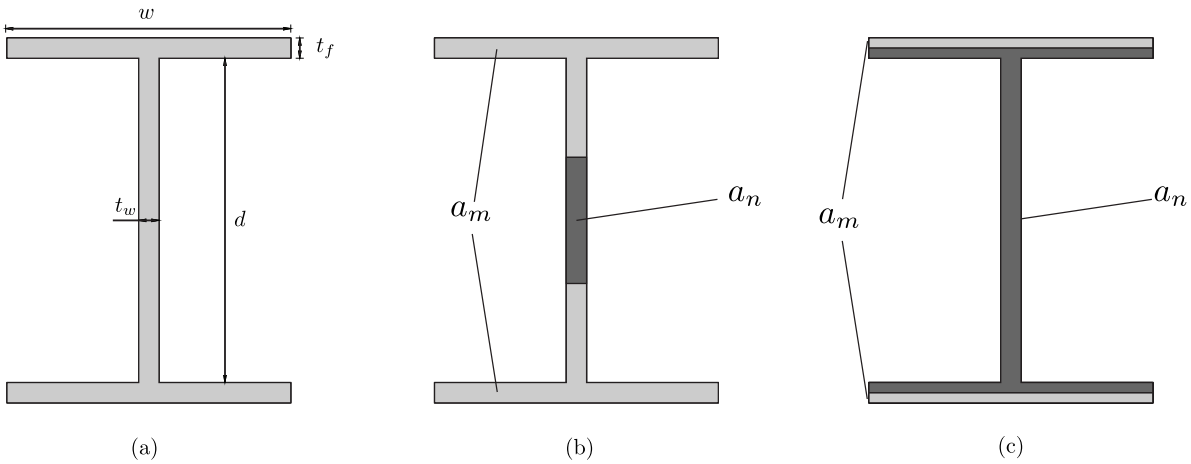

Figure 7.6: Typical I section, (a) size parameters of an I section; (b) an area distribution with a_{N} only in the web; (c) an area distribution with a_{N} also in the flange; a_{N} is the area used to take axial and shear force, and a_{M} is the area used to take moment.

below:

$$\begin{aligned} 7.32t_{\mathrm{f}} \leq (w - t_{\mathrm{w}})/2 \leq 8.1t_{\mathrm{f}} \\ 65.08t_{\mathrm{w}} \leq d \leq 81.36t_{\mathrm{w}} \end{aligned} \tag{7.18}$$

Note that condition (7.18) is specifically for steel with 355MPa as maximum stress and class 2 cross section.

Rearranging condition (7.18) yields:

$$\begin{aligned} 14.64t_{\mathrm{f}} + t_{\mathrm{w}} \leq w \leq 16.2t_{\mathrm{f}} + t_{\mathrm{w}} \\ 65.08t_{\mathrm{w}} \leq d \leq 81.36t_{\mathrm{w}} \end{aligned} \tag{7.19}$$

Defining that $t_f = zt_w$, condition (7.19) could therefore be written as:

$$\begin{aligned} w = (xz + 1)t_{\mathrm{w}} \\ d = yt_{\mathrm{w}} \end{aligned} \tag{7.20}$$

where $14.64 \leq x \leq 16.2$, $65.08 \leq y \leq 81.36$, $z > 0$

Consequently, with (7.20), area a and plastic modulus Z for this section could be written as:

$$a = yt_w^2 + 2(xz^2 + z)t_{\mathrm{w}}^2 = (2xz^2 + 2z + y)t_{\mathrm{w}}^2 \tag{7.21}$$

$$Z = (0.25y^2 + z^2 + yz + xyz^2 + xz^3)t_{\mathrm{w}}^3 \tag{7.22}$$

From (7.21) and (7.22), it is clear that the unit of a is the square of the length, while the unit of Z is the cubic of the length. Hence, a dimensionless relation between a and Z could be defined by the following equation:

$$\frac{Z}{a^{\frac{3}{2}}} = \frac{0.25y^2 + z^2 + yz + xyz^2 + xz^3}{(2xz^2 + 2z + y)^{\frac{3}{2}}} \tag{7.23}$$

Therefore, the following formulation can be used to obtain the maximum plastic modulus for a determined cross-sectional area:

$$\begin{array}{ll} \text{max} & g(x,y,x) = \frac{0.25y^2+z^2+yz+xyz^2+xz^3}{(2xz^2+2z+y)^{\frac{3}{2}}} \\ \text{subject to} & 14.64 \leq x \leq 16.2 \\ & 65.08 \leq y \leq 81.36 \\ & z > 0 \end{array} \tag{7.24}$$

With a numerical non-linear programming solver (e.g. fmincon of MATLAB), the solution of (7.24) could be obtained as:

$$g(x,y,x)_{max} = 2.4734 \quad \text{when} \quad x = 14.64 \quad y = 81.36 \quad z = 1.20 \tag{7.25}$$

This solution leads to:

$$d = 81.36t_w, \quad w = 18.568, \quad t_f = 1.2t_w \tag{7.26}$$

Eqn. (7.26) shows the necessary size constraints for an I section with given cross-sectional area to reach its maximum moment capacity. Note that these size constraints are derived based on a full bending situation. Although in the optimization every member has the possibility to simultaneously take axial force and moment, the proportion between axial force and moment are not known *a priori*. Therefore, one could assume that the section shape is first designed according to the full bending moment situation and the force distribution within this section is considered

later.

As shown in Fig. 7.6b and Fig. 7.6c, for an I section there are two situations for force distribution: (1) axial force exists only in the web; (2) axial force exists in both the web and the flange. With Eqn. (7.26), it can be derived that in the first situation, the section modulus is:

$$Z = 2.4734\sqrt{(a_{\mathrm{M}} + a_{\mathrm{N}})^3} - \frac{2.8054 a_{\mathrm{N}}^2}{\sqrt{a_{\mathrm{M}} + a_{\mathrm{N}}}} \tag{7.27}$$

And for the second situation, the section modulus is:

$$Z = 3.73 a_{\mathrm{M}}\sqrt{a_{\mathrm{N}} + a_{\mathrm{M}}} - \frac{a_{\mathrm{M}}}{6.62\sqrt{a_{\mathrm{N}} + a_{\mathrm{M}}}} \tag{7.28}$$

Eqn. (7.27) and (7.28) can be used to obtain the first-order derivative equation. From Fig. 7.6, it is clear that Eqn. (7.27) should be used when a_n is less than the web area and that Eqn. (7.28) should be used when a_n is larger than the web area. This switch in formulation leads to a non-smooth curve for plastic modulus Z. Therefore, a damping ratio may be introduced within the sequential programming algorithm for a quick convergence. Details about this may be studied in future development.

7.4 Conclusion

In this chapter, a new optimization formulation for identifying combined truss and frame structures has been developed. A sequential conic programming scheme has been used to solve this non-linear formulation. Its implication have been demonstrated in numerical examples with moment loading and restricted design domain. To make this formulation be able to solve more general problems, potential approaches for considering I section and multiple load cases have been proposed. However, more investigation needs to be done on the implementation of the proposed approaches in the future.

Chapter 8

Discussion

8.1 Different optimized solutions under different assumptions

In Chapters 4, 5, and 6, different optimized results are obtained using different assumptions. Specifically, in Chapter 4, pre-existing columns and beams are used; in Chapter 5, no assumption are used; in Chapter 6, only pre-existing beams are used. Generally, this would lead to the most efficient results in Chapter 4 and the most practical results in Chapter 5. However, even for the most practical cases in Chapter 5 (e.g. Section 5.4), only realistic loads and local buckling effects are considered during the optimization. Many more conditions that exist in realistic cases are not considered (e.g. joint cost, global buckling effect, dynamic loading resistance). However, considering lots of realistic conditions in layout optimization for conceptual design may be not suitable for two reasons: (1) the non-linearity of the the problem definition for some of these features means that, even with state-of-the-art mathematical technique, this problem may involve very high computational cost, and the final result is highly likely to be a local optimum; (2) even if the global optimal solution could be obtained, the optimal structure could be very complex, as observed in most Michell structures. Consequently, the optimized results are very difficult to be used for practical cases. Therefore, it is better to consider only limited practical conditions and to use the optimized results in the conceptual design stage to consider the economic efficiency of the structure.

To decide which chapter's optimization approach should be used, one must know the initial conditions and design procedures of the specified design problem. For projects with building

shape fixed and column and beam members that mainly used to take gravity loads and designed separately with lateral stability system, the approaches and results in Chapter 4 may be used. For projects with building shape fixed and gravity load frame designed simultaneously with lateral stability system, the approaches and results in Chapter 5 may be used. For projects with unfixed building shape, the approaches and results in Chapter 6 may be used to find the external building shape and the internal bracing structure. These are illustrated in Table 8.1. Additionally, it has been pointed out in Table 8.1 that the optimization problem with bracing structure and building envelope simultaneously designed under horizontal and vertical loads is not considered in this thesis. This is because the vertical loads on each floor are effectively related to the envelope of the building. However, there appears to be no effective approach to include this relation in the optimization problem. Potentially it is possible to use non-linear constraints in a post-process to address this problem. Nevertheless, more effort is required in future work to investigate this approach.

Optimization loads / Optimization targets	Horizontal load only	Horizontal and vertical loads
Bracing structure only	Addressed in Chapter 4	Addressed in Chapter 5
Bracing structure and building envelope	Addressed in Chapter 6	Need to be addressed in the future work

Table 8.1: Optimization loads and targets of previous chapters

8.2 Optimal intersection angle with pre-existing bars

Assumptions about pre-existing members are an important part of this study because they usually lead to simple and efficient structures. As previously mentioned, Rozvany et al. (2006) and Lewiński (2006) have studied the properties of pre-existing members in optimized structures. Nevertheless, some new properties about pre-existing members have been identified during this study. Therefore, the properties of pre-existing members are summarised and discussed in this section.

Before discussing the properties of pre-existing members, it must be pointed out that there are

situations where pre-existing members may not be part of the optimized structure. An extreme example of this may be a pre-existing member that is located far away from the loads and supports involved in the optimization. However, since the purpose of introducing pre-existing members is to identify simple and efficient structures, these cases attract little interest for the optimization purpose of this study. Therefore, in the cases discussed below, only the situations where the pre-existing bars are used are considered.

There are currently two ways to add a pre-existing bar to the optimization problem: increase the stress capacity of the specified members or impose a positive lower boundary on the cross-sectional area of the specified members. The former is not strictly adding a pre-existing member to the optimization problem, rather, increasing the stress capacity of the concerned members could make the optimization algorithm more inclined to use them. Therefore, both of the approaches could be used to add pre-existing members.

Using the first method, the pre-existing members can be divided into two categories: members with infinite stress capacity and with limited stress capacity. The cost function and adjoint strain of these two types of rods are shown in Fig. 8.1. From this graph, it is clear that cost function and adjoint strain decrease as the stress capacity increases. In the case where the stress capacity is infinite (e.g. Fig. 8.1c), the values of cost function and adjoint strain are both zero. Additionally, for a T-region problem, the adjoint strain obtained by this analysis can be used in the Mohr circle analysis to obtain the optimal angle between the pre-existing bar and the common bar.

Corresponding to the three situations illustrated in Fig. 8.1, the optimal angle problem is considered in these three situations. Firstly, in the absence of a pre-existing bar, as shown in Fig. 8.1a, the angle between the members should be 90°. Secondly, in the other extreme case where the stress capacity of a pre-existing member is infinite, it is demonstrated in Section 4.4.3 that the optimal angle between this pre-existing member and another normal member is 45°. Thirdly, for the intermediate situation between the previous two where a pre-existing member has finite stress capacity, a similar analytical method can be used to derive the optimal intersection angle. Assume that the stress capacities of the two concerned members are σ and $n\sigma$, respectively, in the case of equal compressive and tensile capacity. The adjoint strains of these two bars are therefore ϵ_{xx} and ϵ_{xx}/n. Given this, the Mohr's circles of the pre-existing member and normal member can be obtained as shown in Fig. 8.1b (e.g. small circle for pre-existing member and large circle for normal member). Therefore, based on this Mohr's circle analysis, the optimal intersection angle

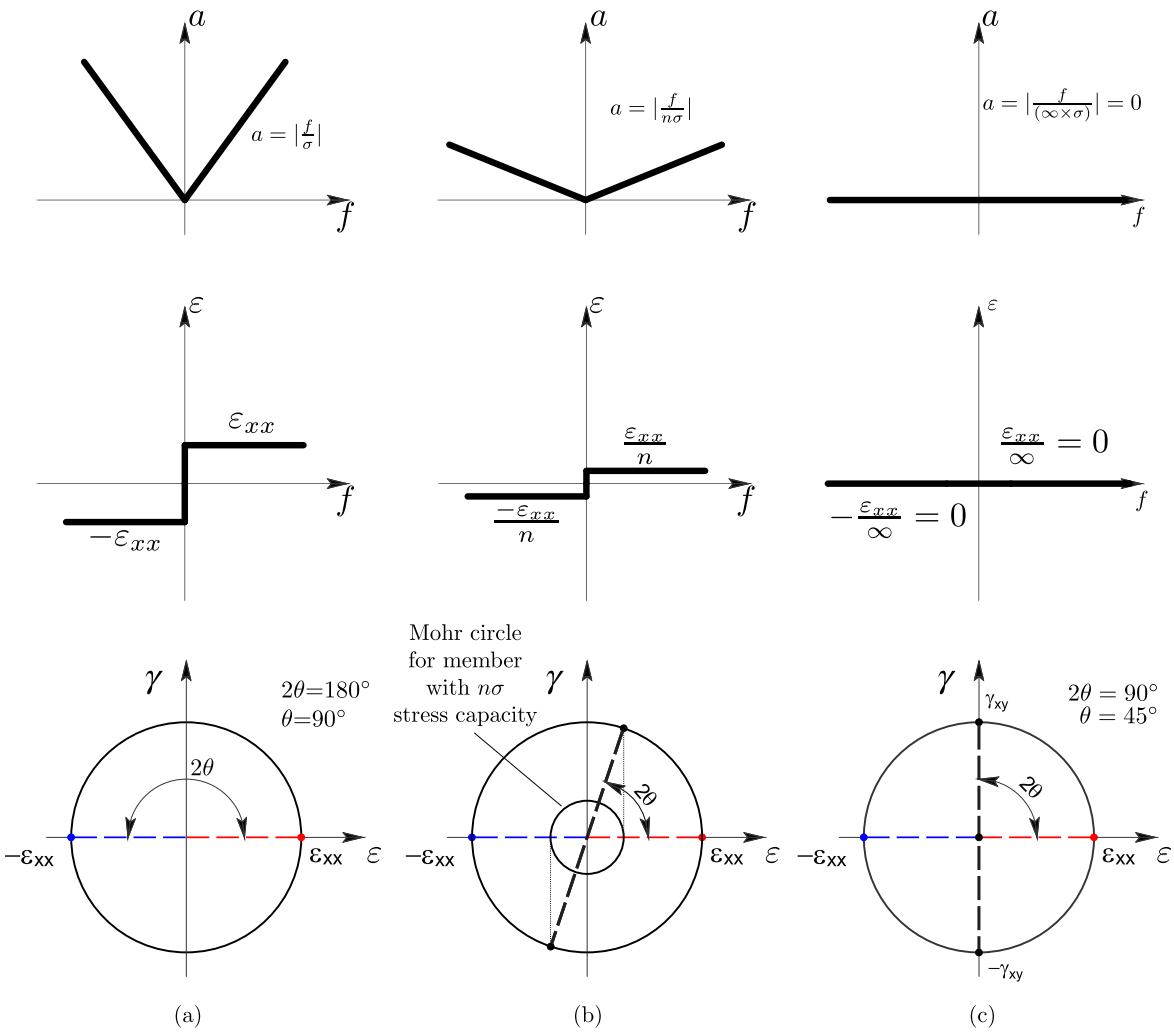

Figure 8.1: Cost function, adjoint strain, and Mohr's circle analysis for three different members: (a) member with normal stress capacity σ; (b) member with increased stress capacity $n\sigma$; (c) member with infinite stress capacity.

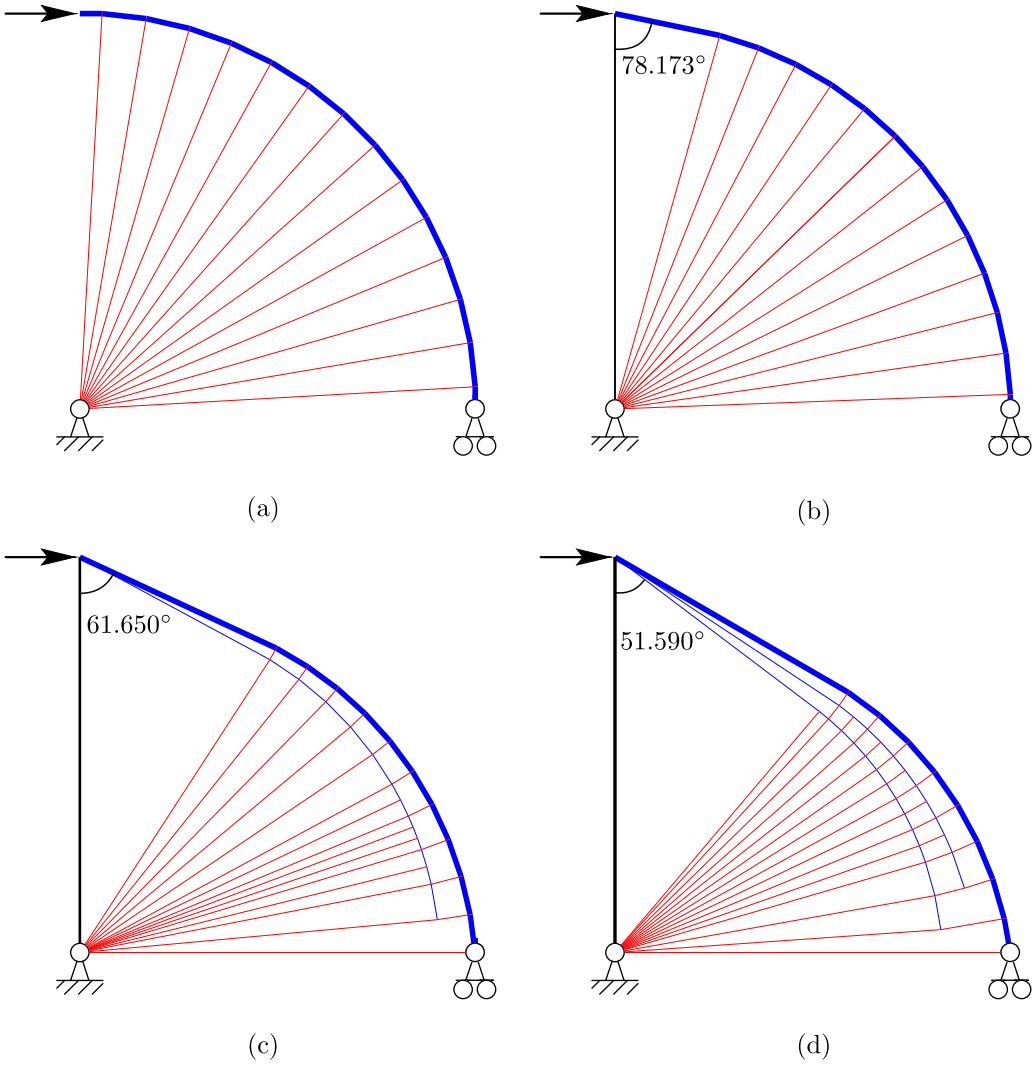

Figure 8.2: Examples for pre-existing members with $n\sigma$ stress capacity and normal members with σ stress capacity:(a) n=1, pre-existing member not used; (b) n=1.1, the theoretical and numerical intersection angles are 77.690° and 78.173°; (c) n=2, the theoretical and numerical intersection angles are 60.000° and 61.650°; (d) n=5, the theoretical and numerical intersection angles are 50.768° and 51.590°; black members represent pre-existing members, and angles shown in the graph are numerical results.

between them can be obtained as:

$$\theta = (\cos^{-1}(1/n))/2 \quad \text{or} \quad \frac{\pi}{2} - (\cos^{-1}(1/n))/2 \tag{8.1}$$

This equation is validated using numerical examples shown in Fig. 8.2. Note that these results are from the approach used in previous chapters that involves both layout and geometry optimization. From the comparison between the numerical value (i.e. obtained from measuring the optimized structure shown in Fig. 8.2) and the theoretical value (obtained using (8.1)), it is evident that the difference is very small. Additionally, a part of this difference is from the numerical solution error. Therefore, the above theory and practice are consistent with each other.

For the second method, the cost function and adjoint strain graph of a member with area lower boundary equal to a_0 are shown in Fig. 8.3 (Rozvany et al. 2006, Lewiński 2006). From this graph, it is clear that there are three different pre-existing bars in this method: fully stressed pre-existing member with area larger than a_0, fully stressed pre-existing member with area equal to a_0, and not fully stressed pre-existing member. In the case of pre-existing rods that are not fully stressed, their properties are in fact the same as those of pre-existing members with infinite stress capacity mentioned in the previous section, which also proved that the optimal intersection angle between this and a normal member is 45 degrees. In the case of pre-existing bars that are fully stressed and have an area larger than a_0, it is shown in Fig. 8.3 that its adjoint strain of this pre-existing member is equal to the adjont strain of a normal member. Consequently, the intersection angle for this kind of member is 90°. For this intermediate situation where the pre-existing member is fully stressed and has an area equal to a_0, its adjoint strain could take any value between $-\epsilon_{xx}$ and ϵ_{xx}. Hence, its optimal intersection angle cannot be predicted using current methods.

It is worth noting that above analysis only apply to T-region situation. For an R-region structure, it has been described in Section 2.5.2 that it only contains strain in one direction. Therefore, according to Hemp's theory described in Section 2.6.2, the minor principal strain can take an arbitrary value between 0 and the limiting value. Based on this point, the Mohr's circle analysis is illustrated in Fig. 8.4. It could be observed that the optimal intersect angle equals to 45° and 90° when the minor principle strain equals to 0 and the limiting value respectively. Therefore, in any R-region structure, the optimal intersection angle between a pre-existing member with infinite strength and a normal member must be between 45° and 90°. This conclusion is consistent with

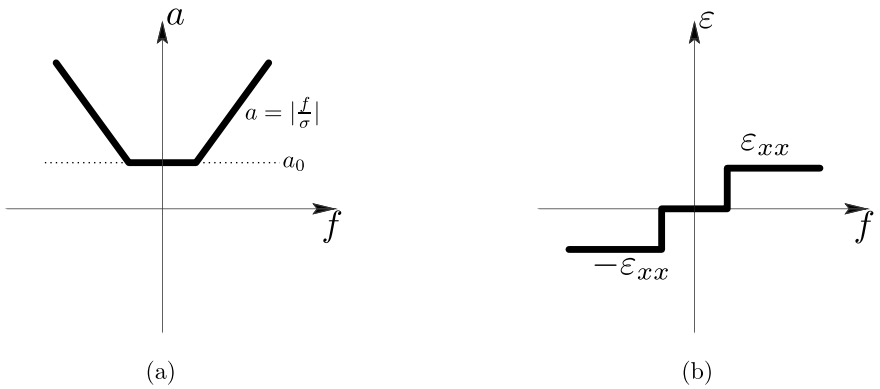

Figure 8.3: Pre-existing member with area lower boundary, where a, f and σ represents area, material cost and adjoint strain : (a) curve of cost function; (b) relation between cost and adjoint strain.

numerical results in Fig. 3.5a and Fig. 6.4a.

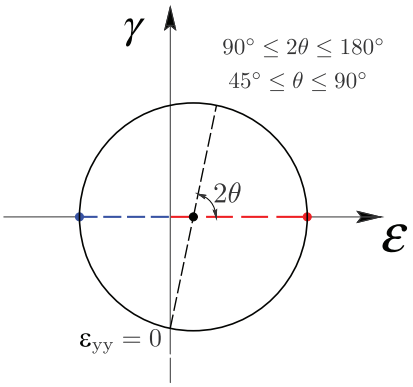

Figure 8.4: Mohr circle analysis for R-region problem, where red, blue and black dash line represents, respectively, bracing member in tension, bracing member in compression and pre-existing member with infinite reserves of strength.

8.2.1 Pre-existing cases with non integer aspect ratio

A 45 degree principle is proposed in Section 4.4.3 and it is proved by Mohr's circle analysis and results from numerical cases with integer aspect ratio (e.g. height : width = 4:1 or 3:1 et al.). For sake of completeness, cases with non-integer aspect ratio are further studied and the results are shown in Fig. 8.5 (case description is show in Fig. 4.1). Note that in cases in this section does not include top horizontal pre-existing members and horizontal loads are applied at both top corners. It can be seen that the intersection angles between normal bracing members and pre-existing members are 45° or very close to 45°. Not all the intersection angles are exactly 45° because of the numerical errors caused by the limited number of nodes used in these cases. For sake of displaying clarity, the node grids used in Fig. 8.5a, b and c are 5×7, 5×11, 5×15

respectively. The numerical error reduces as the increase of node number used in the optimization cases. Therefore, it can be obtained from Fig. 8.5 that in cases with non integer aspect ratio, the form of the optimized structure are adjusted to be more complex to meet the 45° rule.

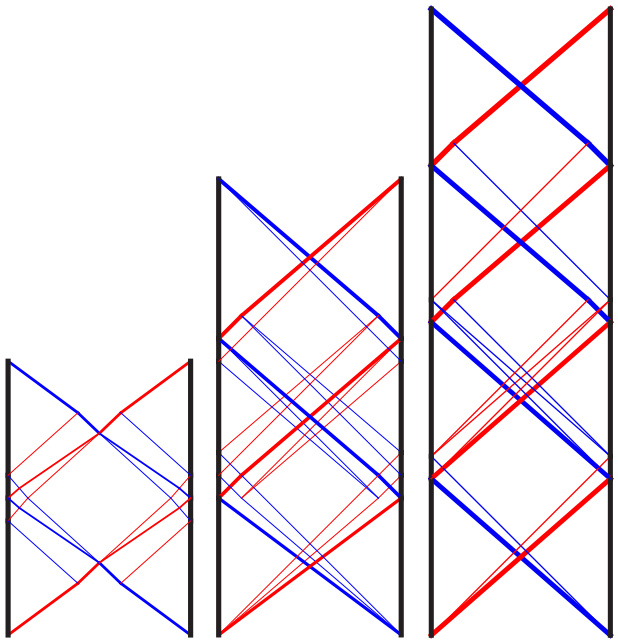

Figure 8.5: Pre-existing cases with none integer aspect ratios, where width : height equals to 1:1.5 in (a), 1:2.5 in (b) and 1:3.5 in (c). Element color key: red = tensile, blue = compressive, black = pre-existing (assuming left to right loading).

Chapter 9

Conclusions

This thesis has focused on the application of layout optimization to the design of bracing; the findings can be summarised as follows:

- For the two transmissible load approaches explored (i.e. the migrating load and the rigid bar approach), clear differences between them have been identified in this study, proved via mathematical and numerical methods. Whilst the migrating load approach is feasible for all situations, the rigid bar approach may output erroneously strengthened structures. The reason for this is the virtual rigid bars that are used to transmit the loads onto the structures may form part of the structure. Therefore, the rigid bar approach should be used with caution, and users should if necessary check whether the optimized structures are feasible without the virtual rigid bars.

- Three different cases have been studied in this thesis: (1) bracing optimized within a pre-existing column-beam frame, (2) bracing optimized with multiple load cases that include both horizontal and vertical loads, and (3) bracing optimized with transmissible loads (and pre-existing beams). The results are compared with standard bracing structures with respect to material consumption and stiffness. In both measures, the optimized structures appear to be better than standard structures. It is worth noting that the use of different assumptions leads to different optimization results, and these results may be chosen for use based on other practical conditions in realistic cases.

- In the cases involving a pre-existing column-beam system considered in Chapter 4, three

different kinds of bracing were analysed. This indicated that conventional cross bracing is in general the most efficient structural solution. In addition, through the analysis of the optimized structures, it was found that tension/compression member pairs with normal strength should intersect pre-existing members with infinite strength at 45° in an optimal structure. This finding was proved via a Mohr'c circle analysis. Additionally, a more general rule for the intersection angle between members with different strength has been identified and included in the discussion.

- In the holistic design cases in Chapter 5, the optimized layout was found to be dominated by only one parameter, formally proved using superposition approach. Since the conditions for the superposition approach are only satisfied for load cases based on the British Standard, the use of different design codes may lead to different results; this is something that is unlikely to have been anticipated by the code writers. In addition, layout optimization has been applied to the design of the frame of a small four storey office building comprising rectangular bays. This led to an unconventional frame layout and a 32% reduction in the mass of material required compared with the equivalent conventional design.

- In Chapter 6, wind loads were treated as transmissible loads and the building envelope identified simultaneously with the inner bracing structure. Simple and efficient structures have been identified for both 2D and 3D scenarios; they may be selected for use based on the real-world conditions pertaining to a specific design project.

- In Chapter 7, a new layout optimization formulation which can consider moment resisting frame members is proposed. In this new approach, members can take axial force only or moment only or axial force and moment simultaneously. Thus new benchmark structures with combined truss and frame members can be identified. Although in most cases, it has been found that pure truss structures are still the optimal results, it has been shown that frame members appears in the optimized results of cases with space restricted design domain and cases with moment loads.

Chapter 10

Recommendations for future work

Areas for further work are indicated below:

- For the transmissible load approach, it has been proved in this thesis that the rigid bar approach and the migrating load approach are mathematically different. Additionally, it has been shown that the rigid bar approach will lead to misleading results in some cases. However, the migrating load approach is also not a perfect solution. Problems such as load splitting and loads transmitted to an arbitrary internal position within the structure. Therefore, it would be useful to use geometry optimization to implement the transmissible load (allowing loaded node to move along a pre-defined transmissible line during the optimization).

- Though bracing optimization cases with different conditions have been studied in this thesis, the load cases considered were relatively simple as was the shape of the design domain. Hence it would be worth applying the same method to building design cases with unusual shapes (e.g. Swiss Re Building in London, CCTV headquarters in Beijing etc.) and also using realistic multiple load cases in the optimization process. It was mentioned previously that doing a 3D optimization with many alternative load cases may lead to structure with high complexity. In relation to this, it would be worth trying to use several primary load cases in the first layout optimization stage and then doing size and/or shape optimization using the remaining, secondary, load cases.

- A optimization approach for combined trusses and frames has been proposed in Section

8. Further development on this approach could focus on the following three aspects: (1) expand the applicability of this approach to make it suitable for 3D cases; (2) consider involving beam members with different cross section shapes in the optimization problem; (3) since the number of variables and constraints in this new approach is much larger than in the truss layout optimization problem, it would be worth investigating methods that can be used to reduce the numerical cost. Since the simplified formulation can be solved via conic quadratic optimization, a ”member adding” method could potentially be developed, utilizing values from the corresponding dual formulation.

References

Airunp (2005), 'Jin Mao Tower', Wikimedia Commons. URL: https://tinyurl.com/yady8p7v, Accessed on: 12 June 2017.

Ali, M. M. (2001), *Art of the skyscraper: the genius of Fazlur Khan*, Rizzoli Intl Pubns.

Ali, M. M. & Moon, K. S. (2007), 'Structural developments in tall buildings: current trends and future prospects', *Architectural science review* **50**(3), 205–223.

Allahdadian, S., Boroomand, B. & Barekatein, A. (2012), 'Towards optimal design of bracing system of multi-story structures under harmonic base excitation through a topology optimization scheme', *Finite Elements in Analysis and Design* **61**, 60–74.

Allaire, G., Jouve, F. & Toader, A. (2002), 'A level-set method for shape optimization', *Comptes Rendus de l'Académie des Sciences - Series I* **334**, 1125–1130.

Allaire, G., Jouve, F. & Toader, A. (2004), 'Structural optimization using sensitivity analysis and a level-set method', *Journal of Computational Physics* **194**, 363–393.

Alsandro (2006), 'Hearst Tower', Wikipedia. URL: https://tinyurl.com/y8c5v3fl, Accessed on: 12 June 2017.

Amstutz, S. (2011), 'Connections between topological sensitivity analysis and material interpolation schemes in topology optimization', *Structural and Multidisciplinary Optimization* **43**(6), 755–765.

Baker, W. (1990), Sizing techniques for lateral systems in multi-story steel buildings, *in* '4th World Congress on Tall Buildings', pp. 868–875.

Baldock, R. (2007), Structural optimisation in building design practice: case-studies in topology optimisation of bracing systems, PhD thesis, University of Cambridge.

Beghini, L. L., Beghini, A., Katz, N., Baker, W. F. & Paulino, G. H. (2014), 'Connecting architecture and engineering through structural topology optimization', *Engineering Structures* **59**, 716–726.

Bendsøe, M. P. (1989), 'Optimal shape design as a material distribution problem', *Structural and multidisciplinary optimization* **1**(4), 193–202.

Bendsøe, M. P. & Kikuchi, N. (1988), 'Generating optimal topologies in structural design using a homogenization method', *Computer methods in applied mechanics and engineering* **71**(2), 197–224.

Bendsøe, M. P. & Sigmund, O. (1999), 'Material interpolation schemes in topology optimization', *Archive of applied mechanics* **69**(9), 635–654.

Bertsekas, D. P., Nedi, A., Ozdaglar, A. E. et al. (2003), *Convex analysis and optimization*, Athena Scientific.

Bobby, S., Spence, S., Bernardini, E., Wei, D. & Kareem, A. (2013), A complete performance-based optimization framework for the design of tall buildings, *in* '11th International Conference on Structural Safety & Reliability (ICOSSAR), New York, USA'.

Bourdin, B. & Chambolle, A. (2003), 'Design-dependent loads in topology optimization', *ESAIM: Control , Optimisation and Calculus of Virations* **9**, 19–48.

Brettle, M. E. & Brown, D. G. (2009), *Steel Building Design: Worked examples for students*, The Steel Construction Institute.

Brown, D. G., Iles, D. C. & Yandzio, E. (2009), *Steel building design: medium rise braced frames, in accordance with Eurocodes and the UK National Annexes*, The Steel Construction Institute.

Burry, J., Felicetti, P., Tang, J., Burry, M. & Xie, M. (2005), 'Dynamical structural modeling: a collaborative design exploration', *International Journal of Architectural Computing* **3**(1), 27–42.

Carroll, C., Cross, P., Duan, X., Gibbons, C., Ho, G., Kwok, M., Lawson, R., Lee, A., Luong, A., McGowan, R. et al. (2005), 'CCTV headquarters, beijing, china: Structural engineering design and approvals', *The Arup Journal* **40**(2), 3–9.

Carroll, C., Cross, P., Duan, X., Gibbons, C., Ho, G., Kwok, M., Li, R., Lee, A., Li, R., Luong, A. & Pope, C. (2008), 'Case study: CCTV Building-Headquarters & Cultural Center', *CTBUH Journal Issue III* .

Chan, A. (1960), The design of Michell optimum structures, PhD thesis, College of Aeronautics Cranfield.

Chiandussi, G., Codegone, M. & Ferrero, S. (2009), 'Topology optimization with optimality criteria and transmissible loads', *Computers & Mathematics with Applications* **57**(5), 772–788.

Cox, H. L. (2014), *The Design of Structures of Least Weight: International Series of Monographs in Aeronautics and Astronautics: Solid and Structural Mechanics*, Vol. 8, Elsevier.

Dantzig, G. B. (1949), 'Programming in a linear structure', *Econometrica* **17**, 73–74.

Darwich, W., Gilbert, M. & Tyas, A. (2007), Optimum structure to carry a uniform load between two pinned supports, *in* '7th World Congress of Structural and Multidisciplinary Optimization, Seoul, Korea'.

Darwich, W., Gilbert, M. & Tyas, A. (2010), 'Optimum structure to carry a uniform load between pinned supports', *Structural and Multidisciplinary Optimization* **42**(1), 33–42.

Dewhurst, P. (2001), 'Analytical solutions and numerical procedures for minimum-weight michell structures', *Journal of the Mechanics and Physics of Solids* **49**(3), 445–467.

Donaldytong (2012), 'Burj Khalifa Tower', Wikipedia. URL: https://tinyurl.com/q9n5hgh, Accessed on: 12 June 2017.

Dorn, W. S., Gomory, R. E. & Greenberg, H. J. (1964), 'Automatic design of optimal structures', *Journal de Mecanique* **3**, 25–52.

EN, C. (1993), 'Eurocode 3: Design of steel structures', *Part1-1: General Rules and Rules for Buildings* .

Foster, N. (2005), 'Modeling the Swiss Re Tower', Architecture Week. URL: goo.gl/DFbtkx, Accessed on: 12 June 2017.

Fuchs, M. B. & Moses, E. (2000), 'Optimal structural topologies with transmissible loads', *Structural and multidisciplinary optimization* **19**, 263–273.

Gilbert, M., Darwich, W., Tyas, A. & Shepherd, P. (2005), Application of large-scale layout optimization techniques in structural engineering practice, *in* '6th World Congresses of Structural and Multidisciplinary Optimization', Rio de Janeiro, Brazil.

Gilbert, M. & Tyas, A. (2003), 'Layout optimization of large-scale pin-jointed frames', *Engineering Computations* **20**(8), 1044–1064.

Gill, P. E., Murray, W., Saunders, M. A., Tomlin, J. A. & Wright, M. H. (1986), 'On projected Newton barrier methods for linear programming and an equivalence to Karmarkar's projective method', *Mathematical Programming* **36**, 183–209.

Graczykowski, C. & Lewiński, T. (2010), 'Michell cantilevers constructed within a half strip. tabulation of selected benchmark results', *Structural and Multidisciplinary Optimization* **42**(6), 869–877.

Guichard, A. (2010), '30 St Mary Axe', Wikipedia. URL: https://tinyurl.com/yasxu48f, Accessed on: 12 June 2017.

Gunel, M. H. & Ilgin, H. E. (2007), 'A proposal for the classification of structural systems of tall buildings', *Building and Environment* **42**(7), 2667–2675.

He, L. & Gilbert, M. (2015), 'Rationalization of trusses generated via layout optimization', *Structural and Multidisciplinary Optimization* **52**(4), 677–694.

He, L. & Gilbert, M. (2016), 'Automatic rationalization of yield-line patterns identified using discontinuity layout optimization', *International Journal of Solids and Structures* **84**, 27–39.

He, L., Gilbert, M. & Shepherd, M. (2017), 'Automatic yield-line analysis of practical slab configurations via discontinuity layout optimization', *Journal of Structural Engineering* **143**(7), 04017036.

Hemp, W. S. (1973), *Optimum structures*, Oxford engineering science series, Clarendon Press.

Holton, I. (2008), 'China World Trade Center Tower', Wikipedia. URL: https://tinyurl.com/ycevzput, Accessed on: 12 June 2017.

Houlsby, G., Liu, G. & Augarde, C. (2000), 'A tying scheme for imposing displacement constraints in finite element analysis', *Communications in numerical methods in engineering* **16**(10), 721–732.

Huang, X. & Xie, Y. M. (2010*a*), 'A further review of ESO type methods for topology optimization', *Structural and Multidisciplinary Optimization* **41**(5), 671–683.

Huang, X. & Xie, Y. M. (2010*b*), 'Evolutionary topology optimization of continuum structures with an additional displacement constraint', *Structural and Multidisciplinary Optimization* **40**, 409–416.

Jovianeye (2011), 'John Hancock Center', Wikimedia Commons. URL: https://commons.wikimedia.org/wiki/User:Jovianeye, Accessed on: 01 January 2017.

Kane, C. & Schoenauer, M. (1996), 'Topological optimum design using genetic algorithms', *Control and Cybernetics* **25**, 1059–1087.

Karmarkar, N. K. (1984), 'A new polynomial-time algorithm for linear programming', *Combinatorica* **4**, 373–395.

Kingman, J., Tsavdaridis, K. & Toropov, V. (2015), 'Applications of topology optimisation in structural engineering: high-rise buildings & steel components', *Jordan Journal of Civil Engineering* **9**(3), 335–357.

Lee, S. & Tovar, A. (2014), 'Outrigger placement in tall buildings using topology optimization', *Engineering Structures* **74**, 122–129.

Lewiński, T. (2006), 'Variational proof of optimality criteria for michell structures with pre-existing members', *Structural and Multidisciplinary Optimization* **32**(1), 81–83.

Lewiński, T. & Rozvany, G. I. (2007), 'Exact analytical solutions for some popular benchmark problems in topology optimization II: three-sided polygonal supports', *Structural and Multidisciplinary Optimization* **33**(4), 337–349.

Lewiński, T. & Rozvany, G. I. (2008), 'Exact analytical solutions for some popular benchmark problems in topology optimization III: L-shaped domains', *Structural and Multidisciplinary Optimization* **35**(2), 165–174.

Liang, Q. Q., Xie, Y. M. & Steven, G. P. (2000), 'Optimal topology design of bracing systems for multistory steel frames', *Journal of Structural Engineering* **126**(7), 823–829.

Maxwell, J. C. (1864), 'On reciprocal figures and diagrams of forces', *The London, Edinburgh, and Dublin Philosophical Magazine and Journal of Science* **27**(182), 250–261.

Michell, A. G. M. (1904), 'The limits of economy of material in frame structure', *Philosophical Magazine* **8**(6), 589–597.

Mijar, A. R., Swan, C. C., Arora, J. S. & Kosaka, I. (1998), 'Continuum topology optimization for concept design of frame bracing systems', *Journal of Structural Engineering* **124**(5), 541–550.

Mlejnek, H. (1992), 'Some aspects of the genesis of structures', *Structural and Multidisciplinary Optimization* **5**(1), 64–69.

Moon, K. S. (2008), 'Optimal grid geometry of diagrid structures for tall buildings', *Architectural Science Review* **51**(3), 239–251.

Moon, K. S. (2012), Braced tube structures for complex-shaped tall buildings, *in* 'Advanced Materials Research', Vol. 450, Trans Tech Publ, pp. 1584–1587.

Moon, K. S., Connor, J. J. & Fernandez, J. E. (2007), 'Diagrid structural systems for tall buildings: characteristics and methodology for preliminary design', *Structural Design of Tall and Special Buildings* **16**(2), 205–230.

Nielsen, M. P. & Hoang, L. C. (2011), *Limit analysis and concrete plasticity*, 3rd edn, Taylor and Francis Group.

Nocedal, J., Wright, S. J. & Robinson, S. M. (2006), *Numerical Optimization*, 2nd edn, Springer.

Pearson, C., E. (1958), Structural design by high speed computing machines, *in* 'Conference on Electronic Computation of the A. S. C. E., Kansas City'.

Prager, W. (1974), *Introduction to structural optimization*, Springer.

Prager, W. & Rozvany, G. I. (1977), 'Optimization of structural geometry', *Dynamical systems* pp. 265–293.

Pritchard, T., Gilbert, M. & Tyas, A. (2005), Plastic layout optimization of large-scale frameworks subject to multiple load cases, member self-weight and with joint length penalties, *in* '6th World Congress of Structural and Multidisciplinary Optimization, CD-ROM proceedings, 10 pages'.

Rees, D. W. A. (2006), *Basic engineering plasticity*, Elsevier.

Renuka, J. & Kumar, M. (2015), 'Effect of configuration on lateral displacement and cost of the structure for high rise steel space frames subjected to wind loads', *International Journal of Research in Engineering and Technology* **04**, 101–113.

Richardson, J. N., Nordenson, G., Laberenne, R., Coelho, R. F. & Adriaenssens, S. (2013), 'Flexible optimum design of a bracing system for façade design using multiobjective genetic algorithms', *Automation in construction* **32**, 80–87.

Rozvany, G. (1998), 'Exact analytical solutions for some popular benchmark problems in topology optimization', *Structural and Multidisciplinary Optimization* **15**(1), 42–48.

Rozvany, G., Bendsoe, M. & Kirsch, U. (1995), 'Layout optimization of structures', *Applied Mechanics Reviews* **48**(2), 41–119.

Rozvany, G. & Hill, R. (1978), 'Optimal plastic design: superposition principles and bounds on the minimum cost', *Computer Methods in Applied Mechanics and Engineering* **13**(2), 151–173.

Rozvany, G. I. N. (1997), 'Partial relaxation of the orthogonality requirement for classical Michell trusses', *Structural Optimization* **13**, 271–274.

Rozvany, G. I. N. & Wang, C. M. (1983*a*), 'On plane Prager-structures', *International Journal of Mechanical Sciences* **25(7)**, 519–527.

Rozvany, G. I. N., Wang, C. M. & Dow, M. (1982), 'Prager-structures: Archgrids and cable networks of optimal layout', *Computer Methods in Applied Mechanics and Engineering* **31**, 91–113.

Rozvany, G. I. & Prager, W. (1979), 'A new class of structural optimization problems: optimal archgrids', *Computer methods in applied mechanics and engineering* **19**(1), 127–150.

Rozvany, G. I., Sokół, T. & Pomezanski, V. (2014), 'Fundamentals of exact multi-load topology optimization–stress-based least-volume trusses (generalized Michell structures) - Part I: Plastic design', *Structural and Multidisciplinary Optimization* **50**(6), 1051–1078.

Rozvany, G., Querin, O., Logo, J. & Pomezanski, V. (2006), 'Exact analytical theory of topology optimization with some pre-existing members or elements', *Structural and Multidisciplinary Optimization* **31**(5), 373–377.

Rozvany, G. & Wang, C. (1983*b*), 'On plane Prager-structures I', *International journal of mechanical sciences* **25**(7), 519–527.

Sala, S. & Candiani, E. (2014), Optimization of tied lateral systems for tall buildings design, PhD thesis, Politecnico di Milano.

Sigmund, O. (2001), 'A 99 line topology optimization code written in matlab', *Structural and multidisciplinary optimization* **21**(2), 120–127.

Sigmund, O. (2011), 'On the usefulness of non-gradient approaches in topology optimization', *Structural and Multidisciplinary Optimization* **43**, 589–596.

Smith, C. & Gilbert, M. (2007), Application of discontinuity layout optimization to plane plasticity problems, *in* 'Proceedings of the Royal Society of London A: Mathematical, Physical and Engineering Sciences', Vol. 463, The Royal Society, pp. 2461–2484.

Soakologist (1998), 'Willis tower', Wikipedia. URL: https://tinyurl.com/y88o8t8a, Accessed on: 12 June 2017.

Sokolowski, J. & Zochowski, A. (1999), 'The topological derivative method in shape optimization', *SIAM Journal on Control and Optimization* **37**(4), 1251–1272.

Stojakovic, E. (2013), 'CCTV Tower', Wikimedia Commons. URL: https://tinyurl.com/y9agww9j, Accessed on: 12 June 2017.

Stromberg, L. L., Beghini, A., Baker, W. F. & Paulino, G. H. (2011), 'Application of layout and topology optimization using pattern gradation for the conceptual design of buildings', *Structural and Multidisciplinary Optimization* **43**(2), 165–180.

Stromberg, L. L., Beghini, A., Baker, W. F. & Paulino, G. H. (2012), 'Topology optimization for braced frames: combining continuum and beam/column elements', *Engineering Structures* **37**, 106–124.

Sulfur (2006), 'The U.S. Bank Center', Wikipedia. URL: https://tinyurl.com/yc5wuby4, Accessed on: 12 June 2017.

Sved, G. (1954), 'The minimum weight of certain redundant structures', *Aust J Appl Sci* **5**, 1–9.

Tangaramvong, S. & Tin-Loi, F. (2015), 'Optimal performance-based rehabilitation of steel frames using braces', *Journal of Structural Engineering* **141**(10), 04015015.

Tata Steel Europe Limited (2016), *Tata Steel sections interactive 'blue book'*, The Steel Construction Institute.

Tyas, A. & Gilbert, M. (2011), 'On transmissible load formulations in topology optimization', *9th World Congress on Structural and Multidisciplinary Optimization* .

Tyas, A., Gilbert, M. & Pritchard, T. (2005), Practical plastic layout optimization of trusses incorporating stability considerations, *in* '6th World Congresses of Structural and Multidisciplinary Optimization, Rio de Janeiro, CD-ROM proceedings'.

Tyas, A., Pichugin, A. & Gilbert, M. (2010), 'Optimum structure to carry a uniform load between pinned supports: exact analytical solution', **467**(2128), 1101–1120.

Vanderbei, R. J. (2001), *Linear programming: foundations and extensions*, 2nd edn, Springer Verlag.

Wang, C. & Rozvany, G. I. N. (1983), 'On plane prager-structuresii: Non-parallel external loads and allowances for selfweight', *International journal of mechanical sciences* **25**(7), 529–541.

Wang, G. R. & Dow, C. (1982), 'Prager-structures: archgrids and cable networks of optimal layout', *Computer Methods in Applied Mechanics and Engineering* **31**(1), 91–113.

WiNG (2010), 'International Commerce Centre', Wikipedia. URL: https://tinyurl.com/yckppcu3, Accessed on: 12 June 2017.

Wright, M. H. (2004), 'The interior-point revolution in optimization: history, recent developments, and lasting consequences', *Bulletin of the American Mathematical Society* **42**(1), 39–57.

Xie, Y. M. & Steven, G. P. (1993), 'A simple evolutionary procedure for structural optimization', *Computers & Structures* **49**(5), 885–896.

Yang, X. Y., Xie, Y. M. & Steven, G. P. (2005), 'Evolutionary methods for topology optimisation of continuous structures with design dependent loads', *Computers and Structures* **83**(12-13), 956–963.

Yazdi, H. M. & Sulong, N. R. (2011), 'Optimization of off-centre bracing system using genetic algorithm', *Journal of Constructional Steel Research* **67**(10), 1435–1441.

Zhou, M. & Rozvany, G. (1991), 'The COC algorithm, Part II: Topological, geometrical and generalized shape optimization', *Computer Methods in Applied Mechanics and Engineering* **89**(1-3), 309–336.